3 3679 00062 5394

BNWL-1898
NRC 1 and 3

GAPCON-THERMAL-2: A COMPUTER PROGRAM FOR CALCULATING THE THERMAL BEHAVIOR OF AN OXIDE FUEL ROD

by

C. E. Beyer, C. R. Hann, D. D. Lanning,
F. E. Panisko, and L. J. Parchen

Report to
Core Performance Branch
Division of Technical Review
Nuclear Regulatory Commission

November 1975

BATTELLE
PACIFIC NORTHWEST LABORATORIES
RICHLAND, WASHINGTON 99352

CONTENTS

LIST OF FIGURES iv
LIST OF TABLES vii
INTRODUCTION 1
SUMMARY AND CONCLUSIONS 5
GENERAL CODE DESCRIPTION 7
DETAILED CODE DESCRIPTION 10
Power History 10
Fission Gas Generation 10
Relocation 11
Densification 12
Conductance Calculations 13
Gas Release 17
Volatile Impurities 24
Dished Pellets and Fuel Axial Thermal Expansion 27
Recycle Mixed-Oxide Fuel 28
Modular Code 29
International System of Units 30
Options 30
Fuel Melting 30
Models Unaltered From Gapcon-Thermal-1 31
PARAMETRIC STUDY 33
CODE VERIFICATION EVALUATION 35
LIMITATIONS AND RECOMMENDATIONS 47
ACKNOWLEDGMENTS 123
REFERENCES 124
APPENDIX A - INPUT VARIABLES FOR GAPCON-THERMAL-2 . . . . . A-1
APPENDIX B - REVISIONS TO FISGAS BY J.L. CARTER B-1
APPENDIX C - MODELS AND DATA UNALTERED FROM GAPCON-THERMAL-1 . . C-1
APPENDIX D - INPUT VALUES TO GAPCON-THERMAL-2 . . . . . D-1

LIST OF FIGURES

1 Typical Fuel Pin Parameters That Influence Fuel-Cladding Heat Transfer Coefficient 51

2 GAPCON-THERMAL-2 Flow Sheet 52

3 GAPCON-THERMAL-2 Flow Sheet (Detail A) 53

4 GAPCON-THERMAL-2 Subroutine Flow Chart 54

5 Comparisons of Gap Conductance Values in GAPCON-THERMAL-2 with GAPCON-THERMAL-1 55

6 A Comparison of the High-Temperature Gas Release Model and the Data 56

7 A Comparison of the High-Temperature Release Model with Hoffman and Coplin's Volume-Average Temperature Model . . . 57

8 A Comparison of the High-Temperature Gas Release Model with Lewis' Model 58

9 UO_2 Surface-to-Volume Ratios as a Function of Burnup . . . 59

10 Measured Surface Area as a Function of Percent Theoretical Density for Sintered UO_2 60

11 Predictions of the Low-Temperature Gas Release Model . . . 61

12 Schematic of Fuel Model for Pressure Calculations 62

13 Parametric Study: Base Case, Restructuring, Constant Power, Best Estimate Relocation 63

14 Parametric Study: Conservative Relocation, Densification, Conservative Gas Release, Delayed Gas Release 64

15 Parametric Study: Cladding Elastic Deformation, Plastic Fuel, Rigid Fuel, Larger Plenum 65

16 Parametric Study: Densification and Best Estimate Relocation, Densification Delayed Fission Gas Release and Best Estimate Relocation, Dished Fuel Pellets, Smaller Plenum 66

17 Parametric Study: Sorbed Gas, High Fill Gas Pressure, High U^{235} Enrichment, Different Axial Power Shape 67

18 Difference Between GAPCON-THERMAL-2 Predictions and HPR-129, IFA-116 Experimental Data 68

19 Difference Between GAPCON-THERMAL-2 Predictions and HPR-129, IFA-117 Experimental Data 69

20 Fuel Temperatures Versus Heat Rating, Experimental Data from Various Irradiation Tests in Halden Reactor 70

21 Fuel Temperatures Versus Fabricated Gap Size, Experimental Data from Various Irradiation Tests in Halden Reactor . . . 71

LIST OF FIGURES (contd)

22 GAPCON-THERMAL-2 Predictions of IFA-130 72

23 GAPCON-THERMAL-2 Predictions of IFA-131 73

24 GAPCON-THERMAL-2 Predictions of Capsule II, WCAP-2923 . . . 74

25 GAPCON-THERMAL-2 Predictions of Capsules I and II, WCAP-2923 75

26 GAPCON-THERMAL-2 Prediction of Sample HBA, HPR-80 76

27 GAPCON-THERMAL-2 Prediction of Sample HBB, HPR-80 77

28 GAPCON-THERMAL-2 Prediction of Sample HCA, HPR-80 78

29 GAPCON-THERMAL-2 Prediction of Sample HCD, HPR-80 79

30 GAPCON-THERMAL-2 Prediction of Sample HBC, HPR-80 80

31 GAPCON-THERMAL-2 Prediction of Sample HCC, HPR-80 81

32 GAPCON-THERMAL-2 Prediction of Fuel Centerline Temperature Versus Linear Heat Rating for Sample HCD1, HPR-80 82

33 GAPCON-THERMAL-2 Prediction of Fuel Centerline Temperature Versus Heat Rating for Sample HBB, HPR-80 83

34 GAPCON-THERMAL-2 Prediction of Fuel Radial Temperature Profile for Sample LFD, AECL-2662 84

35 GAPCON-THERMAL-2 Prediction of Fuel Radial Temperature Profile for Sample LFH, AECL-2662 85

36 GAPCON-THERMAL-2 Prediction of Fuel Radial Temperature Profile for Sample LFM, AECL-2662 86

37 GAPCON-THERMAL-2 Prediction of Fuel Radial Temperature Profile for Sample DFB, AECL-1676 87

38 GAPCON-THERMAL-2 Prediction of Fuel Radial Temperature Profile for Sample DFD, AECL-1676 88

39 GAPCON-THERMAL-2 Prediction of Fuel Radial Temperature Profile for Sample DFE, AECL-1676 89

40 GAPCON-THERMAL-2 Prediction of Fuel Centerline Temperature Versus Linear Heat Rating for Sample IFA-3, AE-318 90

41 GAPCON-THERMAL-2 Prediction of Fuel Centerline Temperature Versus Linear Heat Rating for Sample IFA-4, AE-318 91

42 GAPCON-THERMAL-2 Prediction of Fuel Centerline Temperature Versus Linear Heat Rating for Sample IFA-10, AE-318 92

43 A Comparison of GAPCON-THERMAL-2 Predictions with Grain Growth Measurements from CEA-R-3358, Sample 4112-AE1 . . . 93

LIST OF FIGURES (contd)

44 A Comparison of GAPCON-THERMAL-2 Predictions with Grain Growth Measurements from CEA-R-3358, Sample 4112-BE1 . . . . .

45 A Comparison of GAPCON-THERMAL-2 Predictions with Grain Growth Measurements from CEA-R-3358, Sample 4112-AE2 95

46 A Comparison of GAPCON-THERMAL-2 Predictions with Grain Growth Measurements from CEA-R-3358, Sample 4112-BE2 96

47 A Comparison of GAPCON-THERMAL-2 Predictions with Grain Growth Measurements from CEA-R-3358, Sample 4110-AE1 97

48 A Comparison of GAPCON-THERMAL-2 Predictions with Grain Growth Measurements from CEA-R-3358, Sample 4110-BE1 98

49 A Comparison of GAPCON-THERMAL-2 Predictions with Grain Growth Measurements from CEA-R-3358, Sample 4110-AE2 99

50 A Comparison of GAPCON-THERMAL-2 Predictions with Grain Growth Measurements from CEA-R-3358, Sample 4110-BE2 100

51 A Comparison of GAPCON-THERMAL-2 Predictions with Grain Growth Measurements from CEA-R-3358, Sample 4113-AE1 101

52 A Comparison of GAPCON-THERMAL-2 Predictions with Grain Growth Measurements from CEA-R-3358, Sample 4113-AE2 102

53 A Comparison of GAPCON-THERMAL-2 Predictions with Grain Growth Measurements from CEA-R-3358, Sample 4113-BE1 103

54 A Comparison of GAPCON-THERMAL-2 Predictions with Grain Growth Measurements from CEA-R-3358, Sample 4113-BE2 104

55 A Comparison of GAPCON-THERMAL-2 Predictions with Grain Growth Measurements from CEA-R-3358, Sample 4111-AE1 105

56 A Comparison of GAPCON-THERMAL-2 Predictions with Grain Growth Measurements from CEA-R-3358, Sample 4111-AE2 106

57 A Comparison of GAPCON-THERMAL-2 Predictions with Grain Growth Measurements from CEA-R-3358, Sample 4111-BE1 107

58 A Comparison of GAPCON-THERMAL-2 Predictions with Grain Growth Measurements from CEA-R-3358, Sample 4111-BE2 108

LIST OF TABLES

1	Alphabetical Listing of INPUT Parameters for GAPCON-THERMAL-2	109
2	Fission Yields Used for Thermal Flux Irradiation	110
3	Thermal Fission Cross Sections Used for the Heavy Metal Atoms	111
4	Data Base Used to Correlate Gas Release Model	112
5	Base Input for Parametric Study.	113
6	Summary of Parametric Study	114
7	IFA 116 and 117 Condensed Fuel Assembly Power History	115
8	GAPCON-THERMAL-2 HPR-129, IFA-116 Comparison	116
9	GAPCON-THERMAL-2 HPR-129, IFA-117, Pins 1 and 3 Comparison.	117
10	GAPCON-THERMAL-2 HPR-129, IFA-117, Pins 5 and 6 Comparison.	118
11	GAPCON-THERMAL-2 AECL-2662 and -1676 Gas Release Comparison.	119
12	GAPCON-THERMAL-2 Other AECL Gas Release Comparisons	120
13	GAPCON-THERMAL-2 Grain Growth Radii AECL-2588, X-23301 and X23303 Comparisons	121
14	GAPCON-THERMAL-2 CEA-R-3358 Gas Release Comparison	122

GAPCON-THERMAL-2: A COMPUTER PROGRAM FOR CALCULATING THE THERMAL BEHAVIOR OF AN OXIDE FUEL ROD

C. E. Beyer, C. R. Hann, D. D. Lanning,
F. E. Panisko, and L. J. Parchen

INTRODUCTION

This document describes the computer code GAPCON-THERMAL-2 which is a light water reactor (LWR) fuel thermal performance prediction code.

GAPCON-THERMAL-2 is an updated version of GAPCON-THERMAL-1.[1] Both of these codes were prepared by Battelle-Northwest for the Core Performance Branch of the Nuclear Regulatory Commission. This version of GAPCON-THERMAL-2 is being published to consolidate the numerous changes in the code that occurred since the publishing of the GAPCON-THERMAL-1 report, September 1973. GAPCON-THERMAL-2 should not be used as a fuel design code but as one of several calculational tools for reactor fuel steady-state thermal performance and to provide input for accident analyses. Some models used in the code provide best estimate as well as conservative predictions. No effort was made to adjust the code to agree with data; however, each of the individual models in the code is based on the best available data.

An analytical model for calculating the heat transfer coefficient (gap conductance) between the fuel and cladding eventually evolves into a series of complex, interacting models which cannot be treated separately. Physical phenomena must be adequately modeled mathematically with a self-consistent approach to even crudely simulate the dynamic situation in a fuel rod. A computational model for simulating fuel thermal performance should consider many phenomena and the effect of changes in any one of these on all the others. Figure 1[2] depicts the type of interactions associated with fuel thermal behavior that must be considered by the fuel modeler. Inability to accurately model some phenomena can have relatively large effects on the calculation while relatively large errors in other models may have a relatively small effect.

The high fuel temperatures calculated as a result of assuming instantaneous densification and isotropic shrinkage of the pellet also produce high fission gas release fractions. The released fission gases change the gas composition thereby reducing the conductivity of the gas. Two factors offsetting the rapidly changing gas compositions are gap closure mechanisms and the gradual decline in rod power associated with fuel depletion. The gap closure mechanisms that have the most pronounced effects are those associated with thermal expansion, fuel swelling, cladding creepdown, and radial relocation of the fuel via cracking. All four phenomena are difficult to describe quantitatively to the accuracy desired (a few tenths of a mil) for gap conductance calculations. Linear thermal expansion for UO_2 has been measured with some success; however, there is considerable dispute over what type of algorithm should be used to expand the fuel under in-reactor conditions, i.e., large temperature gradients. A large number of qualitative observations on fuel cracking and fuel swelling have been made but very little success has been achieved in quantifying these two phenomena.

The computed results from an analytical model should relate to the observations made during the irradiation or the results of postirradiation examinations. Comparison of the analytical results with experimental observations is an essential test of both the computer code and the mathematical models of the phenomena being simulated. Discrepancies between computed results and observations can be attributed to either uncertainties in the models or poorly characterized experiments. Many computer codes developed to simulate fuel performance are adjusted to agree with specific observations. Such codes should be checked against a wide range of independent data that were not used in the development of the models comprising the code.

Models for calculating gap conductance are often compared with reported values calculated from experimental data. A number of assumptions usually have to be made by the experimenter to calculate a gap conductance from the data. These assumptions lead to an accumulation of error in the estimation of fuel surface temperature from which the temperature difference and

thus the gap conductance is calculated. Most of the reported gap conductance values are based on interpretation of microstructural features observed in the fuel after completion of the irradiation. These microstructural boundaries include the once molten fuel radius, the columnar grain growth radius, and the equiaxed grain growth region. These features represent isotherms that existed in the fuel at some time during operation. Disagreement still exists as to the temperatures associated with the above boundaries. Various experimenters also disagree as to what features define the boundaries and what values to use for UO_2 thermal conductivity. Accordingly, the gap conductances reported by any one experimenter may be internally consistent for his particular test but should not be compared directly with the gap conductances calculated from other experiments with a different set of assumptions. The comparison of predicted values with various reported values is not entirely valid, unless the gap conductances are calculated in a consistent manner for all the experiments.

A more consistent method of comparing an analytical model with experimental data is to compare the model with the variable that was measured in the experiment. These variables usually include fission gas release fractions, microstructural boundaries, and the output of thermocouples located in the fuel. These comparisons are also somewhat limited because very few well-characterized experiments have been published for thermal reactor fuels. Evaluating reports containing experimental data usually reveals relatively large uncertainties in heat ratings, dimensional tolerances, physical characteristics of the fuel, and flux depressions.

Thermal performance codes are important to help assure the continued safe operation of nuclear reactors which includes predicting the outcome of postulated accident situations. However, this code currently does not have the capability to predict fuel rod behavior during or following a reactor transient. GAPCON-THERMAL-2 should not be used for fuel rod design; it is one of several calculational tools for fuel performance and for input to accident analyses.

Included in this report is a summary of the code description and conclusions about its predictions followed by a description of the code and pertinent models. Also included are the results of a parametric study, a comparison of the codes predictions with open literature experimental data, and the code limitations. A listing of the code is given in the User's Guide.[3]

SUMMARY AND CONCLUSIONS

GAPCON-THERMAL-2 is an updated version of GAPCON-THERMAL-1[1] for calculating light-water reactor fuel thermal performance. Close detail is given to the calculation of the fuel-cladding thermal gap conductance. A complete description of the code is presented with emphasis describing the major revisions. These include an added steady-state power history capability, improved fission gas generation model, fuel relocation and densification models, improved gap conductance, and fission gas release models plus the added ability to account for volatile impurities, dished pellets, mixed oxide fuel and molten UO_2. The gas release and relocation models provide as a user option either best estimate or conservative predictions.

The code requires little computer running time; for example, 2 min on a CDC 6600 or UNIVAC 1108 to compute the thermal conditions at 4 axial locations in 3 fuel pins for 12 time steps. This, coupled with small required core storage, should permit rapid multiple runs at low cost to the user.

An evaluation of the code was performed using data from 61 fuel rods or specimens reported from 14 irradiation tests. Predicted temperatures, pressures, and gas release fractions were generally higher than the reported values. Some predictions for a power history case were made (Figure 19) which show the difference between the calculated temperatures and pressures and the measured values.

All the predictions presented here were made using the best estimate fuel relocation and gas release models. The densification model was not used; however, the effect of using the densification model can be seen in the results of the parametric study included in this report.

This version of the code has limitations in such areas as gap closure rate, restructuring rate and associated effects, asymmetric radial heat transfer, axial heat transfer, detailed fuel-cladding mechanical analysis, and power transient conditions.

Finally, the predictions of a code like GAPCON-THERMAL-2 can never be better than the reported or measured experimental values. As better results from instrumented irradiation tests and out-of-pile experiments become available, better predictions by computer codes will be possible.

GENERAL CODE DESCRIPTION

GAPCON-THERMAL-2 calculates the gap conductance, temperatures, pressures and stored thermal energy in a nuclear fuel rod. The code calculates these values for a fuel rod during its operation--following its power history. The current version uses 50 fuel radial nodes and between 1 and 20 axial fuel nodes for as many as 15 time-power steps. The code does not contain a specific fuel cracking model but does calculate a gap closure using an empirical fuel relocation model. Other code limitations are limited restructuring, no asymmetric fuel-cladding heat transfer, no helium sorbtion and no plastic deformation associated with fuel-cladding mechanical interaction. Also, the neutron cross sections used in the code may not be appropriate for all reactor conditions (see Appendix B). A flow sheet showing the order of the calculations is given in Figures 2 and 3; the subroutine call sequence is shown in Figure 4.

The code requires certain input to perform the necessary calculations. As many as 66 different input variables may be used but as few as 10 are sufficient. An alphabetical listing of the input parameters is given in Table 1. At the beginning of a computation all but six of these variables are preset to zero through the subroutine called BLKDAT. The nonzero values of the six variables are shown in Table 1.

Following the preset operation the input values are read and written through the subroutine named INPT. Some preliminary calculations are performed; for example, the cold gap size is calculated from the input fuel and cladding dimensions, the proper fuel and cladding material properties in BLKDAT or from INPT are made available to the main program, GAPCON and the fuel radial flux depression through the subroutine DEPRES or from INPT are determined. The basic initial data (both input and calculated) are written through the subroutine INPUT. The amounts of krypton and xenon fission gases generated are calculated for the end of each time step for each axial node; these values are saved for use later. Subroutine FISSES calculates the appropriate times and powers to be used for the fission gas generation calculations in FISGAS.

The time step sequence begins with time equal to zero days. No iteration on gas release is required for time equal to zero; however, for subsequent time steps the iteration-to-convergence scheme is used within each time step.

The axial node calculations start with the node nearest the coolant inlet. The fission gas plenum is assumed to be near the coolant outlet. Fuel relocation and/or densification, if they are required, are calculated using subroutines RELOC and DENSF, respectively. Next, cladding and fuel radial temperature profiles are calculated using an assumed gap conductance. Cladding temperatures are calculated in GAPCON and fuel temperatures in RTEMP. The cladding and fuel thermal expansions and other radial displacements (strain from internal and external pressures and fuel swelling) are computed. The amount of reactive volatile consumed as well as the amount of krypton and xenon released by the fuel are calculated. The subroutine GASREL performs the latter calculations. The convergence scheme for gap conductance starts each iteration at the calculation for the cladding and fuel temperature.

The gap conductance for each node is calculated using parameters for the fuel, gap, and the cladding. The gap conductance consists of the radial heat transfer by gas conduction, fuel-cladding solid-solid conduction and radiation from the fuel to the cladding. Conductance through the gas is based on work by Lanning and Hann[4] using a model proposed by Ross and Stoute.[5] The fuel and cladding temperature jump distances are calculated by the Lloyd model.[6] The conductance due to solid-solid contact is calculated by a modified Mikic-Todreas model.[7] A concentric fuel-cladding gap containing a homogeneous gas with complete mixing is assumed. An iteration-to-convergence scheme is used to determine the gap conductance. Calculations within this iteration loop include fuel and cladding temperatures, thermal expansions, gap size, gas thermal conductivity, interfacial pressure between fuel and cladding if gap is closed and finally, gap conductance. The iteration scheme checks for similar slopes in the approach to convergence and makes adjustments for either the under-damped, oscillating, or over-damped case. After convergence on gap conductance for one node, identical

calculations are repeated for each axial node. The fuel column axial thermal expansion is calculated taking pellet dishing into effect after the calculation for the last axial node.

Next, the internal gas content based on the gas release from each node is calculated and then compared with the assumed value. An iteration-to-convergence scheme similar to that used with gap conductance is used with the gas release fraction. After convergence of gas release fraction, the final computed results are written by use of subroutine OUTPUT for each axial node; optional output may be obtained for the peak power node and a table from subroutine AXPRNT which summarizes the thermal conditions of axial nodes for the current time step. Subroutine OUTPUT writes fuel stored energy values calculated in subroutines CARL and HCAP. After the output for the final time step is written, the code reads in data for the next problem. A detailed description of the salient models, algorithms, and options in the code are given below.

DETAILED CODE DESCRIPTION

A detailed description of the updated portions of the code is given below. A listing of the code is in the User's Manual.[3]

POWER HISTORY

The power history simulation in the code uses constant power for each finite time step; a maximum of 15 steps is permitted. The powers for the first two times must be greater than zero and all subsequent powers must be greater than or equal to zero. The power history dependent models in the code are gas release, relocation and densification. These models are treated as irreversible phenomena. At any time step other than the first for each axial node the current gas release, relocation and densification values are compared with the values used in the previous time step. Relocation and densification displacements will not decrease if lesser values are subsequently calculated. However, relocation is not permitted to cause fuel-cladding interfacial pressure. The fission gas release algorithm depends on all previous gas release values. For more information on these particular models or algorithms, refer to the particular model description given in this report.

FISSION GAS GENERATION

The calculation of the amount of generated krypton and xenon fission gases is done by a different method than used in GAPCON[8] and GAPCON-THERMAL-1. The mathematical models for fission gas generation in subroutine FISGAS in GAPCON-THERMAL-2 do not require that time start at zero as in earlier versions of the code, but use time increments. This was the main modification in the code that was required to be able to follow a fuel pin power history. Another addition in FISGAS includes the transmutation to plutonium of uranium-238 by resonance absorption of neutrons and subsequent gas production from fissioning of this plutonium. The fissioning of plutonium in the as-fabricated fuel and the subsequent production of krypton and xenon had been in the code. A review by J. L. Carter [9] of Battelle-Northwest of the FISGAS model used in GAPCON and GAPCON-THERMAL-1 and a description of FISGAS in GAPCON-THERMAL-2 are given in Appendix B.

Tables 2 and 3 give thermal yield and thermal cross sections that are used in FISGAS to calculate the fission gas inventory. Note that the values are for 2200 m/sec neutron velocity.

RELOCATION

Relocation as used here is the early-in-life reduction in gap size due to athermal fuel cracking and outward movement. It is postulated that such relocation is a function of fuel power, power cycling, fabricated gap, burnup and/or irradiation time. The accurate measurement and prediction of such relocation is currently not feasible.

During irradiation, ceramic fuels are subjected to thermal stress which can be relieved by fuel strain. The UO_2 can strain by plastic flow at temperatures above ∿1200°C, and by cracking at temperatures below ∿1200°C.[71] The crack volume in solid fuel comes from the fuel-cladding gap. Normal crack healing does not restore the void volume to the gap but moves it toward the fuel centerline. By a series of cracking and crack healing cycles the void volume in the gap can be transferred to the fuel centerline.

The model for the change in the fuel diameter was defined as

$$\left[\alpha\left(\frac{B}{1+B}\right) + \beta P + \gamma\right] GAP/100.$$

Results of linear regression were $\alpha = 40$, $\beta = 0.8$ and $\gamma = 1$ with a correlation coefficient of 0.4 and a residual deviation of 17%. The model, in subroutine RELOC, is based on linear regression analysis of experimental data from the open literature. Some uncertainty exists in the correlation due to both the inaccuracy associated with each datum point and the scatter among the available data. The correlation is based on 84 experimental data points used in an Exxon report[10] plus 33 additional data in a Belgonucleaire report[11] and 16 data points from a CEA report.[12] The model is described as

$$DELGD = \left[40\left(\frac{B}{1+B}\right) + 0.8P + 1\right] GAP/100 \qquad [1]$$

$$\text{with } B = EXP\ (-4 + BURNUP^{1/4}) \qquad [2]$$

where DELGD is the increase in fuel diameter (inches) due to relocation at a power, P, (kW/ft) with an as-fabricated cold gap, GAP, (inches) for a burnup, BURNUP, (MWd/MTM).

The conservative model which gives less relocation is DELGD = DELGD - 0.28 GAP using the standard deviation of 17%. The 95% upper bound for a normal distribution for a one-sided test is $1.65\sigma = 0.28$. This relocation correlation can be improved as better experimental data become available.

One of the better relocation correlations based on a consistent set of experimental irradiation data was presented by Dutt, Baker and Chastain at HEDL.[13] Their correlation was developed using cold gap measurements from the ceramographic cross sections of $\sim UO_2$ - 25 wt% PuO_2 fuel irradiated in EBR-II. The experimental data used by them showed a minimum 0.0009-inch closure for $\sim$1/4 inch diameter fuel with a fabricated 0.0051-inch gap; the maximum was 0.0075-inch with similar fuel and a 0.010-inch fabricated gap. The Dutt et al. correlation gives increasing gap closure with increasing cold gap, fuel power, power cycles and burnup; the correlation predicts within $\sim\pm$1 mil the range of the data. The HEDL experimental data were not used in correlating the model used in GAPCON-THERMAL-2 because of the differences in fuel size and composition, surface temperatures and power densities.

The algorithm associated with our fuel relocation relates to the fuel-cladding gap. For each axial node at each time step the relocation is calculated. If the calculated amount at any time step is less than the amount used during the previous time step, the current time step uses the larger amount. However, relocation is not permitted to cause fuel-cladding interfacial pressure, i.e., relocation is reduced until the interfacial pressure becomes zero or until relocation is zero. This algorithm is not an accurate representation of true fuel behavior, however, to provide a better algorithm the uncertainties in relocation and contact conductance data must be reduced.

DENSIFICATION

The densification model in GAPCON-THERMAL-2, developed by R. O. Meyer[14] calculates the reduction of the fuel radius as a function of irradiation time and differential density. The radial shrinkage, DELPI, is calculated as

$$\text{DELPI} = -\left\{ M \ln[\text{Burnup}] + B \right\} \text{DFS} \cdot \rho/4 \qquad [3]$$

where the used burnup is a maximum of 2000 MWd/MTM, and

$B = -1.6094M$ if the fuel starting density is less than 92% T.D.

otherwise [4]

$B = -2.996M.$

And, $M = \Delta\rho/(7.601-1.6094)$ if the starting density is less than 92% T.D.

otherwise,

$M = \Delta\rho/(7.601-2.996)$

where, $\Delta\rho$ is the difference in fuel density from the as-fabricated and the re-sintered fuel. If burnup is less than 20 then DELPI = 0.

Because no radial expansion is permitted, if the calculated value is greater than zero it is set equal to zero. The algorithm in the code assumes densification is irreversible; the maximum radial reduction calculated through the current time step is always used for calculations in the current time step.

CONDUCTANCE CALCULATIONS

The gap conductance is composed of three terms:

$$h_{gap} = h_{solid} + h_{gas} + h_{radiation} \qquad [5]$$

h_{solid}	h_{gas}	$h_{radiation}$
conductance through points of contact	conductance through the gas	conductance by radiation from fuel to cladding

The first two terms have been modified in GAPCON-THERMAL-2 from GAPCON-THERMAL-1. The criterion for contact has also been modified. (The first term contributes only after contact has occurred if the contact is not due to relocation). These modifications are discussed below. Refer to Reference 4 for their derivation.

The Model for h_{gas}, Before and After Contact Occurs

In GAPCON-THERMAL-1, the model for h_{gas} before contact was

$$h_{gas} = 12\ k_{gas}/(th + g_1 + g_2) \qquad [6]$$

after contact,

$$h_{gas} = 12k_{gas}/(C(R_1+R_2) + g_1 + g_2) = 12\ k_{gas}/\Delta X \qquad [7,8]$$

The criterion for contact was $th \leq C(R_1+R_2)$ [9]

in the above equations, for h_{gas} in Btu/hr-ft^2-°F,

k_{gas} = thermal conductivity of interfacial gas (Btu/hr-ft-°F) (calculated by Chapman-Enscog theory[15])

th = radial gap thickness (inches)

R_1, R_2 = mean surface roughness of fuel and clad (inches)

g_1, g_2 = the temperature jump distance at the fuel and at the clad (inches)

C = a dimensionless constant dependent on fuel-clad contact pressure P. The dependence of C on P was deduced from the Ross-Stoute data to be as follows:

$C = 1.98 \exp(-0.000088\ P)$, P in psi

ΔX = effective gap width at contact (inches)

The quantity $\Delta X = k_{gas}/h_{gas}$ was deduced from the Ross-Stoute measurements of h_{gas} in various gases. A calculated value of ΔX for each experimental value was computed from the model in Equation [8], using the values for contact pressure, gas temperature and surface roughness given by Ross and Stoute.[5] The measured and calculated values were then compared by linear regression. The result, i.e., the "line of best fit" was as follows:

$$\Delta X_{meas.} = 1.8\ \Delta X_{calc.} - 0.000005 \text{ (inches)} \qquad [10]$$

In GAPCON-THERMAL-2, this regression result was used in calculating h_{gas} after contact has occurred. Thus, we write

$$h_{gas} = k_{gas}/\Delta X_{regression} = k_{gas}/(1.8(C(R_1+R_2) + g_1 + g_2) - 0.000005, \qquad [11]$$

but it is necessary for h_{gas} to remain a continuous function from non-contact to contact (i.e., as th decreases until contact occurs). Thus the model for h_{gas} before contact and the criterion for contact have to be altered. The simplest alteration is to change the model before contact to:

$$h_{gas} = k_{gas}/(th + 1.8\ (g_1+g_2)) \qquad [12]$$

and change the criterion for contact to:

$$th \leq 1.8C\ (R_1+R_2) = 3.6\ (R_1+R_2) \qquad [13]$$

With these changes, h_{gas} is still not completely continuous because of the constant -0.000005 which occurs in the model after contact. But this slight discontinuity does not affect convergence.

The new criterion for contact effectively states that contact occurs when the gap narrows to 3.6 times the sum of the roughness. The waviness and mismatch of the fuel-clad interface and the nonuniformity of their peak heights cause some contact before the gap completely closes.

The Calculation of Temperature Jump Distance

In GAPCON-THERMAL-2, temperature jump distances are calculated from the Lloyd equation[6]

$$g_i = \frac{k_{gas} \times 6.8 \times 10^{-5}\ \text{(inches)}}{\sum_j \frac{a_j P_j}{M_j T_i}} \qquad \begin{array}{l} i = 1,2 \\ j = 1,\ldots N \end{array} \qquad [14]$$

where

P_j = partial pressure of the jth gas (psi),

M_j = molecular weight of the jth gas,

a_j = the accommodation coefficient of the jth gas (a function of temperature)

T_i = temperature at the ith interface (°K) before temperature jump.

The Lloyd equation replaces a different equation used in GAPCON-THERMAL-1, which did not include accommodation coefficients explicitly. Measurements by Ullman et al.[16] for xenon and helium on UO_2 show that accommodation coefficients do vary between gas species and vary significantly with temperature. Therefore the Lloyd equation, which explicitly incorporates accommodation coefficients into the calculation of the temperature jump distance, was chosen.

The temperature dependence of accommodation coefficient, a, for xenon and helium are taken directly from the Ullman data in the form:

$$a_{He} = 0.425 - 2.3 \times 10^{-4} T, \text{ T in °K} \qquad [15]$$

$$a_{Xe} = 0.749 - 2.5 \times 10^{-4} T \qquad [16]$$

For a gas other than xenon and helium and for the mixed gases, a_j, is estimated from a linear interpolation based on molecular weight (M_j):

$$a_j = (a_{Xe} - a_{He}) \frac{(M_j - 4)}{128} + a_{He} \qquad [17]$$

The Calculation of h_{solid}

The term h_{solid} is calculated by a modification of the Mikic-Todreas model[7] defined as

$$h_{solid} = \frac{5k_m}{(R_1^2 + R_2^2)^{1/2}} \left(\frac{P}{H}\right)^n \left(\frac{R_1}{\lambda_1}\right) \qquad [18]$$

where

$$k_m = \frac{2k_1k_2}{k_1+k_2} \qquad [19]$$

k_1, k_2 are conductivities of fuel and clad, respectively, in Btu/hr-ft - °F,

$\left(R_1/\lambda_1\right)$ is a dimensionless ratio of fuel surface roughness and wavelength $R_1 R_2$ are in inches.

$\left(\frac{P}{H}\right)$ is the dimensionless ratio of interfacial pressure to Meyer hardness of the cladding,

$n = 1.0$ for (P/H) above 0.01,

$n = 0.5$ for (P/H) below 0.0001, and

$\left(\frac{P}{H}\right)^n = 0.01$ for $0.0001 < (P/H) < 0.01$.

Note that $\left(\frac{R_1}{\lambda_1}\right)$ is estimated by GAPCON-THERMAL-2 as

$$\left(\frac{R_1}{\lambda_1}\right) = \exp\left(0.5825 \ln R_1 - 5.738\right) \qquad [20]$$

where R_1, the mean fuel surface roughness is in microinches.

This equation [20], is a correlation of measurements of surface profiles by Dean[17] and Rapier, Jones, and McIntosh.[18]

The model, [18], ties together the data of Rapier[18] and Ross and Stoute[5] and fits the highly scattered data of Ross and Stoute nearly as well in the least-squares sense as the original Ross and Stoute model.

Overall Effect on Conductance

The net effect of the replacement of previous models for h_{gas} and h_{solid} with those just described is to lower the total gap conductance at contact by 20 to 30%, depending on the surface roughness and the gas mixtures involved. Before contact the net effect is negligible; see Figure 5 which shows a comparison of the GAPCON-THERMAL-1 and 2 calculated gap conductances.

GAS RELEASE

High temperature (>1200°C) gas release from UO_2 fuel is an important consideration in steady-state reactor safety calculations because of its effect on the fuel-to-cladding gap conductance and thus fuel temperatures

and fuel rod internal gas pressures. Conservative and best-estimate correlations for gas release are needed to define gap conductance and internal pressure values in the rod before accident calculations can be performed. Several methods for calculating the high temperature fission gas release have been proposed[19-25] but the results vary widely. However, most investigators agree that high temperature gas release is a nonlinear phenomenon which is dependent upon local conditions in the fuel, with fuel temperature being the primary controlling parameter. The large uncertainties that are inherent in estimating fuel temperatures often preclude a reliable correlation for gas release. These uncertainties in determining fuel temperatures, plus the inherent differences in the models themselves, account for the lack of agreement between previously proposed models.

Low temperature (<1200°C) gas release from fuel with burnups of less than 20,000 MWd/MTM is typically in the range of 2% or lower. The release from low temperature fuel is not as significant as the high temperature release because the gap conductance and internal rod pressures change very little when gas release is on the order of 2%. A low temperature release model is included to extend gas release predictions below temperatures of 1200°C.

High and low temperature models included in GAPCON-THERMAL-2 were developed[26] to provide an improved method for predicting gas release from UO_2 fuel. The high-temperature release model was fit to a consistent and well-characterized set of 45 data points using a multiple-linear regression code. The low temperature release model is one developed by Bellamy and Rich[27] and is compatible with the high-temperature model (i.e., extends gas release predictions to temperatures below 1200°C where the high-temperature model is not applicable).

To reduce the variability in the high temperature gas release data the following criteria for the selection of data were used:

- Stoichiometric UO_2 (O/M 2.00 ± 0.005)

- A relatively constant power history--maximum power over the life of a fuel rod could not be more than 15% greater than the time average power.
- Short fuel columns and relatively flat axial power distributions--axial $\frac{\text{peak}}{\text{avg.}}$ power ≤ 1.15.
- Fuel temperatures were either measured or could be inferred from microstructural changes.

A review of data from 65 sources provided 18 sources for further evaluation. Data from 7 sources[28-33] (Table 4) met the criteria listed above and supplied the 45 data points used for fitting the model. The range of heat ratings, fuel centerline temperatures and release fractions are also listed in Table 4.

The high temperature release model is based on experimental evidence supplied by Lewis[19,34] and other investigators[28,31] and is divided into three regions of gas release:

$$F = AX_1 + BX_2 + CX_3 \qquad [21]$$

where

F = fraction of gas released

X_1 = fractional amount of fission gas produced in the temperature region 1200 to 1400°C

X_2 = fractional amount of fission gas produced in the temperature region 1400 to 1700°C (region of equiaxed grain growth)

X_3 = fractional amount of fission gas produced in the temperature region 1700°C to 2790°C.

A = fraction of gas released from region X_1

B = fraction of gas released from region X_2

C = fraction of gas released from region X_3.

The fractional amount of gas produced in each of these regions (X_1, X_2 and X_3) is estimated by taking the ratio of the cross-sectional area between the temperatures that bound the region to the total cross-sectional area of the pellet. The effects of flux depression are also included. The cross-sectional areas of each temperature region are obtained from the radial temperature profiles.

Using a multiple linear regression code, the model was fit to the reduced data (X_1, X_2 and X_3) to obtain the coefficients A, B, and C associated with each temperature region. The X_1 and X_2 variables are linearly dependent on each other (i.e., $X_1 = GX_2$) and regressing X_1 against X_2 gives G = 0.727. This dependency arises from the fact that if two isotherms, such as the 1700 and 1400°C boundaries used to obtain X_2, are known within the radial cross section of the fuel, then any other temperatures and their location can be defined. The regression analysis was performed with the terms X_2 and X_3 to obtain the coefficients B' = 0.177 and C = 0.807 with a correlation coefficient of 0.980 and a residual standard deviation of 0.047 in fraction of gas released. The coefficient B' obtained in the regression analysis is a combination of the A and B coefficients of our model. Since X_1 can be related in terms of X_2 the model can be expressed in the following manner:

$$F = A\,(BX_2) + BX_2 + CX_3 \qquad [22]$$

The coefficient B' obtained from regression analysis can be expressed by

$$B' = AG + B \qquad [23]$$

and since B' = 0.177 and G = 0.727 a value for either A or B can be chosen on the basis of previous experimental evidence to get the other coefficient. Experiments have been conducted in which small cores of fuel were ultrasonically drilled at various distances from the centerline of the pellet to determine the concentration of retained fission gas across the pellet radius. These experiments indicate that less than 10% of the gas produced in the 1200 to 1400°C range (X_1) and 10 to 40% in the region of equiaxed grain growth (X_2) is released. To be consistent with this evidence, 5% release was

selected for region X_1 which yields 14.1% for the equiaxed region (i.e., $B = B' - A \cdot G = 0.177 - 0.05\ (0.727) = 0.141$) to obtain the best estimate high temperature model:

$$F = 0.051\ X_1 + 0.141\ X_2 + 0.807\ X_3 \qquad [24]$$

An attempt was also made to define the effects of density and burnup on gas release, however a statistical treatment of the data found no such dependency over the range of the data--91.3 → 98% TD and 400 → 18,300 MWd/MTM, respectively.

Predicted percent release as determined from the model is compared with the experimental data in Figure 6. The upper dashed line in this figure is the upper 95% confidence limit of our data which can be represented with the following relationship:

$$F = 0.050\ X_1 + 0.141\ X_2 + 0.807\ X_3 + 1.68\ (0.002112 + 0.0052\ X_2^2 - 0.00269\ X_2\ X_3 + 0.00217\ X_3^2)^{1/2} \qquad [25]$$

where F, X_1, X_2 and X_3 are the same variables used in the best estimate model.

The statistical significance of this upper limit is that there is 95% confidence that future gas release data, which meet the criteria we have used in selecting data, will lie below this line. This 95% upper limit equation is used as the conservative estimate for gas release in the code (see the input variable IGAS).

A comparison of the best estimate model to models that have been proposed by other investigators[19,23] is shown in Figures 7 and 8. Figure 7 shows the data and the relationship Hoffman and Coplin used in their volume-average temperature model. Also included is the proposed high-temperature model expressed in terms of volume-average temperature, which was accomplished by selecting a typical commercial BWR fuel rod[a] and varying the

(a) Changing the fuel rod design will shift the curve represented by the model. In most cases the shift is small for a particular reactor type because fuel rod designs are usually similar.

power ratings while holding gap conductance constant at 1000 Btu/hr-ft^2-°F to assure the same fuel surface temperature as a function of power. The resulting temperature distributions were used to predict a value for gas release from the model and to calculate a volume-average fuel temperature to be used in plotting the curve for the high-temperature model (Figure 7). This figure indicates that the scatter in the data used by Hoffman and Coplin is much larger than the scatter in the data used for the model developed here, as represented by the 95% confidence band. The 95% confidence band in Figure 8 bounds 95% of our data. This comparison provides additional support for the fact that the parameters controlled in the selection of the data do indeed lead to substantial amounts of variance between gas-release data. The relationship used here is also less conservative for volume-average fuel temperatures between 900 and 1524°C, which is the operating range of the peak power rods within most commercial LWRs. For example, at a volume-average temperature of 1200°C (fuel operating at ∿13 kW/ft) the Hoffman and Coplin model would predict a 24% increase while the best estimate model would predict 13%.

Figure 8 shows a comparison of the model with the Lewis[19] model in terms of a volume-average temperature for a typical BWR fuel design. As seen here, the Lewis model is much more conservative. This is not too surprising since Lewis intended the model to be conservative.

The low-temperature gas release model proposed by Bellamy and Rich[27] was modified for use in GAPCON-THERMAL-2. The Bellamy and Rich model was selected because it was the only one found in the literature that supplied and adequately described data applicable to LWR UO_2 fuel. The model expresses low-temperature gas release in terms of the effective surface-to-volume ratio of the fuel, the fission rate, and the irradiation time in the following manner:

$$F = \frac{S}{V} \ell \left[\frac{3}{4} - \frac{3}{\nu f t} \left\{ 1 - \exp\left(- \frac{1}{4} \nu f t\right)\right\}\right] \qquad [26]$$

where

F = fraction of gas release

S/V (%TD,BU) = effective surface-to-volume ratio of the fuel (a function of density and burnup), (cm^{-1})

ℓ = recoil range of fission fragment (7×10^{-4} cm)

ν = volume of fuel ejected from the fuel surface by "knock-out" (2×10^{-21} cm^3)

f = fission rate, (fissions/cm^3/sec)

t = irradiation time, (sec)

This relationship was derived by Bellamy and Rich from gas-release data obtained from fuel rods over a wide range of burnups (7,000-43,000 MWd/MTM). Fuel centerline temperatures were less than 1250°C for all the data. Their data show a marked increase in gas release for burnups greater than 26,000 MWd/MTM. The increase is believed to arise partly from the interconnection of grain boundary gas bubbles and partly from the fracture under thermal stress of grain boundaries weakened by gas bubbles which increases the effective surface area of the fuel. This behavior is substantiated by the appearance of fuel structures at high burnups which show extensive intergranular porosity and grain boundary cracking. A plot of the effective surface-to-volume ratios, as determined from the data and equation of Bellamy and Rich for low temperature gas release, is shown in Figure 9. The data in Figure 9 are from fuel with an as-manufactured density of 98% TD. The increase in $\frac{S}{V}$ fits an exponential function fairly well for burnups greater than 17,000 MWd/MTM by the following relationship:

$$\frac{S}{V} \text{ (at burnup X)} = \frac{S}{V} \text{ (initial) } 0.1938 \exp (0.0301X) \qquad [27]$$

where

$\frac{S}{V}$ (initial) = initial surface-to-volume ratio a function of the fuel density.

X = burnup in atom percent

The functional relationship given in Figure 10 for the $\frac{S}{V}$ (initial) ratio in terms of the fuel as-manufactured theoretical density was taken from Lewis.[35] By substituting the relationship for the surface-to-volume ratio as a function of burnup (Equation 27) into Equation 26, results from the low-temperature release model can be compared with the data of Bellamy and Rich, as shown in Figure 11. The model predictions agree very well with this set of data. No attempt was made to correlate the low-temperature release model to a large volume of data as was done with the high-temperature release model. This approach makes the accuracy of the model somewhat uncertain; however, the model adequately describes low-temperature gas release to within ±1% release.

If any molten fuel is predicted by the code, 100% of all the generated fission gases is assumed to be released from that molten fuel.

The code uses a fission gas release algorithm which was developed by Notley[77] and based on experimental data from Soulhier and Notley.[83] Release fractions for each axial node are calculated for each time step and these are used to calculate the total fission gas release up through the current time step. The algorithm assumes that later-in-life temperature increases will eliminate any previous history of lower release fractions and thus uses the current release fraction. A time interval where release fractions have decreased will use the current (lower) release fraction only to calculate gas release during the current time step and which will then be added to the releases calculated in previous steps.

VOLATILE IMPURITIES

A study was made on the fuel volatile impurity release rates and the subsequent reaction rates of these gases with the cladding.[36] The conclusions of the study are outlined below.

- Essentially all the volatile impurities in the fuel are released above 1000°C.

- The release rates are rapid, (nearly total release within 30 min).
- Sorbed gas content in oxide fuel is typically 0.01 to 0.05 cm^3/g.
- Sorbed gas composition varies with pellet sintering and storage atmospheres; however, the composition still varies significantly with constant sintering and storage atmospheres.
- The most common sorbed gas constituents are H_2, H_2O, O_2, N_2, CO and CO_2.
- All H_2, H_2O and O_2 in a typical BWR fuel rod react within a day.
- Sparse reaction rate data for N_2, CO and CO_2 indicate each of these gases will react in a typical BWR fuel rod with zircaloy cladding within 40 days; however, the uncertainty in these data are large, i.e., a factor of 2 uncertainty in the reaction rates.
- Puncturing fuel rods after $\sim$ 60 days full-power operation and analyzing the extracted gases resulted in trace, $< 10^{-4}$ cm^3/g, quantities of sorbed gas.[37]

The results of this study were used in GAPCON-THERMAL-2 to model the behavior of hydrogen, moisture, nitrogen, CO_2 and CO.

The total quantity of sorbed gas is input by the variable S in units of cubic centimeters of gas at standard pressure and temperature per gram of fuel. The mole fraction of each gas H_2 and H_2O, N_2, and CO_2 and CO are input by the variables XH, XN, and XCO, respectively. The code does not distinguish between H_2 and H_2O nor between CO_2 and CO because it was experimentally difficult to determine in what form these gases existed under fuel operating conditions. All sorbed gas is released instantaneously.

The hydrogen and moisture contribution, XH, is assumed to react with the cladding immediately upon release which is consistent yet conservative with the conclusions stated above. However, if the user wants to assume that the H_2 does not react with the clad, the user needs to input NOH $\neq$ 0.

The total amounts of nitrogen and carbon monoxide that will react with the zircaloy cladding are calculated and subtracted from the amount initially present. The remaining amount is included in subsequent calculations for gap conductance and fuel pin internal pressure. The reaction equations are given below.

The reaction inverse temperature,

$$RTCIK = 1/[(TCI - 32)1.8 + 273] \quad [28]$$

where, TCI = cladding inside temperature, °F

The moles of nitrogen and carbon monoxide gas capable of reacting for any axial node are:

$$MREACN = GRECN/28.02 \quad [29]$$

and,

$$MREACO = GRECO/28.01 \quad [30]$$

where,

$$GRECN = \sqrt{REACN}\ (T) \quad (Z4) \quad [31]$$

$$GRECO = [REACO\ (T) + C] \quad (Z4) \quad [32]$$

T = time, sec

C = 4.2×10^{-5} g/cm^2

Z4 = cladding inside surface area for the axial node, cm^2

REACN = reaction rate constant for N_2 which experimental evidence indicates is relatively constant at 0.667×10^{-15} (g/cm^2)^2-sec over the temperature range of interest (500-300°C).

REACO = reaction rate constant for CO which is dependent on the inverse temperature RTCIK, defined above.

The values for <u>REACO</u>, the reaction rate constant, are determined by a linear interpolation of the following set of data:

Reaction Temperature °C	Inverse Temperature $°K^{-1}$	Reaction Rate Constant for Carbon Monoxide g/cm^2-sec
255	1.876×10^{-3}	2.09×10^{-7}
311	1.699×10^{-3}	3.80×10^{-7}
340	1.622×10^{-3}	4.93×10^{-7}
387	1.513×10^{-3}	7.21×10^{-7}
425	1.429×10^{-3}	9.48×10^{-7}

DISHED PELLETS AND FUEL AXIAL THERMAL EXPANSION

In order to improve pin pressure calculations, axial expansion of the fuel into available void volumes was included in GAPCON-THERMAL-2. Axial expansion is computed from thermal expansion and fission product swelling of each axial segment in the fuel column. Fuel axial thermal expansion into the plenum is computed using the Conway, Fincel and Hein[38] coefficient of linear expansion and either the fuel plastic temperature or the temperature at the edge of the dish. The plastic temperature is used if pellet dishing is not present or if the temperature at the edge of the dish is greater than the plastic temperature. Fuel that is above the plastic temperature is assumed to flow into available local void volume (dish, porosity, etc.). The plastic temperature can be input into the code by the user with the variable name TPLAS (See Appendix A), otherwise the code assumes TPLAS = 1200°C.[71]

The fuel swelling contribution to expansion into the plenum is assumed to be one-third of the volume increase predicted from the Geithoff, Kersten and Bummerer[39] model for fission product swelling.

Fuel expansion into the dish volume occurs by thermal expansion and fuel swelling based on the Geithoff model. Thermal expansion into the dish is computed using the Conway, Fincel and Hein coefficient for thermal expansion,[38] the volume average temperature of the dish, and the length of the axial fuel node minus the depth of the dish.

The GAPCON-THERMAL-1 code did not consider fuel dishing, consequently, in an effort to improve the accuracy of the calculation of internal pin

pressures, a simple algorithm for pellet dishing was included in GAPCON-THERMAL-2. Dish volumes are approximated by a void in the form of a short right cylinder as shown in Figure 12 as the hatched area, with the radius of the dish being the radius of the cylinder. The code considers one dish per axial segment. The following information has to be input into the code if pellet dishing is desired, see Appendix A for definition of input variables.

(a) The amount of dish volume available in the fuel column is to be input in terms of percent fuel column volume (PRCDH).

Example:

PRCDH = (total dish volume/total fuel columm volume) x 100

(b) The radius of the dish (RADS).

The dish volumes at operating conditions (includes thermal expansion into the dish) affect the pin pressure like the other void volumes (plenum and fuel-to-cladding gap). A V_{local}/T_{local} relationship is used where T_{local} is the volumetric average temperature of the dish. If the calculated dish volumes become negative, the volumes are set equal to zero.

RECYCLE MIXED-OXIDE FUEL

The properties in the code for recycle mixed-oxide fuel below ~5 wt% PuO_2 are the same as those for UO_2 except for theoretical density, thermal conductivity and melting (solidus) temperature.[40]

- the PuO_2 theoretical density is 11.46 g/cm^3; the mixed-oxide theoretical density is the weighted fraction of this value and 10.96 for the UO_2.
- the thermal conductivity of recycle mixed-oxide equals the UO_2, Lyons et al.,[41,42] values reduced by ~1% per percentage PuO_2 up to and including 5 wt% PuO_2.
- the melting temperature, T_m, is equal to the UO_2 value reduced 5°C per percentage PuO_2 and further reduced 32°C per 10,000 MWd/MTM burnup.

It should be noted that DEPRES should not be used for flux depression calculations for mixed-oxide fuels, these values should be provided by the user.

MODULAR CODE

This version of GAPCON-THERMAL is programmed so that calculations for most of the fuel models are separated into discrete subroutine packages. It is hoped that with this feature, calculational models different than those used in the code can easily be replaced with a user's model, thereby eliminating the need to rewrite complete codes to essentially duplicate thermal performance calculations. The following list briefly identifies each subroutine:

INPT - provides the input values
DEPRES - calculates radial flux depression
INPOUT - writes input values
FISSES - controls the time and power steps for the fission gas calculations
POWDIS - calculates power for fission gas, cladding and fuel temperatures
FISGAS - calculates the generated fission gas
RELOC - calculates radial fuel relocation
DENSF - calculates radial fuel densification
RTEMP - calculates radial fuel temperature profile
EXPAND - calculates radial fuel thermal expansion
GASREL - calculates gas release rate
OUTPUT - writes pertinent nodal information
HCAP - calculates volumetric-averaged fuel heat capacity
CARL - calculates fuel rod stored energy
AXPRNT - writes summary of pertinent nodal information.
BLKDAT - contains the data used by the program
HTCW - calculates water coolant film coefficient
MOVEAA - transforms a one dimensional matrix
MOVEKA - fills a one dimensional matrix with a constant
TCOR - Function - calculates LWR fuel thermal conductivity
TEPP - Function - does linear interpolation with two arrays
TERP - Function - does linear interpolation with one array
OMEXP - Function defined as 1 - EXP (-X)
CORROS - calculates Zr oxide thickness from coolant reaction

INTERNATIONAL SYSTEM OF UNITS

This version of the code was modified to provide answers in the International System of Units (SI units) as well as in somewhat conventional English units. The ASTM Metric Practice Guide, E 380 72E was used for the conversion of units. Output which summarizes the information for all the axial nodes also includes a set of equations for unit conversion.

OPTIONS

The code has several models to help describe fuel behavior, but at certain times determined by the user some of these models may not be appropriate. In addition, it is sometimes useful to compare final calculated results with and without the use of a certain model. For these reasons there are options in the code that permit the user to easily switch on or off a particular model. These models that can be activated by the user are listed on Page 32 along with the names of the subroutines in which they reside, and the names and values of the control switch to activate and deactivate a computation. One additional option was added using variable IT which will permit input as burnup values in place of irradiation time in days. For additional details see Appendix A.

FUEL MELTING

This version of the code includes a model to accommodate analyses involving molten fuel. Based on the fuel melting temperature the melt radius is calculated using the radial temperature profile. Next the volume of molten fuel is calculated followed by the volume of porosity available from the melt assuming the molten fuel is 100% dense. The fuel expansion due to the solid-to-liquid transformation is determined using 9.6% $\Delta v/v$ for the phase change.[72] Finally, the fuel radial and axial expansion due to the liquid fuel is calculated assuming isotropic expansion of the fuel after the porosity has been filled. The gas release model assumes 100% release from the molten fuel of the generated fission gases.

MODELS UNALTERED FROM GAPCON-THERMAL-1

A number of models used in GAPCON-THERMAL-2 are from GAPCON-THERMAL-1. These models are listed below and their descriptions are given in Appendix C.

- Fuel thermal conductivity, porosity correction, thermal expansion, restructuring, swelling, stored thermal energy and flux depression
- Cladding properties, elastic deflection and creep
- Gas pressure and conductivity
- Power and coolant temperature profiles
- Axial segments for analyzing power profiles
- Radiation heat transfer
- Radial temperatures
- Water heat transfer film coefficient.
- Linear interpolation of data

LISTING OF OPTIONS IN GAPCON-THERMAL-2

Model	Subroutine Name	Switch Name	Switch Value Activate	To Deactivate
Cladding creep	GAPCON	ICREEP	>0	≤0
Cladding strain due to coolant and internal gas pressures	GAPCON	ICDF	≠0	0
Best Estimate - Conservative - Gas Release	GASREL	IGAS	0 ≠0	
Peak - Average - Input Power	GAPCON	IPEAK	0 ≠0	
Stored Energy from HCAP and CARL	OUTPUT	ISTOR	≠0	0
Conservative - Best Estimate - Fuel Relocation	RELOC	IRELOC	<0 >0	0
Alter print of flux depression values	GAPCON	IRL	>0	≤0
Fuel Densification	DENSF	IDENSF	≠0	0
Retard gas release by one time step	GAPCON	IRELSE	≠0	0
Zirconium - Stainless Steel - Special - Cladding	GAPCON	NCLAD	0 <0 >0	
Zr-2 - Zr-4 - Zirconium Cladding	GAPCON	ZCLAD	≤0. >0.	NCLAD ≠0
UO_2 - Recycle Mixed Oxide - Special - Fuel Thermal Conductivity	GAPCON	NFUEL	0 <0 >0	
Calculate - Special - Flux Depression	DEPRES	NFLUX	0 >0	<0
Hydrogen gas effects included	GAPCON	NOH	≠0	0
Supplied axial power profiles for each and every time step	GAPCON	NPRFIL	≠0	0
Set inside cladding temperature to local coolant temperature	GAPCON	KOOL	>0	≤0
Water - Special - Coolant Film Coefficient	HTCW GAPCON	SIGHF	≤0 >0	
Fuel Restructuring	GAPCON	FRSIN	FRSIN>FRDEN	FRSIN≤FRDEN

Note: The term "special" as used in this list designates an item supplied by the user.

PARAMETRIC STUDY

A parametric study was performed to determine the effect of different input parameters and options on calculated fuel centerline temperature and internal gas pressure. The input values for the base case are shown in Table 5 and include 94% T.D. fuel with a 0.477-inch diameter, clad in a Zr-2 tube with a fuel-clad diametral gap of 0.012 inches. The 12-ft long fuel column was divided analytically into 10 equal axial segments. The relative axial power generation varied from 0.35 near the rod ends to 1.19 near the column center. Seven equal time steps were used beginning at 0 days and ending after 360 days. The power history consisted of startup at 14.5 kW/ft followed by 60 days each at 14.5, 13.5, 0.0, 11.0, 17.0, and 13.0 kW/ft. The calculated fuel centerline temperatures and rod internal gas pressures for this base case are shown graphically in Figure 13a. The predicted fuel centerline temperature at beginning of life was 2100°C then 2560, 2570, 285, 2400, 2810, and 2614°C after each successive 60-day period. The corresponding rod internal gas pressures calculated were 38 psi at beginning-of-life then 144, 270, 162, 346, 575 and 698 psi. These data are shown as dots (for temperatures) and circles (for pressures) on Figure 13a.

The 20 plots show the effect of varying one or more input parameters. For example, Figure 13b shows the dashed lines resulting directly from Figure 13a. The calculated data points resulting when fuel restructuring to 96.5% T.D. is assumed are shown as dots for fuel centerline temperatures and circles for rod internal gas pressures. Small changes relative to the base case were calculated. For this example after 360 days irradiation the fuel peak temperature was calculated to be ∿50C° lower and rod internal gas pressure ∿10 psi higher relative to the base case. These numerical differences for the fuel restructuring case as well as the other parametric cases are given in Table 6.

Another example showing the effect of allowing fuel relocation, using the best estimate model in the code, is illustrated in Figure 13d.

Again, the dashed lines reproduced from Figure 13a represent the base case results while the dots and circles give the calculated temperatures and pressures during the power history with fuel relocation. Permitting relocation decreased the fuel temperatures and the pin pressures. At end-of-life the resultant values were ∿800°C and ∿450 psi lower for the case with best estimate relocation relative to the base case (with no relocation). The interaction effects of two parameters are illustrated by comparing the results from: (a) the best estimate relocation and (b) densification to 97% T.D. with (c) best estimate relocation and densification. Table 8 shows that at end of life (a) above reduces the peak fuel temperature and pin pressure 800°C and 450 psi while (b) increases these 300°C and 110 psi; however, these combined effects result in a 30°C and 10 psi increase which are all relative to the base case (with no relocation or densification).

CODE VERIFICATION EVALUATION

This section presents the results of the GAPCON-THERMAL-2 predictions of reported experimental data from 61 fuel rods or specimens from 14 irradiation tests. The predictions are made using the best estimate values from the fuel relocation and fission gas release models. Also certain assumptions were made by us in order to provide sufficient input to the code. The actual input values for some of the predictions are given in Appendix D.

Essentially all of the reported irradiation tests were taken as potential candidates for code evaluation. However, in reports where much significant data were absent, the tests were not used. Detailed power history reports on highly instrumented fuel assemblies such as HPR-129[29] were rare. The type of input used by the code is shown in Table 1. The following irradiation tests or reports were used in the code evaluation:

Test Identification		Reference
IFA-116, IFA-117	HPR-129	(29)
IFA-130, IFA-131	---	(73)
Capsule I and II	WCAP 2923	(74)
Samples	HPR-80	(76)
Rods	AECL-2662	(30)
Rods	AECL-1676	(32)
Samples and Rods	AECL-2588	(78)
IFA-3, 4, 10	AE-318	(75,82)
Rods	CEA-R-3358	(33)

Reference 29 presents data from two 8-rod fuel assemblies, IFA-116 and IFA-117. Reported irradiation data included assembly power, periodic internal gas pressures, and fuel centerline temperatures in the pins. Also provided was information needed to calculate individual rod powers along with rod average burnups and the assembly axial power profiles for various times during the irradiation.

A limited effort was made to completely model the power history of the rods in these assemblies because of the large number of required constant power time steps and the uncertainties associated with obtaining the requisite data for each of these steps from the graphs in Reference 29. Instead, specific data at 12 times were used to simulate the actual irradiation history. See Appendix D for the complete listing of input values to the code for these irradiation tests. Table 7 gives the power histories for these two fuel assemblies.

Data for these times for rods 1 and 5 in IFA-116 and 1, 3, 5 and 6 in IFA-117 included rod mean burnup and assembly axial power ratio in addition to a table for finding the fractional rod power for the various axial power ratios.

Rod powers were calculated from the assembly power for each of the 12 given times. The rod average linear heat ratings were calculated using the active length of fuel. The duration of each time step for the constant power step was calculated using the rod average burnup and the previously mentioned rod power. The input to the code (given in Appendix D) includes fabrication parameters, rod power and time at power. Code input for rod 5 of IFA-116 included time-dependent axial power profiles. These profiles were calculated for each of the 12 time steps using the given axial power ratio, TG1/TG2, where TG1 and TG2 represent the output from gamma thermometers used in the irradiation test. A sinusoidal series equation given in Reference 29 was used to calculate the relative flux for each time step at 5 equally spaced locations along the length of the fuel column.

The fuel assemblies condensed power history is given in Table 7. Table 8 lists the measured mean burnup, temperature and pressure followed by the GAPCON-THERMAL-2 predictions for fuel rods 1 and 5 in IFA-116. The last column in Table 8 gives the code input linear heat ratings for both pins for the 12 time steps.

End-of-life burnups were just over 4000 MWd/MT UO_2 with fuel temperatures over 2000°C and internal rod pressures above 150 psi (Table 8). Pin linear heat ratings were sometimes greater than 21.5 kW/ft.

Tables 11 and 12 give the corresponding information for fuel rods 1, 3, 5 and 6 in IFA-117; Figures 18 and 19 summarize the results, showing the differences between the predicted and measured pin temperatures and pressures. The code predictions are based on our calculations using the assumed 12-step power history and the given experimental data of burnup and an assembly power rating. The assembly power rating was not constant, although it was assumed to be constant during the time-step.

As illustrated in Figures 18 and 19, the code generally predicts higher fuel temperatures and pin internal pressures. Some possible reasons for the discrepancy include the usual experimental uncertainties associated with inaccurate temperatures, the determination of assembly power, and particularly the determination of the rod power as a function of time at various axial locations. In addition there are uncertainties associated with the physical dimensions of the rods.

To obtain some idea of the possible magnitude of variations in experimental results an analysis was made of several Halden irradiation tests. These results are shown in Figures 20 and 21. Figure 20 shows the relatively large variation in reported fuel centerline temperatures as a function of gap size for 5 ± 1, 10 ± 1, and 15 ± 1 kW/ft linear heat ratings. The variations at constant power may be as little as 100 or as large as 700°C. A replot of some of the same data is shown in Figure 21. Here the variation is shown in the reported fuel centerline temperatures as a function of heat rating for fuel pins with a fabricated gap of 0.006 ± 0.001 inches. At 10 ± 1 kW/ft linear heat rating the reported fuel temperatures range from below 1000 to above 1500°C.

Two other Halden reactor irradiation tests used in the code evaluation were IFA-130 and IFA-131.[73] These two assemblies each contained 12 fuel rods (pellet and powder UO_2). IFA-130 had rods with 90 and 94% T.D. pellet fuel with 0.0087-inch fabricated fuel-cladding gap for the 90% T.D. fuel; no gap size was reported for the 94% T.D. fuel. IFA-131 contained 94% T.D. pellet fuel rods with 0.006-, 0.008- and 0.012-inch fabricated fuel-cladding gap. Fuel centerline temperature as a function of linear heat rating was graphically reported. See Appendix D for the input values used by the code for these predictions. The results of the code predictions are shown in Figures 22 and 23. The code predicted temperatures that were 100 to 300°C higher.

Balfour, Christensen and Ferrarri reported the results of three highly instrumented UO_2 irradiation tests.[74] One capsule (No. III) contained $UO_{1.94}$ and was not used in the code evaluation. The code input for these large diameter capsules I and II are given in Appendix D. The results of the code predictions are shown in Figures 24 and 25. The effects of the relocation on fuel centerline temperatures are also shown in Figure 25 for these capsules which had a fabricated gap of over 0.024 inches; however, almost all of the gap closure was due to fuel thermal expansion.

HPR-80 Data[76]

These data consist of centerline temperatures determined by thermocouples located in the fuel. Fuel densities were 96% T.D. and 98% T.D., pellet diameters were ∿0.440 inches, and all sorbed gas was assumed to have reacted with the fuel or cladding. The predicted BOL values for both the 0.002- and 0.006-inch gap rods agree with the experimental values (Figures 26 to 31). Predictions for the HBA and HBB rods (Figures 26 and 27) are high (∿100°C) for heat ratings >13 kW/ft but are still within the uncertainty given. A comparison of GAPCON-THERMAL-1 predicted BOL temperatures to the GAPCON-THERMAL-2 temperatures shows only a few degrees change for the

0.002-inch gap rods while the 0.006-inch gap rods show a 170 to 200°C drop in centerline temperatures (Figures 30 and 31) with the GAPCON-THERMAL-2 prediction in very good agreement with the data. The experimental uncertainties in power and thermocouple readings were obtained from reported estimates.

Kajaerheim and Rolstad[76] also reported power versus temperature values for two of the fuel rods which indicated a temperature increase of about 60 to 80°C after burnups of 4200 and 4300 MWd/MT UO_2. A comparison of GAPCON-THERMAL-2 predictions at these burnups with the measured temperatures (Figures 32 and 33) shows good agreement up to ∿10 kW/ft where the predicted values start to deviate from the reported values, resulting in a 110°C overprediction at ∿12 kW/ft (the highest power measured). The GAPCON-THERMAL-2 predicted temperature rise with burnup is due to the fission gas degradation of the fill gas.

AECL-2662

Notley et al.[30] have reported grain growth and gas release measurements from rods irradiated for approximately 108 full-power days. Pellet diameters and diametral gaps were a nominal 0.7638- and 0.004-inches, respectively. Power histories were not provided for these rods and peak powers ranged from 7% to 15% higher than the time-averaged powers. This makes it difficult to accurately simulate fuel performance; however, comparison has been made between GAPCON-THERMAL-2 predictions and experimental data for three argon-filled rods (LFD, LFH and LFM) which showed the minimum power variance (∿7%). The time-averaged heat ratings were used for the code calculations due to the lack of a power history. A comparison of the code's predicted temperature profiles and the grain growth data (Figure 34, 35 and 36) shows a general overprediction by the code for both BOL and EOL temperatures with the exception of rod LFD which shows BOL temperatures slightly underpredicted. The effect of a 7% variance in power on both BOL and EOL

temperatures would contribute approximately ±80°C uncertainty at the grain growth boundaries. The code predicts a large temperature increase to occur from BOL to EOL (∿300°C increase in centerline temperature) caused by the fission gas degradation of the fill gas with burnup.

A comparison of predicted and measured fission gas release fractions for these three rods (Table 11) shows an overprediction by the code with the LFD rod being only slightly overpredicted.

The general overprediction by the code for these rods is consistent with the previous results, which shows the code begins to overpredict temperatures and gas release when fuel temperatures and heat ratings exceed 2000°C and 20 kW/ft.

AECL-1676[32]

Notley et al.[32] have reported grain growth and gas release measurements from rods irradiated for ∿18 full-power days. Pellet diameters and diametral gaps were a nominal 0.748- and 0.003 - inches, respectively. As in AECL-2662, the detailed power histories were not given; however, the time-averaged powers and the peak powers and their times of occurrence are given. Three rods from these tests (DFB, DFD and DFE) were selected for comparison against GAPCON-THERMAL-2 predictions because of the relatively small difference (5 to 8%) between average and peak powers. The predicted temperatures of these rods at their peak heat ratings in comparison with the grain growth data shows (Figures 37, 38 and 39) the code to overpredict temperatures. There seems to be a general trend of the higher the heat rating the larger the overprediction. A comparison of predicted and measured fission gas release fractions (Table 11) also shows a significant overprediction by the code. These results are similar to the previous data comparisons which also show the code overpredicts at the higher temperatures and heat ratings.

Soulhier and Notley[83]

The purpose of this test was to evaluate the effects of power changes on gas release. Essentially four separate power histories were run in these tests; the first set of rods was held at a relatively high power (∿22 kW/ft) for a period of time and then reduced to a lower power (∿13 kW/ft) for continued irradiation; the second set was irradiated with a power history in reverse of the first set. The third set was held at the constant high power level while the fourth set was held at the lower power level to provide a standard data base for evaluation of the rods with varying power history. Consequently, these data provide a good opportuntiy to check the ability of GAPCON-THERMAL-2 to follow a power history which was one of the major reasons for updating the code. The initial cold fuel-to-clad gap size of these pins was very small (nominally 0.002 inches) which precludes any checks on how well the code models fuel relocation for these power histories.

The power histories and gas release data are presented in Table 12 along with the GAPCON-THERMAL-2 predictions. There is very good agreement between the predicted gas release for the three rods with varying power histories (samples AZB, AZC and AZJ) and the experimental results indicating the code does an adequate job of modeling the power history effects of gas release. A comparison of the GAPCON-THERMAL-2 predictions of the four rods (samples AZM, AZL, AZR and AZT) with a relatively high (22 kW/ft) constant power history and the experimental results shows the code overpredicts gas release by 6 to 12% release for three of the rods. Results are similar to other comparisons of the code which show the code overpredicts temperatures for rods with centerline temperatures >2000°C and heat ratings >20 kW/ft. In contrast, the code underpredicted gas-release by 2 to 4% release for data from the two rods (AZD and AZE) operated at a constant low power (∿13 kW/ft).

AECL-2588

Bain[78] reported on a wide range of experimental data which consisted of very short irradiations (10 to 40 min) in the hydraulic rabbit and

longer-term irradiations (∿40 full-power days) in a pressurized water loop. GAPCON-THERMAL-2 comparisons have been made on the longer-term irradiations only (X-23301 and X-23303 tests). Pellet diameters for these tests were 0.7047 and 0.6902 inches, diametral gaps were 0.0142 and 0.0292 inches, and the fill gas was argon. A comparison of GAPCON-THERMAL-2 beginning-of-life predictions of equiaxed grain growth boundaries (assumed to be 1400°C) and the reported values (Table 13) show that the code overpredicts this data by 2 to 14%. Previously predicted values from GAPCON-THERMAL-1[1] are also included in Table 13. A comparison of predictions from the two codes show GAPCON-THERMAL-2 to predict slightly higher temperatures for the smaller 0.0142-inch gap rods and significantly lower temperatures for the 0.0291-inch gap rods. The relocation and fuel melting models in GAPCON-THERMAL-2 are the primary contributions to the lower temperatures predicted for the larger gap rods. The slight temperature increase for the smaller gap rods is due to the new contact conductance model which predicts lower gap conductances for fuel-to-cladding contact.

AE-318[75,82]

Devold[75,82] reported centerline temperatures for three different fuel rods determined from thermocouple measurements. The pellet diameters were 0.4953 and 0.4909 inches with fuel-to-cladding gaps of 0.0071 and 0.0051 inches and a 96% T.D. fuel density. The temperatures measured were essentially BOL values. The predicted results (Figure 40) for IFA-3 (0.0071-inch gap) compare very well with the measured results between the range of heat ratings given, 1 to 9 kW/ft. However, the code under-predicts temperatures for the remaining two rods (IFA-4 and IFA-10). The IFA-4 rod is underpredicted (Figure 41) by the largest amount (300 to 400°C) even though the IFA-3 and IFA-4 rods were identical except for enrichment (1.5% and 6%, respectively). An anomaly between the experimental results exists because the higher enrichment rod (IFA-4) should have resulted in slightly lower temperatures when compared to IFA-3. The author suggests[75] that the gap sizes were not the same for

the two rods. However, a run with GAPCON-THERMAL-2 making the IFA-4 gap size 1 mil larger only raised the centerline temperature by ∿50°C, indicating that the IFA-4 gap size would have to be ∿2 times larger (7 mils versus 13 to 14 mils) than IFA-3 to account for the temperature differences. The IFA-10 rod was also nearly identical in design to the other two rods with the exception of gap size and enrichment, 0.0051 mils and 2.5%, respectively. The code overpredicts the mean of this data by 130 to 200°C (Figure 42) with the largest deviation at the peak heat rating (∿13 kW/ft). However, the temperature measurements at the peak heat rating show a considerable amount of variance (∿200°C difference) among the data making the lower temperature data points within 100°C of the code predictions.

The experimentally measured temperature differences between nearly identical fuel rods, especially between IFA-3 and IFA-4, can possibly be explained by an accumulation of errors from the thermocouple measurements, estimation of powers, and variance in initial gap size. Another contributing source may be in gap closure kinetics which is postulated to be a relatively fast phenomenon occurring relatively early in life. Possibly the IFA-4 temperature measurements were made on the first excursion to power so that very little relocation took place. The IFA-3 temperature measurements were made after a few days of accumulated burnup allowing the fuel to relocate and reduce the gap size.

CEA-R-3358 Data

The data reported by Janvier et al.,[33] consisted of grain growth measurements obtained from rods irradiated for two or four reactor cycles. Pellet diameters were a nominal 0.510 inches and diametral gaps ranged from 0.004 to 0.012 inches. Nominal burnups achieved for the two series of lists were 3000 and 6000 MWd/MTM. Rod powers varied between 3% to 30% from the time-averaged powers over the irradiation period with peak powers occurring at the first startup and the last startup with the highest

powers generally occurring at the start of the last cycle. The power history makes it difficult to determine the operating condition that controlled grain growth. Initial power conditions may have established the microstructure observed during the postirradiation examination, but the high powers toward the end-of-life may also have controlled the grain growth. There are many complicating factors that make it difficult to relate the structure observed in a postirradiation examination with a temperature at a particular point in the irradiation history. These factors include the variation of gap conductance with time and the production of fission products that can act as impurity atoms to inhibit grain growth towards end-of-life.

Bain[79] reported that 2 weeks operation at about 2000°C eliminated any evidence of a molten zone. Similar restructuring of the columnar grain growth region and the equiaxed grain growth region could also occur with new temperature conditions erasing old boundaries. An irradiation test by MacDonald[80] suggests that equiaxed grain growth was retarded by previous irradiation history. The test consisted of reirradiating a rod that had achieved 484 full-power days at 50% higher power. MacDonald's calculations suggested the diameter of grain growth should have increased about 0.050 inches for an additional 22 full-power days whereas the measured amount was as low as 0.010 inches. MacEwan and Hajaski[81] (as reported by MacDonald) showed that grain growth was inhibited for samples irradiated below 1500°C and subsequently raised to 1500 to 1750°C for an additional 290 hours. Thus, the magnitude and deviation of power changes during irradiation could have a pronounced effect on grain growth because of the time-temperature relationship and the effect of fission-induced impurities.

The power conditions that established the grain growth observed in the CEA-R-3358 tests were not determined. We attempted to simulate the thermal behavior by comparing GAPCON-THERMAL predictions based on: 1) beginning-of-life (BOL) powers and temperatures and 2) peak centerline temperatures (in most cases this corresponds to maximum end-of-life powers) achieved during the irradiation history. The fuel temperatures were plotted as a function of fuel radius with the quoted grain growth measurements

superimposed. The uncertainty box for the grain growth data represents the authors reported dimensional uncertainties and our estimate of ±100°C on the grain growth temperature. A columnar grain growth temperature of 1700°C and an equiaxed grain growth temperature of 1400°C was assumed based on earlier analysis.[26,87] All of the sorbed gas was assumed to have reacted with the cladding and fuel.

The rods with similar temperatures for beginning-of-life and peak conditions, samples 4110 and 4112 (Figures 43 through 50) show good agreement between predicted temperatures and grain growth measurements with the predicted temperature profiles falling within or near the uncertainty boxes. These rods have a fuel-to-clad gap size of 4 to 5 mils. The BOL and peak temperatures for the 4113 samples also show reasonable agreement with grain growth measurements (Figures 51 through 54) even though the differences between BOL and peak centerline temperatures were ∿300°C. BOL temperatures fall within the lower portion of the uncertainty box (excluding 4113-BE1) and peak temperatures within the upper portion. The exception to the above was sample 4113-BE1 (Figure 53) where both predicted BOL and peak temperatures were higher than grain growth temperatures. The predicted BOL and peak temperatures for the 4111 samples (Figures 55 through 58) also bracket the uncertainty boxes for grain growth as they did for the 4113 samples; however, the predicted peak temperatures are substantially higher than the grain boundary isotherms while the BOL temperatures are underpredicted by a larger degree than in the 4113 samples. These results were not unexpected, however, since the BOL and peak centerline temperatures for the 4111 samples differ by 550 to 750°C. Both the 4111 and 4113 rods have fuel-to-cladding gap sizes of ∿12 mils.

A comparison between the CEA-R-3358 measured gas release values and those predicted by GAPCON-THERMAL-2 are presented in Table 14. The code predicts 0.03 to 0.16 higher gas release fractions for the large gap rods (4111 and 4113 samples) while 5 of the 8 rods with smaller gaps (4110 and 4112 samples) show good agreement with the measured values (within ±0.02 release fraction).

Several postulated effects could explain the above results. If the BOL rod powers set the grain growth boundaries and if we have overestimated the grain growth boundary temperatures by 100 to 150°C, good agreement would be obtained with the 4111 and 4113 BOL temperatures. However, all the 4110 and 4112 grain growth temperatures would then be overpredicted. A more likely situation is that while BOL temperatures may establish the initial grain growth boundaries, higher temperatures are required later in life to move the boundaries due to fission product impurities pinning. This would support the experimental work of MacDonald[80] discussed earlier. Alternatively, deficiencies in modeling for burnup effects and rods with relatively large fuel-to-clad gaps (≥12 mils) would explain the code's overprediction of gas release for the 4111 and 4113 rods.

Another source of error in the calculation of these temperatures and gas release fractions is the reported heat ratings which are probably no better than ±10%. Nominal heat ratings given for the power histories were used in these calculations.

LIMITATIONS AND RECOMMENDATIONS

GAPCON-THERMAL-1 was modified to provide a more appropriate calculational tool for computing gap conductance values in thermal reactor fuels. This version of the code, GAPCON-THERMAL-2, still contains certain limitations to its application. These limitations stem principally from the sparsity of well-characterized data for establishing performance models and for checking the calculational models. Since the code is based on empirical models as well as first principles, the lack of well-characterized data can result in a conservative calculation. We have been unable to locate much well-characterized data for thermal reactor fuel, with large diametral gaps, especially in the 10 to 15 kW/ft range. Most of the data contain enough experimental uncertainties to preclude anything but a best estimate calculation. Furthermore, some information concerning initial conditions or operating history is usually either completely lacking or is inconsistent with other information in the report. Evaluation of data reported in the open literature is continuing, but a definite need exists for good data applicable to commercial fuel in the operating range of interest.

To further improve the thermal performance modeling capability of the code, efforts are being applied to better delineate the following performance and operational characteristics of the fuel. Additional revision and validation of the code will be made as additional data becomes available.

- gap closure
- restructuring
- asymmetric heat transfer
- neutron cross sections
- helium sorbtion
- fuel cladding mechanical interaction
- cladding crud and corrosion
- thermal transients
- flux depression burnup dependence

Gap Closure

The area of gap closure is currently a limiting aspect of the GAPCON-THERMAL code because of the lack of data on the kinetics and magnitude of gap closure.

Sources of gap closure include cladding elastic contraction and creep, as well as fuel thermal expansion, swelling and cracking. Fuel relocation typically provides the most gap closure; however, very little well-characterized, quantitative data have been published to model early-in-life gap closure caused by a combination of fuel swelling and fuel cracking. The phenomena are currently not completely understood and are not currently amenable to a rigorous analytical solution.

Restructuring

Restructuring or grain growth is an important factor in oxide fuel temperature calculations because the formation of the central void reduces the heat flow path while the densification improves the thermal conductivity of the fuel. Calculated effects depend on the amount of sintering, the temperature at which sintering begins, and the sintering kinetics. The void distribution will affect other calculations such as fuel dimensional changes. Restructuring should be treated as a continuous time-dependent process. GAPCON-THERMAL contains a time-dependent relationship for columnar grain growth,[44] but we have not compared the model with others available. Some controversy exists as to the temperatures associated with the microstructural changes and the postulated densities in the restructured regions. For example, reported equiaxed grain growth temperatures vary from 1300 to 1700°C, and columnar grain growth temperatures range from 1600 to 2200°C. Restructured fuel densities vary from 92% T.D. to 100% T.D. Some of the scatter can be attributed to the use of different assumptions for calculating the fuel temperatures from an experiment and the difficulty of measuring residual porosity. Temperature gradients and pore morphology would also influence

the results. Although commercial fuel does not typically operate at powers sufficiently high to produce restructuring, the availability of a restructuring option will provide capability to model overpower conditions and additional experimental data.

Asymmetric Heat Transfer

Only heat transfer in the radial direction and a concentric pellet within the cladding are considered. The conditions in an operating fuel pin typically are asymmetric, and the concentric case has been shown[45] to give higher fuel temperatures. The concentric heat transfer in GAPCON-THERMAL contributes to the higher temperature predicted by the code for large hot gaps. Consequently, comparison of the code with experimental results becomes more conservative as the hot gap increases. However, other phenomena such as gap closure caused by thermally induced cracking probably are the largest sources of disparity between calculated and experimental values for large hot gaps.

Neutron Cross Sections

All the neutron cross sections in the code are for 2200 m/sec neutron velocities at room temperature. More appropriate values like those from the Westcott formulation may be required if more accurate flux and fission gas values are needed. This code should not be used to determine accurate neutron flux values. The fission gas generation values are sufficiently accurate for the current technology.

Helium Adsorption

The current version of the code does not account for any helium adsorption by the fuel but when quantitative data become available, a model for this effect can be added. Helium adsorption can be modeled by reducing the initial fill gas pressure.

Fuel-Cladding Mechanical Interaction

GAPCON-THERMAL-2 does not have an adequate engineering mechanics base to couple cladding and fuel deformations with the thermal routines in the code. Efforts are currently directed to coupling the pressure-induced

elastic and creep deformation of the cladding to all axial segments and the internal gas pressure. Additional work is being conducted to provide a basis for modeling the elastic and inelastic deformation of fuel and cladding induced by differential thermal expansion and fuel swelling.

Cladding Crud and Corrosion

This version of the code does not completely model cladding-coolant chemical interactions. The changes in cladding mechanical properties due to hydrogen absorption are not determined. The crud thickness (inches) may be input by the user through the variable CRUDTH. The code uses a low crud thermal conductivity value of 0.23 Btu/hr-ft-°F[84]

A late addition was made to the code to include oxidation of the Zircaloy cladding by the coolant. The calculation of zirconium oxide thickness and the associated temperature change is made in the subroutine CORROS.[85] The rates of reaction are modeled for PWR ($0 < ICOR < 3$) or BWR ($ICOR \geq 3$) coolant conditions. The GAPCON-THERMAL-2 user is cautioned that CORROS will probably not correctly model the oxidation rates for any specific reactor. The zirconium dioxide thermal conductivity used in CORROS is calculated by an equation given in Reference 86 based on out-of-pile data on high density zirconia.

Thermal Transients

Thermal transients cannot be modeled with this or the preceding versions of the code. Thermal equilibrium is assumed throughout the calculations. Power changes are assumed to occur instantaneously with zero thermal and mechanical resistance.

Flux Depression Burnup Dependence

The values of the flux depression used by the code are independent of time and power so there are no burnup dependent flux depression calculations. To estimate the possible effects due to burnup on fuel pin behavior the user can input burnup-modified flux-dependent values.

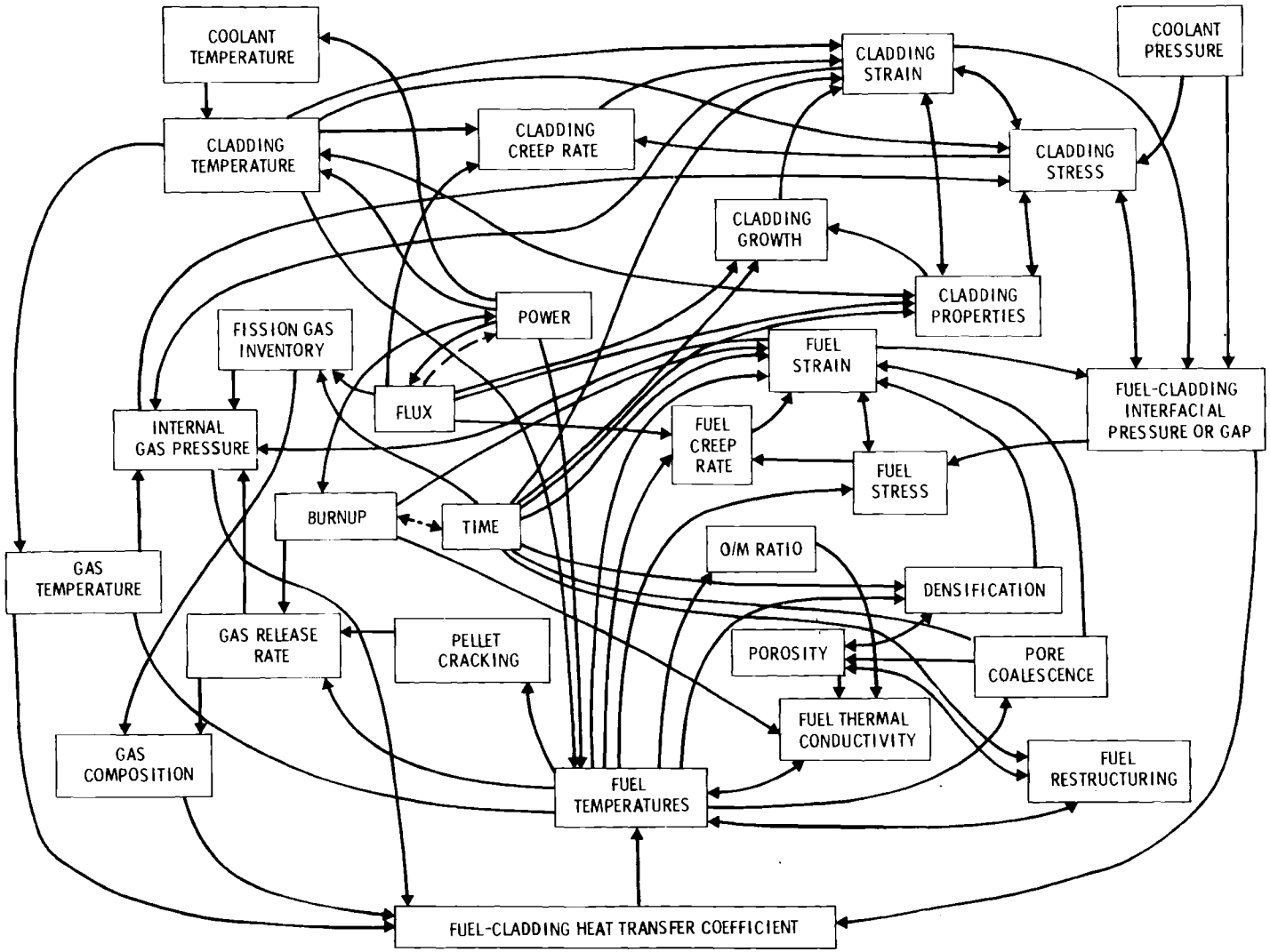

FIGURE 1. Typical Fuel Pin Parameters That Influence Fuel-Cladding Heat Transfer Coefficient

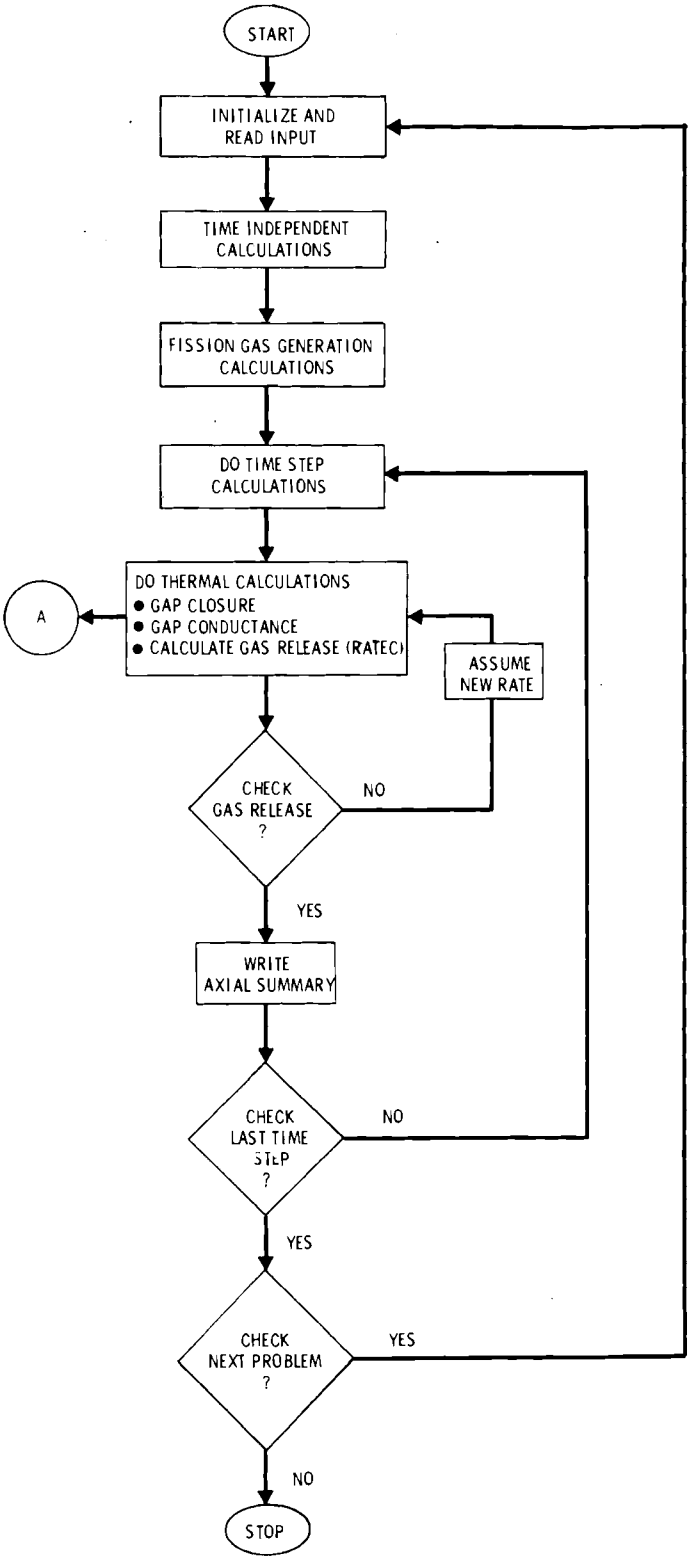

FIGURE 2. GAPCON-THERMAL-2 Flow Sheet

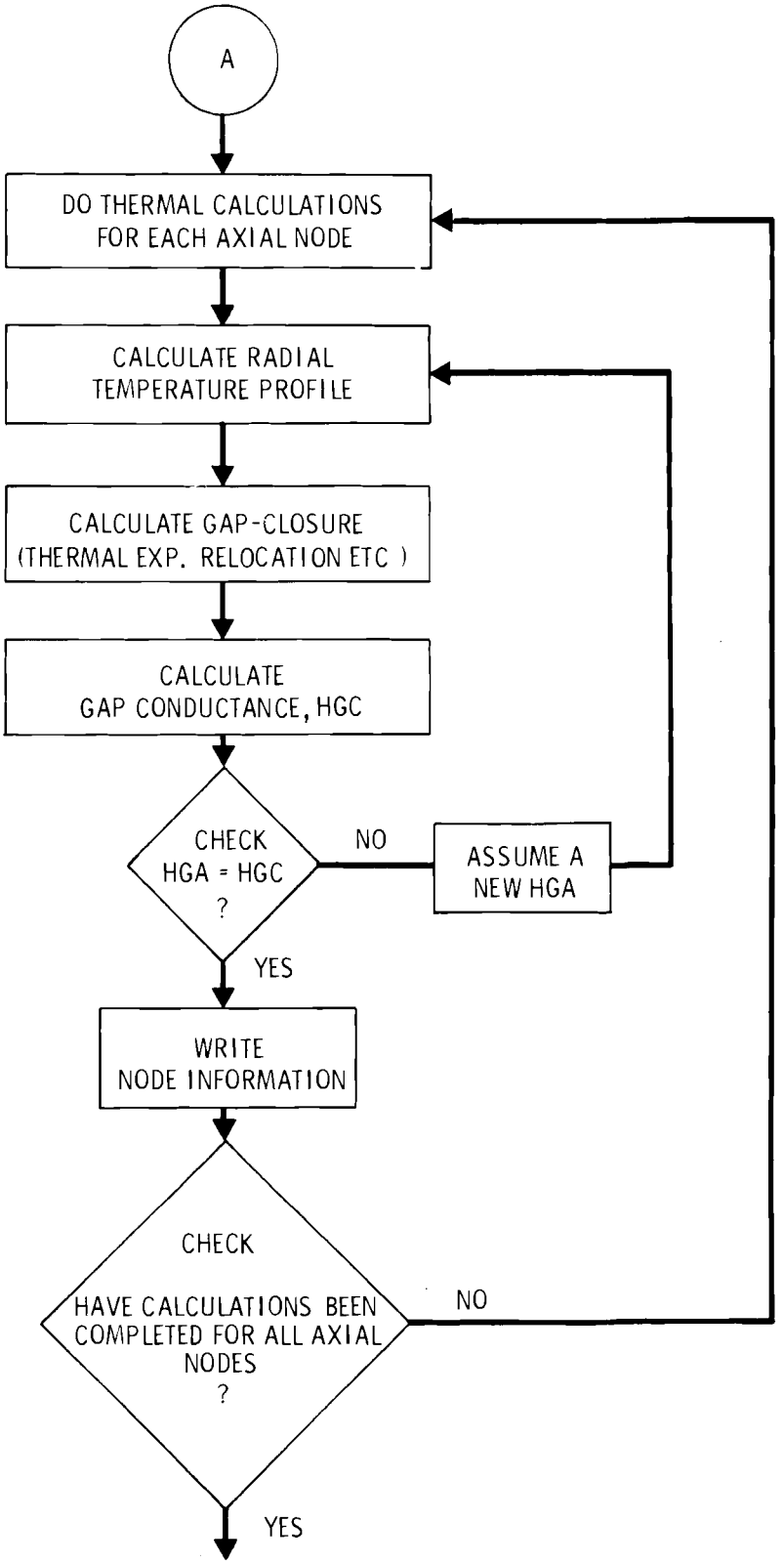

FIGURE 3. GAPCON-THERMAL-2 Flow Sheet (Detail A)

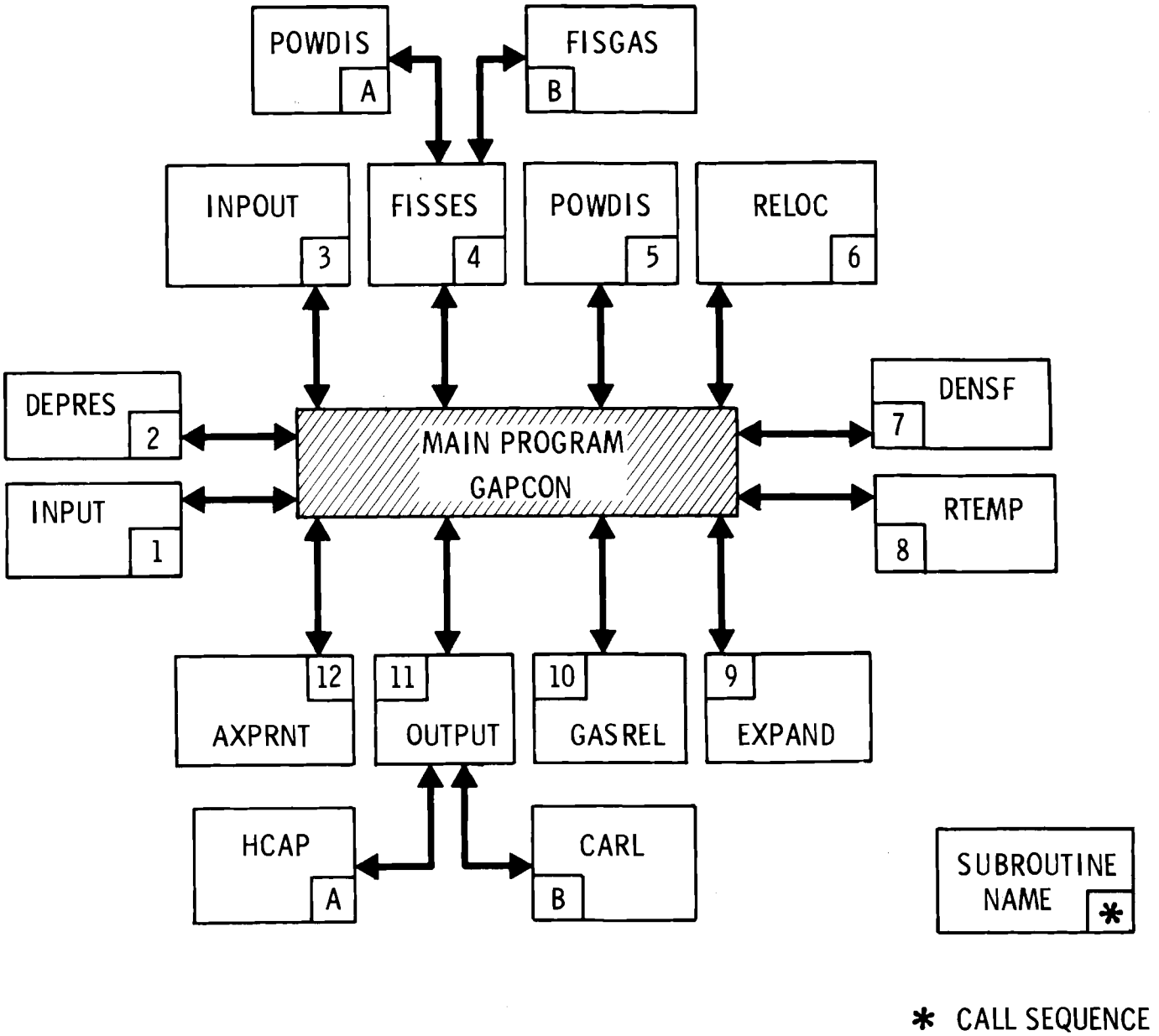

FIGURE 4. GAPCON-THERMAL-2 Subroutine Flow Chart

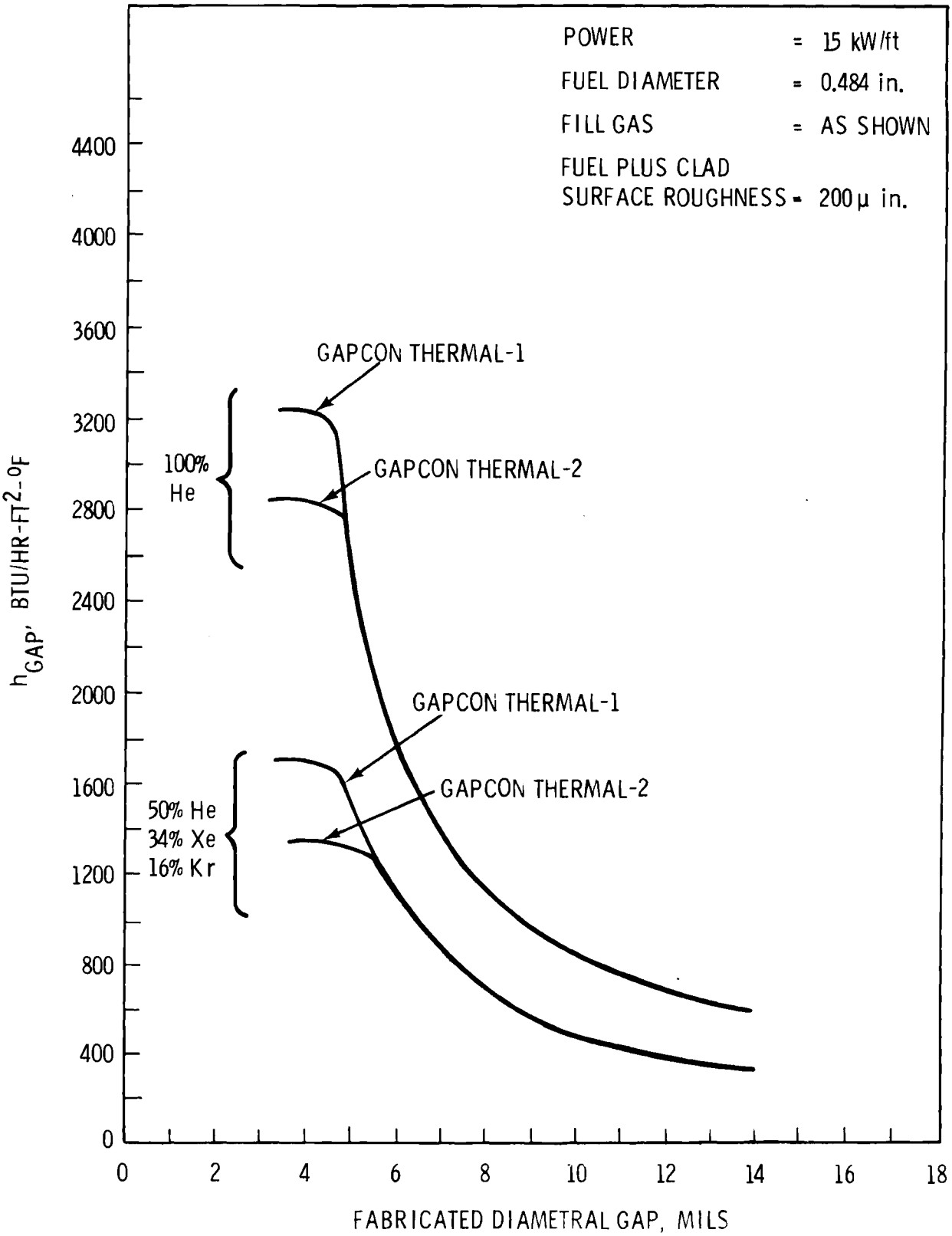

FIGURE 5. Comparisons of Gap Conductance Values in GAPCON-THERMAL-2 With GAPCON-THERMAL-1

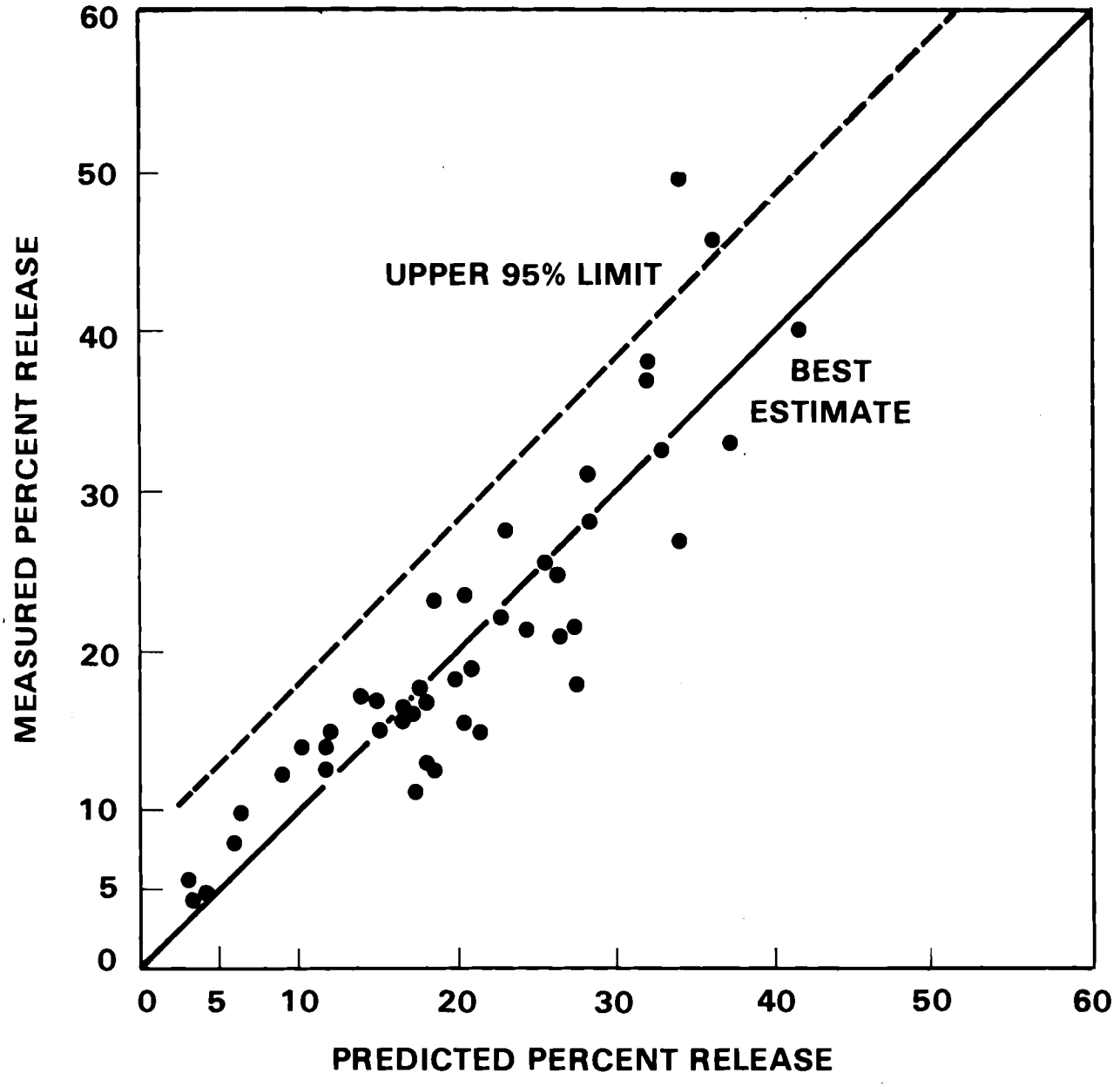

FIGURE 6. A Comparison of the High-Temperature Gas Release Model and the Data

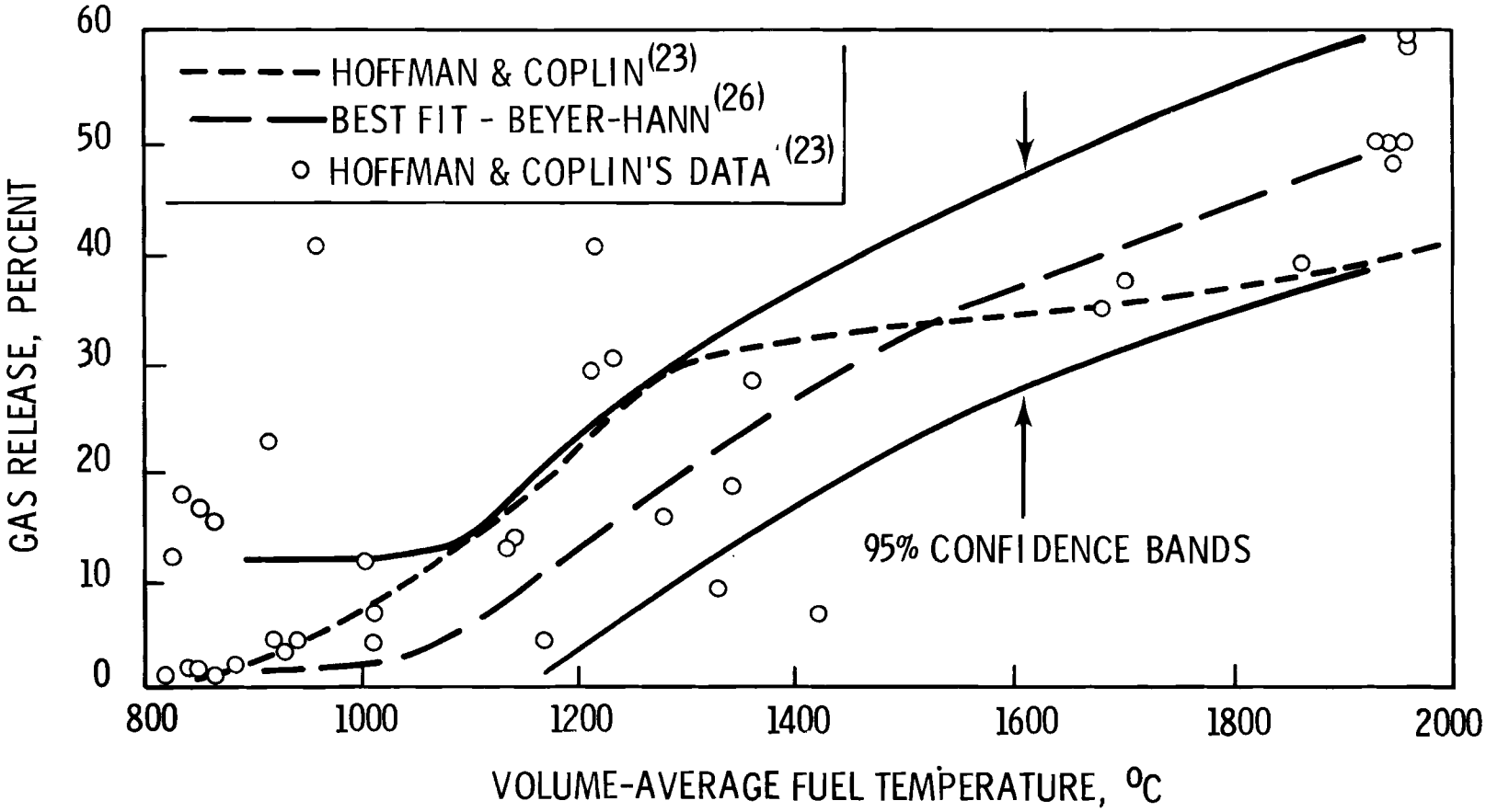

FIGURE 7. A Comparison of the High-Temperature Release Model with Hoffman and Coplin's Volume-Average Temperature Model

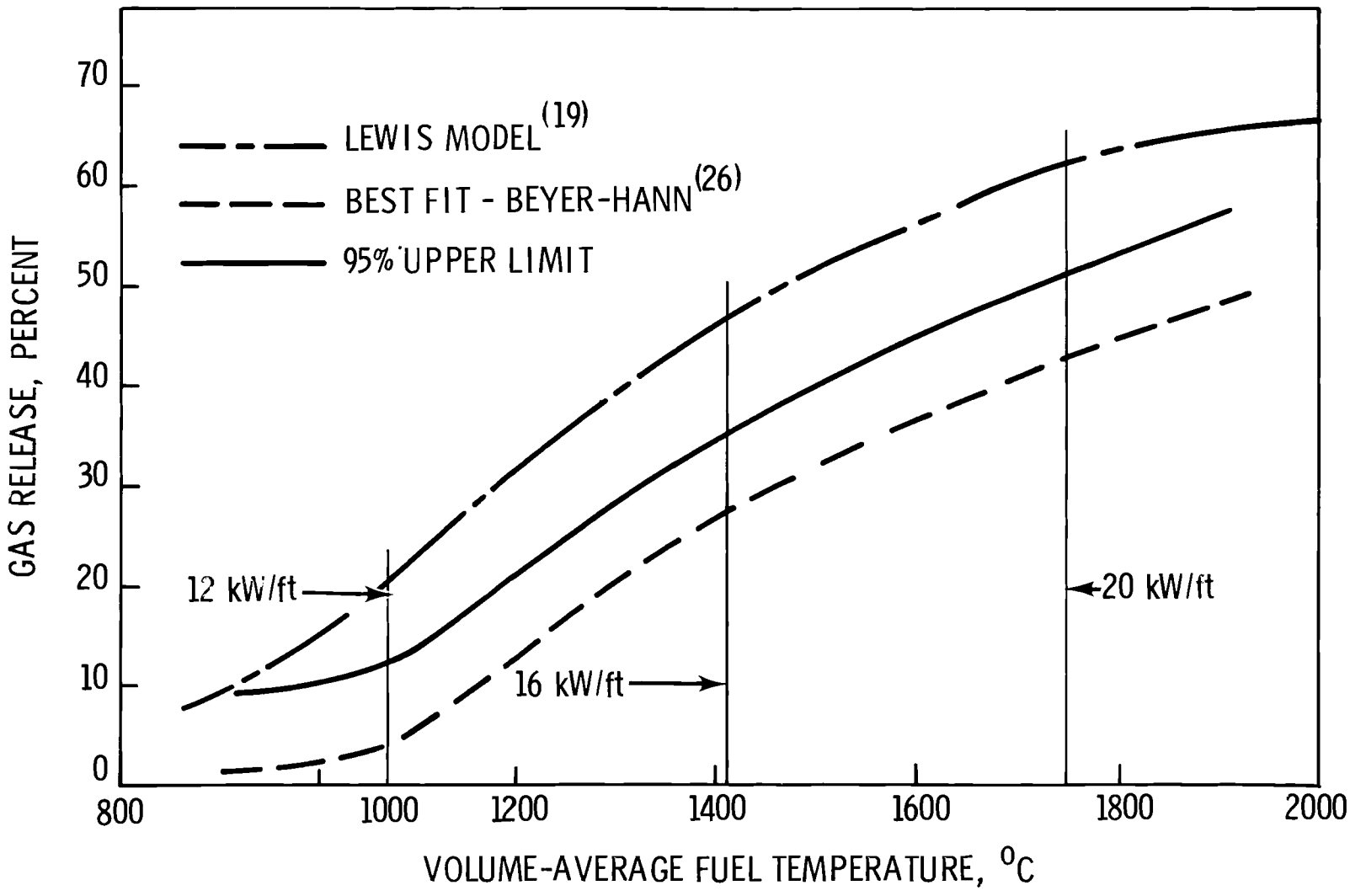

FIGURE 8. A Comparison of the High-Temperature Gas Release Model with Lewis' Model

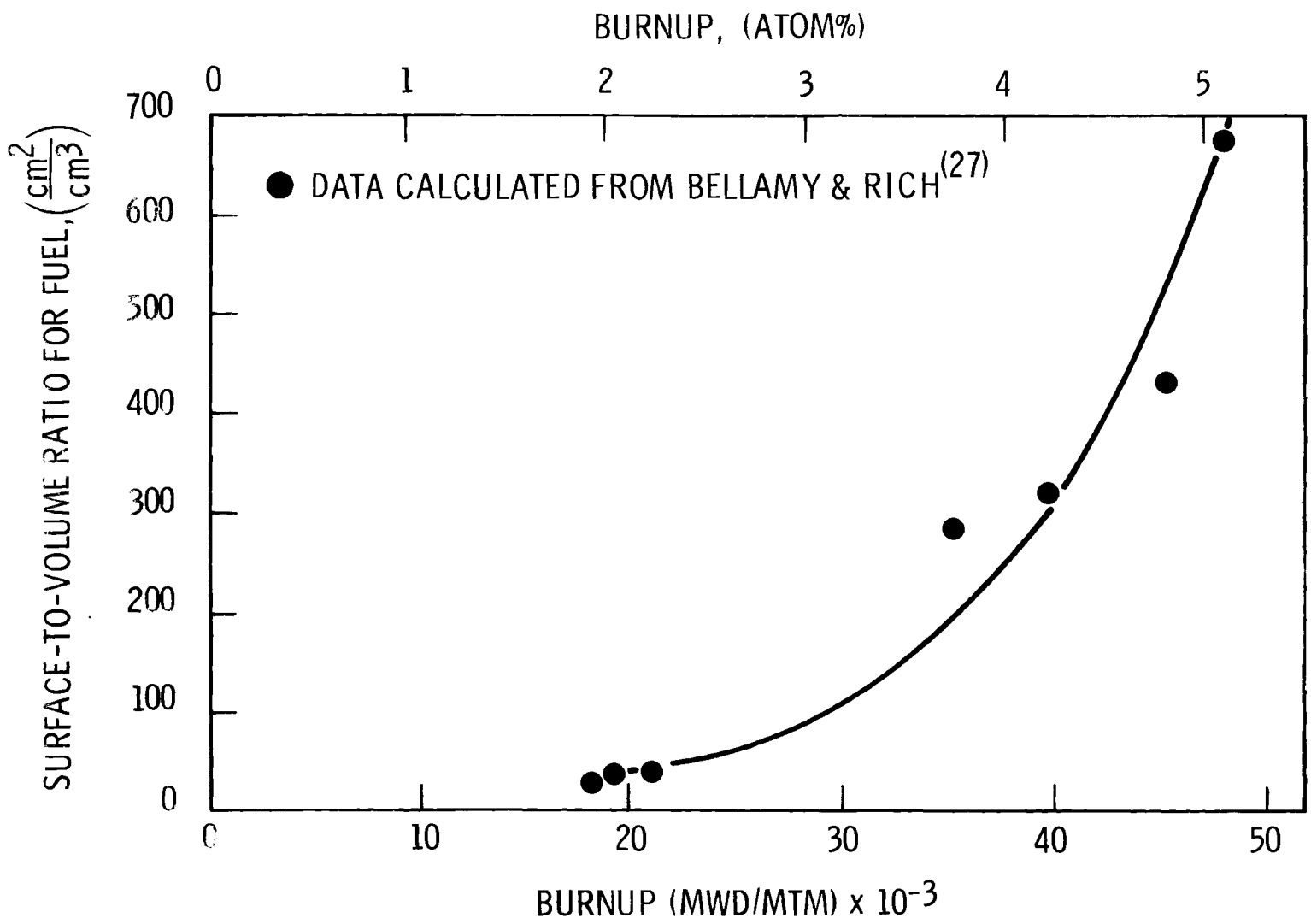

FIGURE 9. UO_2 Surface-to-Volume Ratios as a Function of Burnup

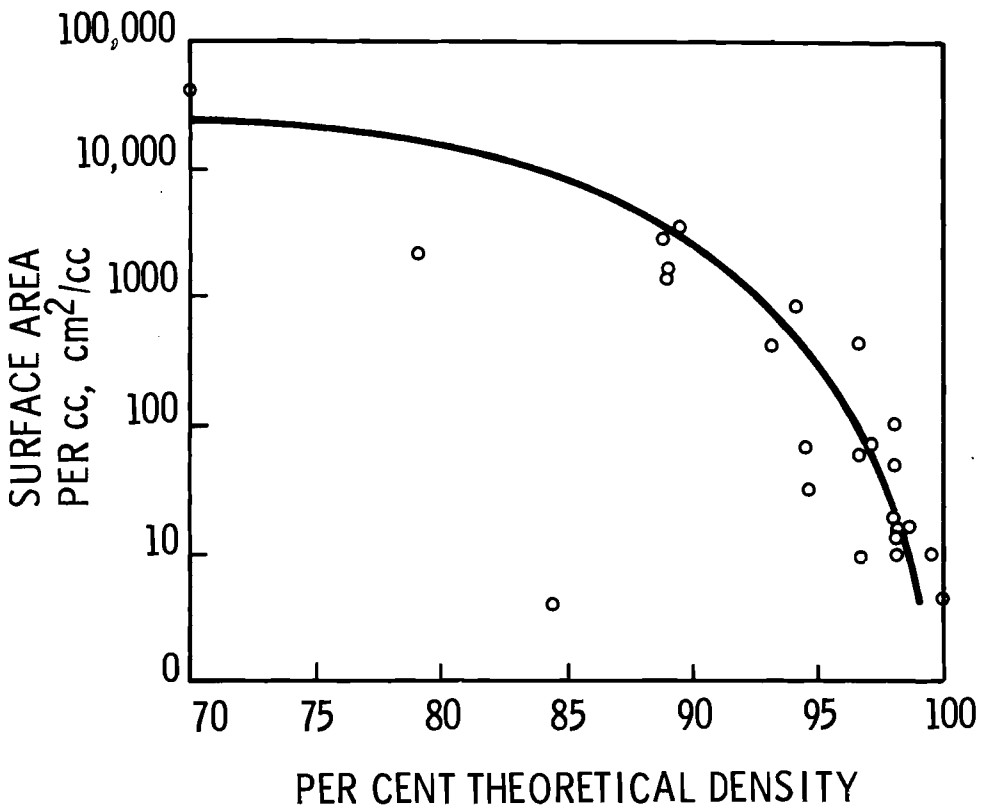

FIGURE 10. Measured Surface Area as a Function of Percent Theoretical Density for Sintered UO_2[35]

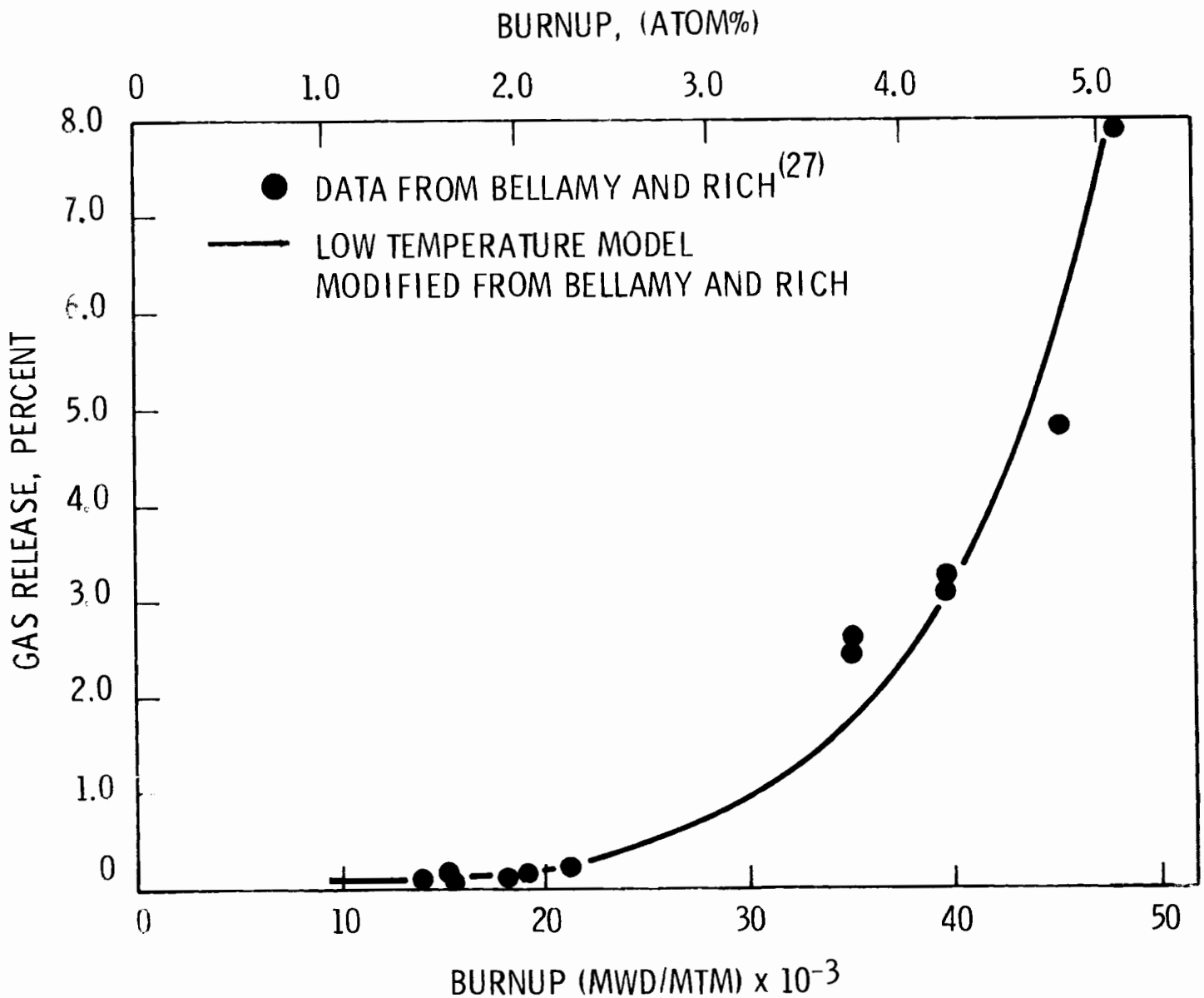

FIGURE 11. Predictions of the Low-Temperature Gas Release Model

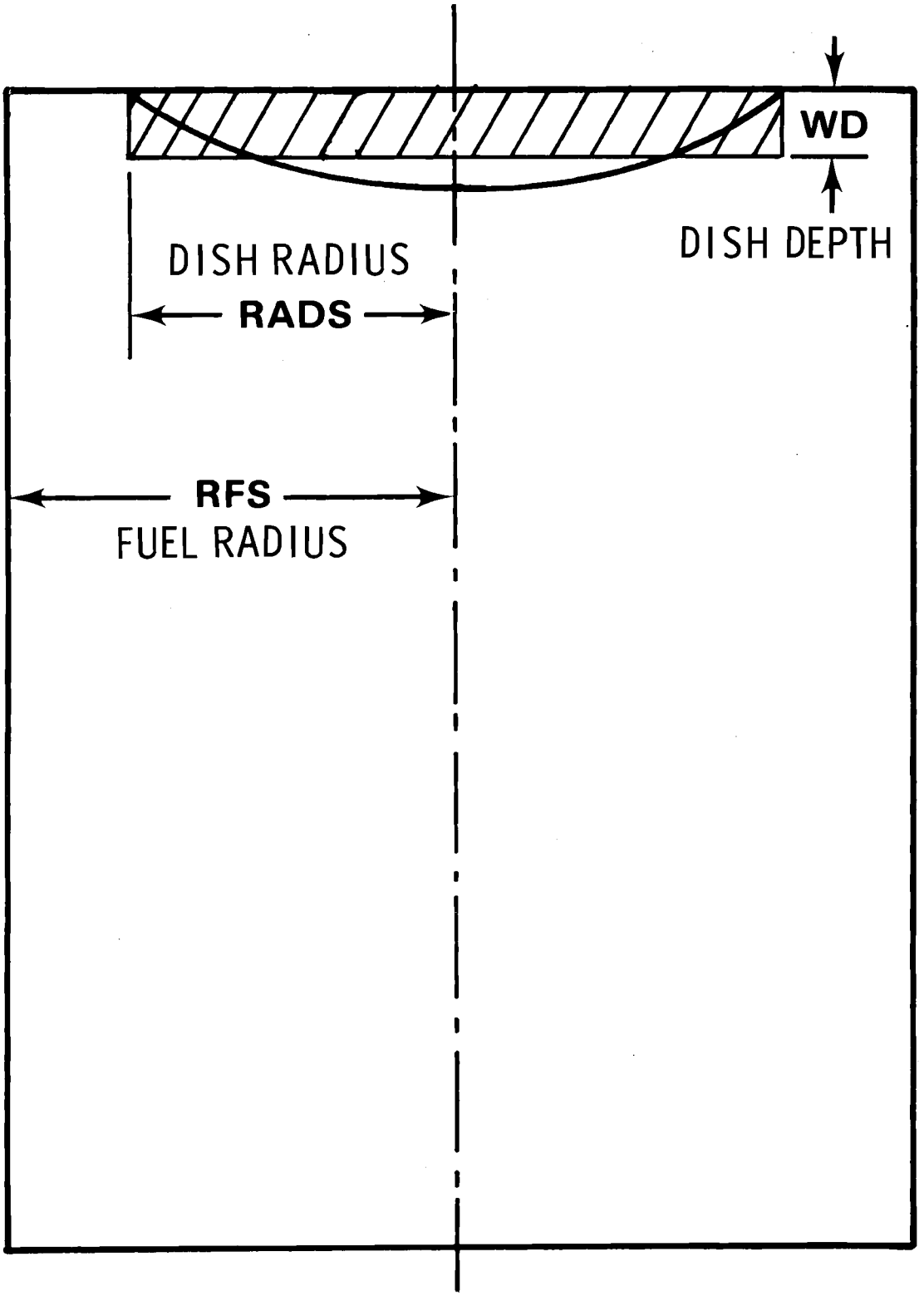

FIGURE 12. Schematic of Fuel Model for Pressure Calculations

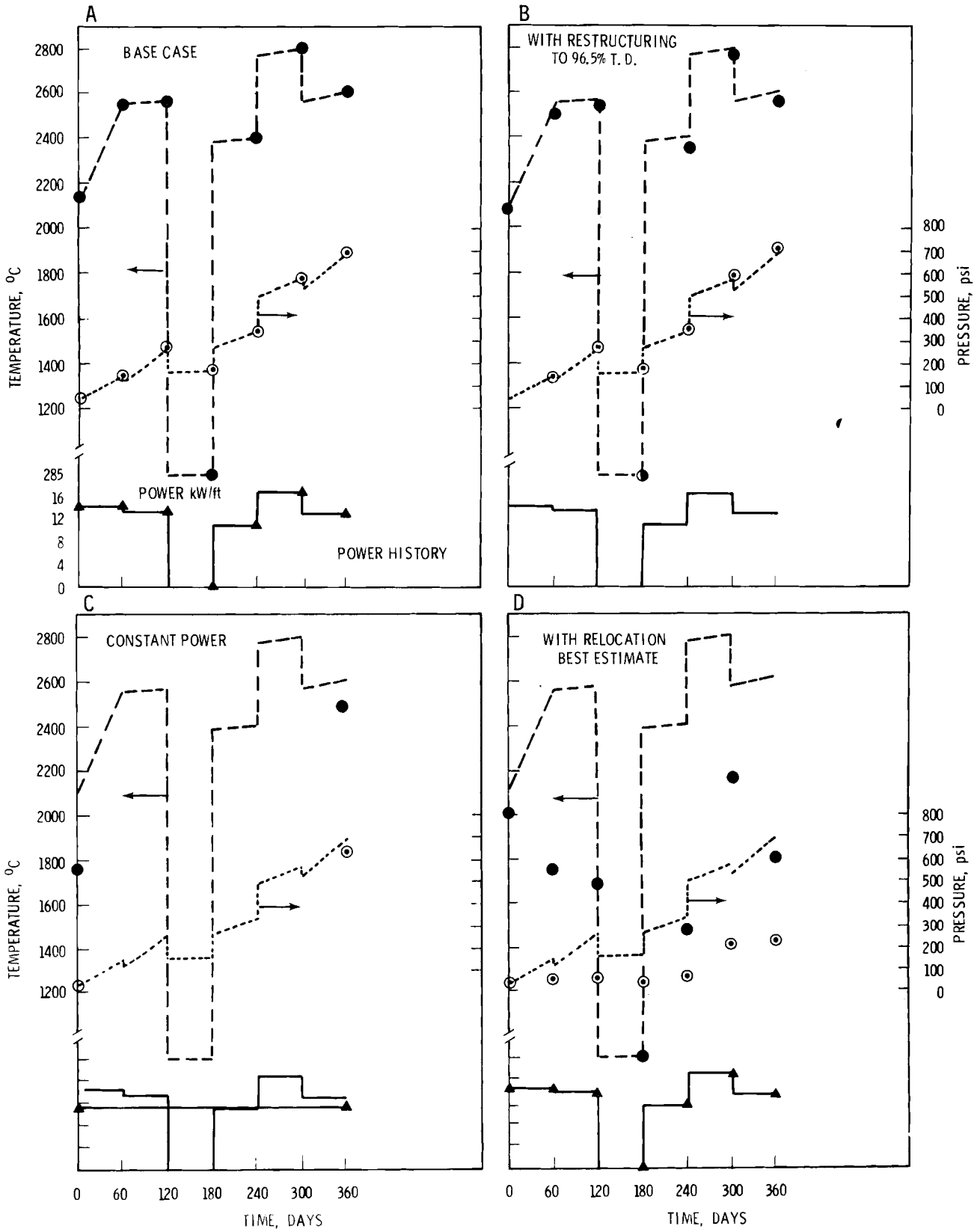

FIGURE 13. Parametric Study: Base Case, Restructuring, Constant Power, Best Estimate Relocation

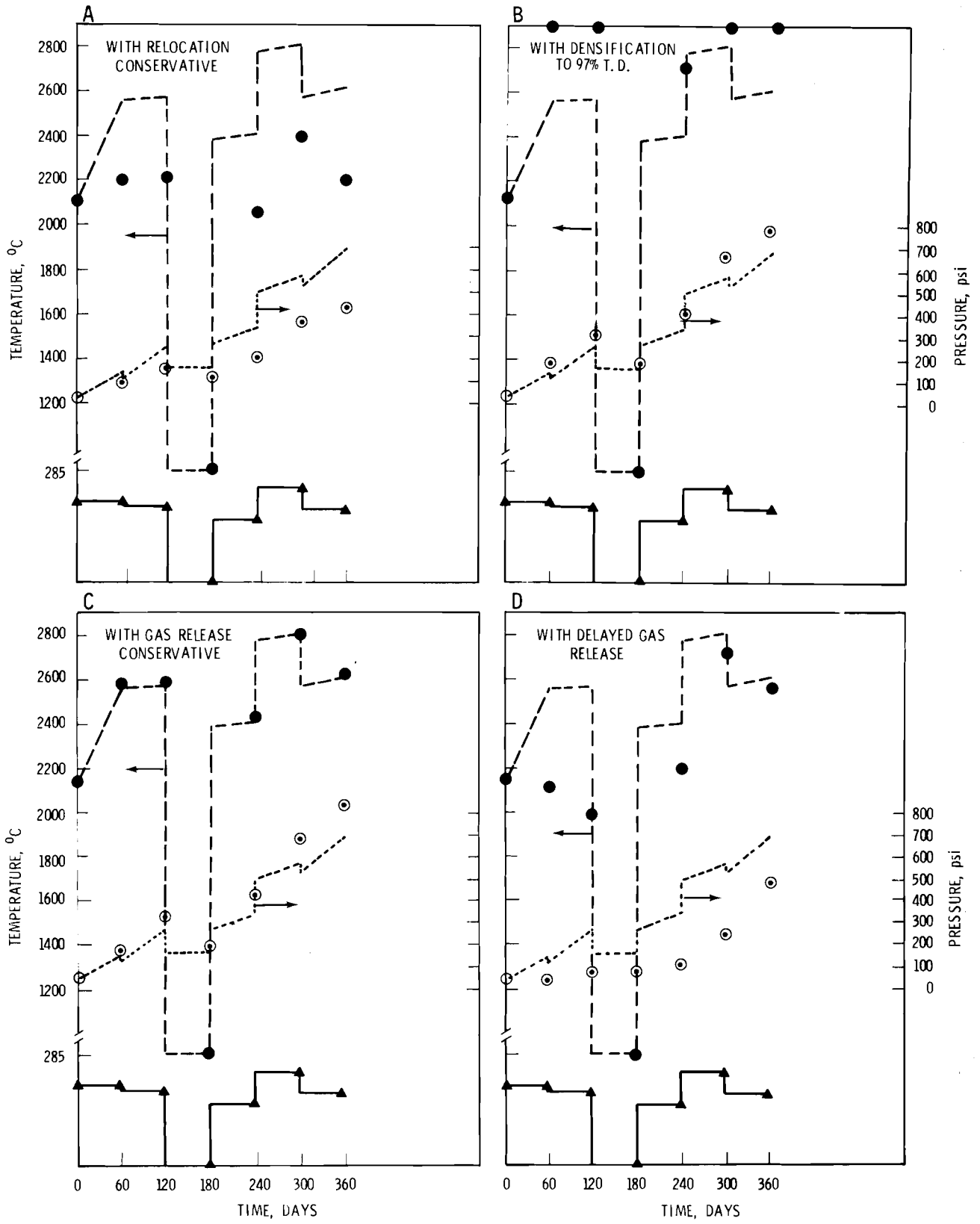

FIGURE 14. Parametric Study: Conservative Relocation, Densification, Conservative Gas Release, Delayed Gas Release

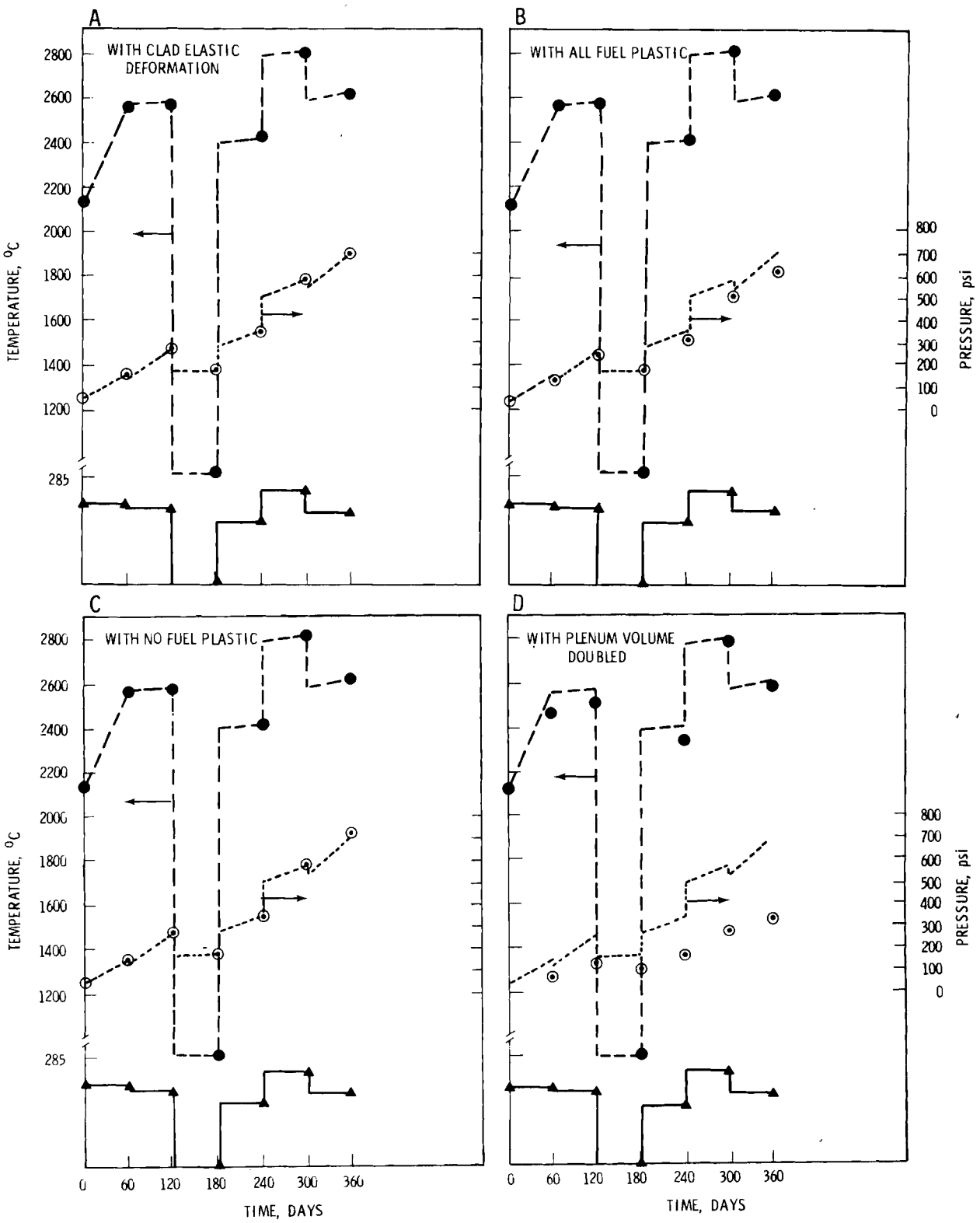

FIGURE 15. Parametric Study: Cladding Elastic Deformation, Plastic Fuel, Rigid Fuel, Larger Plenum

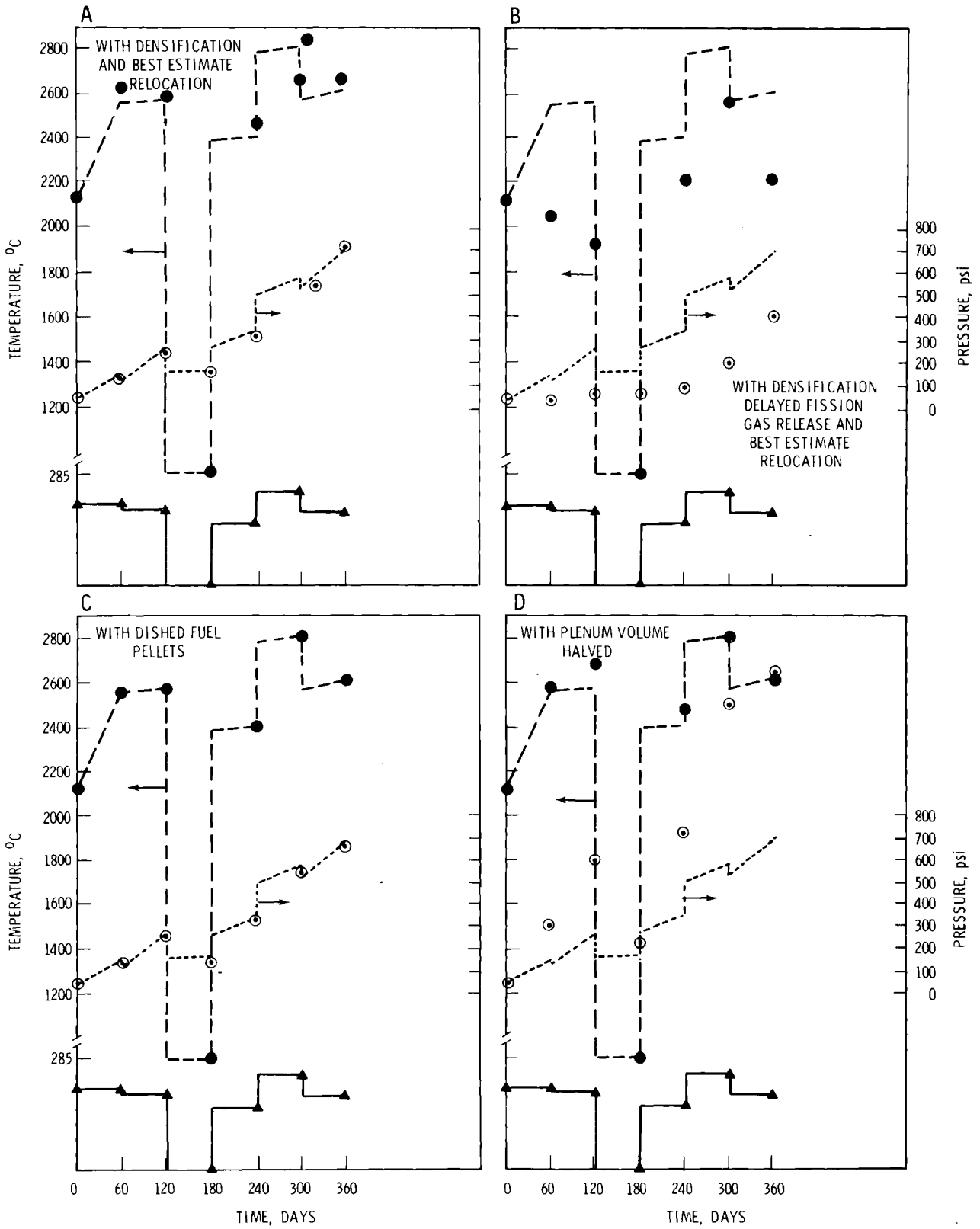

FIGURE 16. Parametric Study: Densification and Best Estimate Relocation, Densification Delayed Fission Gas Release and Best Estimate Relocation, Dished Fuel Pellets, Smaller Plenum.

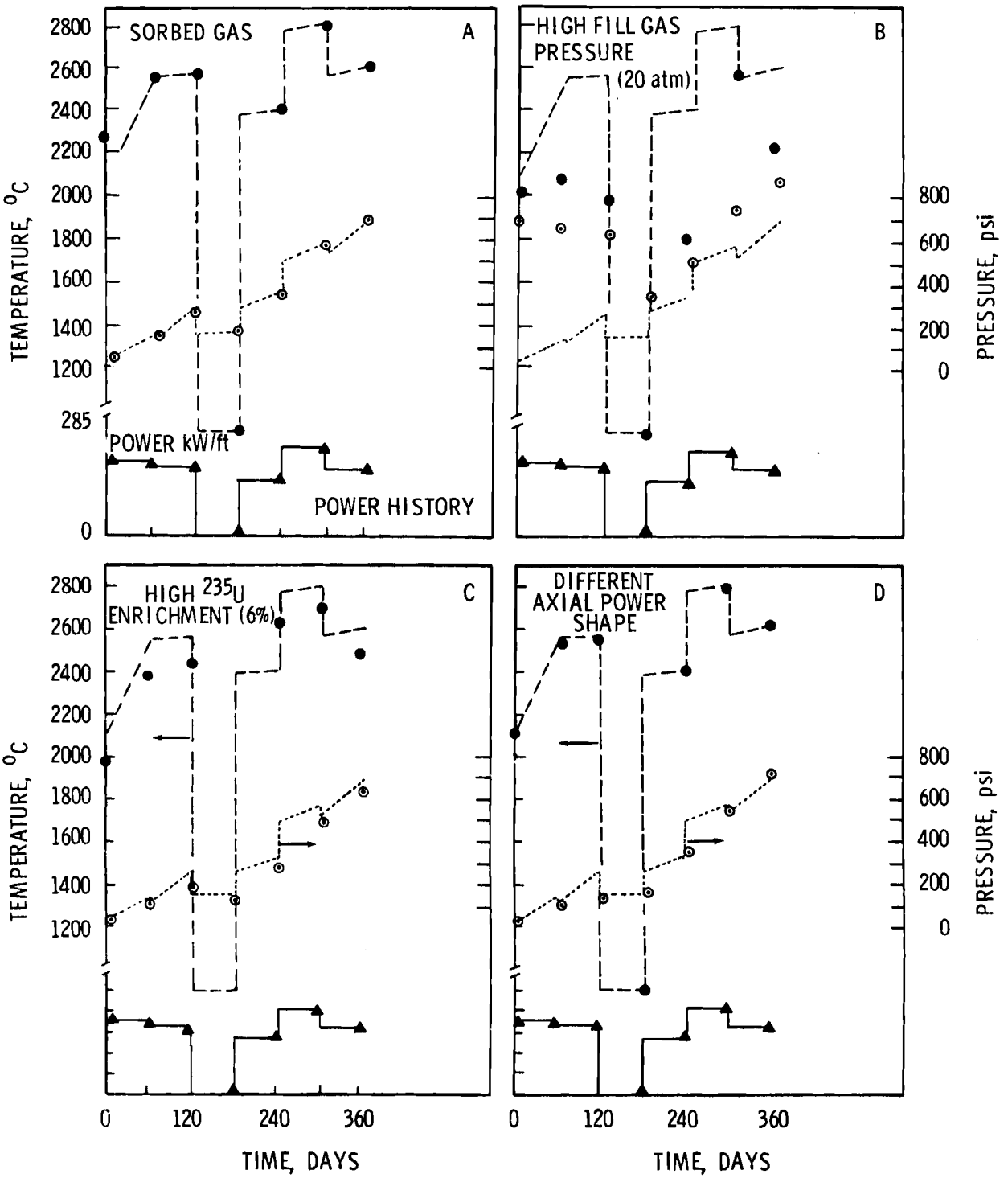

FIGURE 17. Parametric Study: Sorbed Gas, High Fill Gas Pressure, High U^{235} Enrichment, Different Axial Power Shape

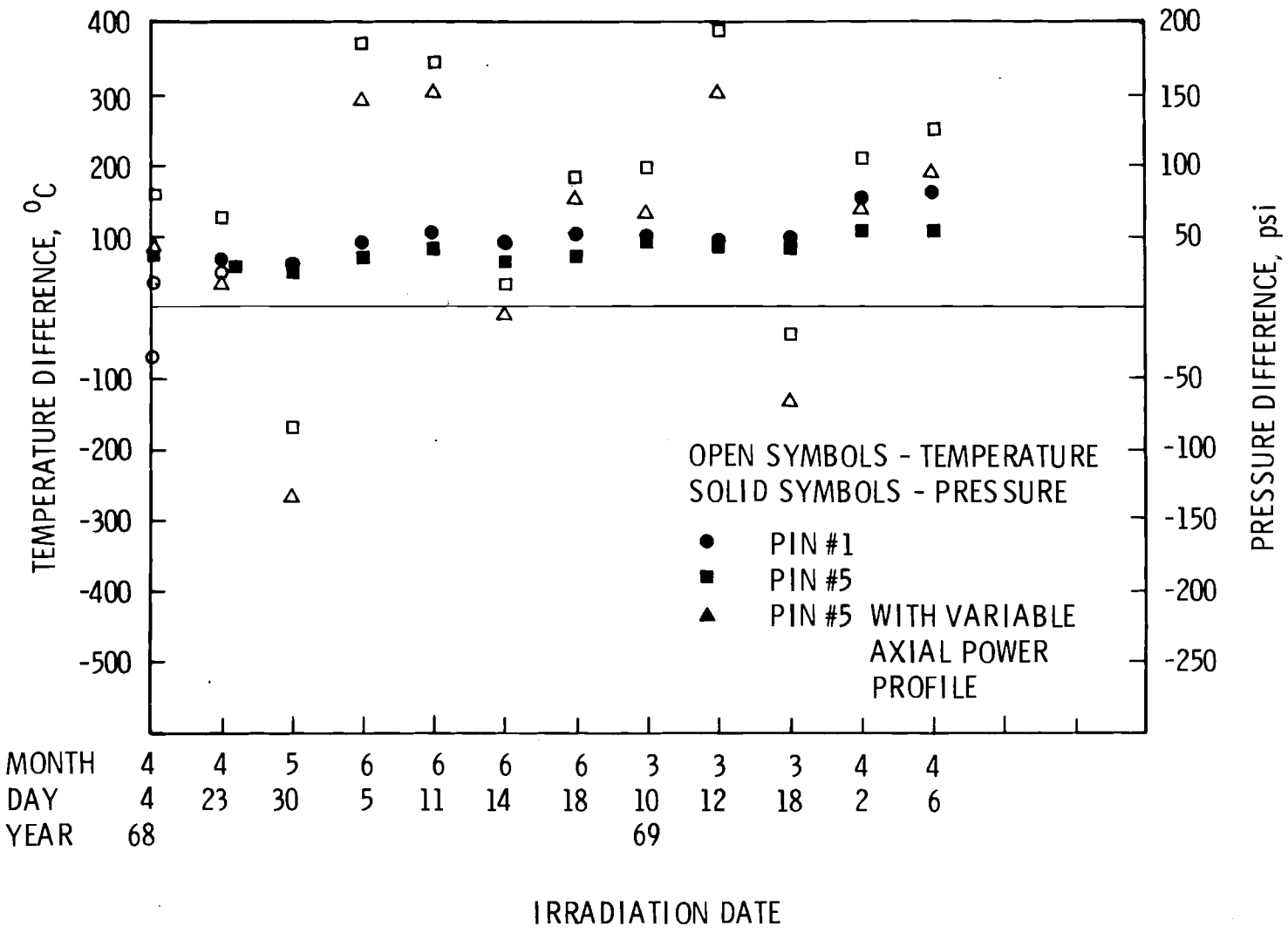

FIGURE 18. Difference Between GAPCON-THERMAL-2 Predictions and HPR-129, IFA-116 Experimental Data

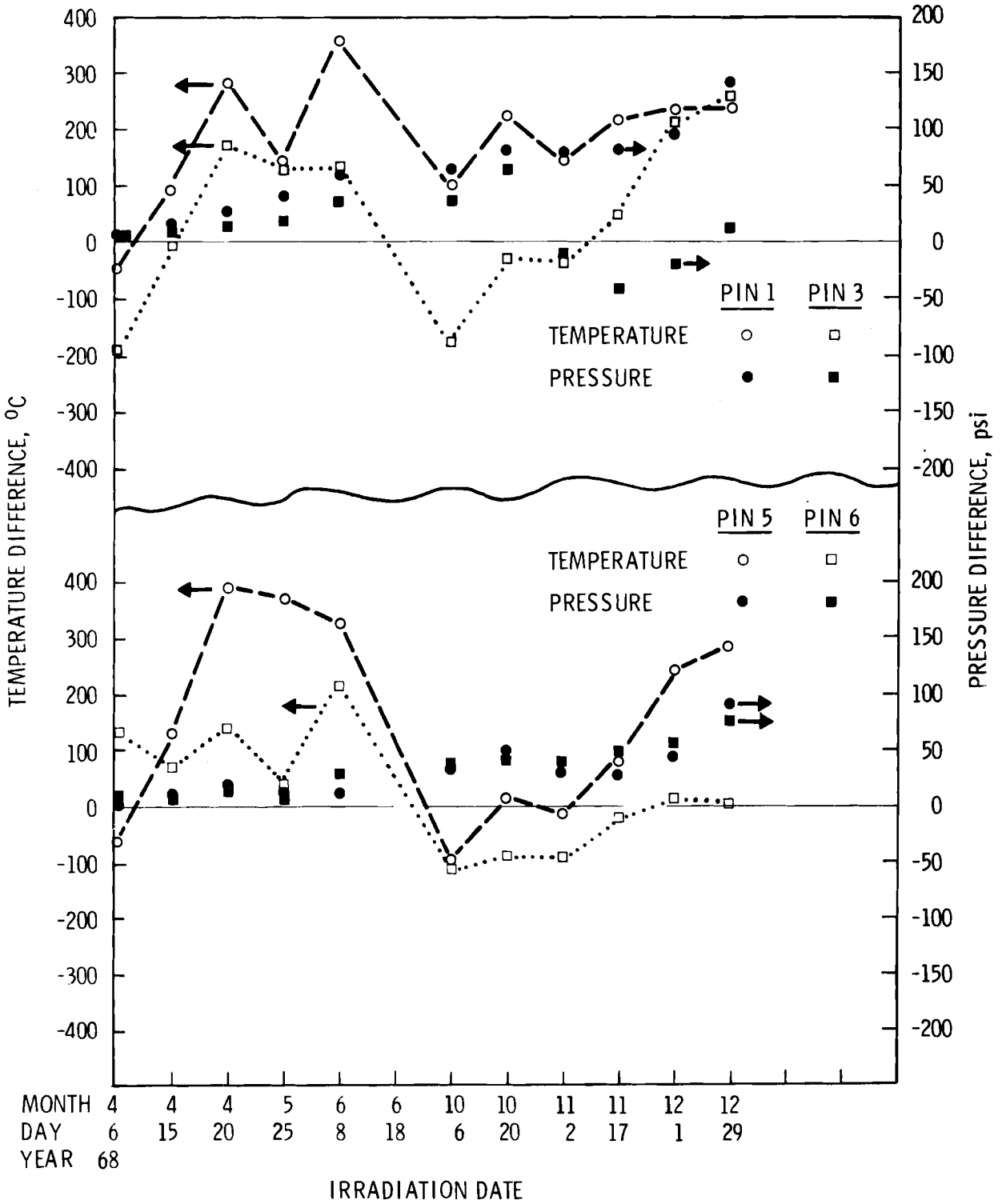

FIGURE 19. Difference Between GAPCON-THERMAL-2 Predictions and HPR-129, IFA-117 Experimental Data.

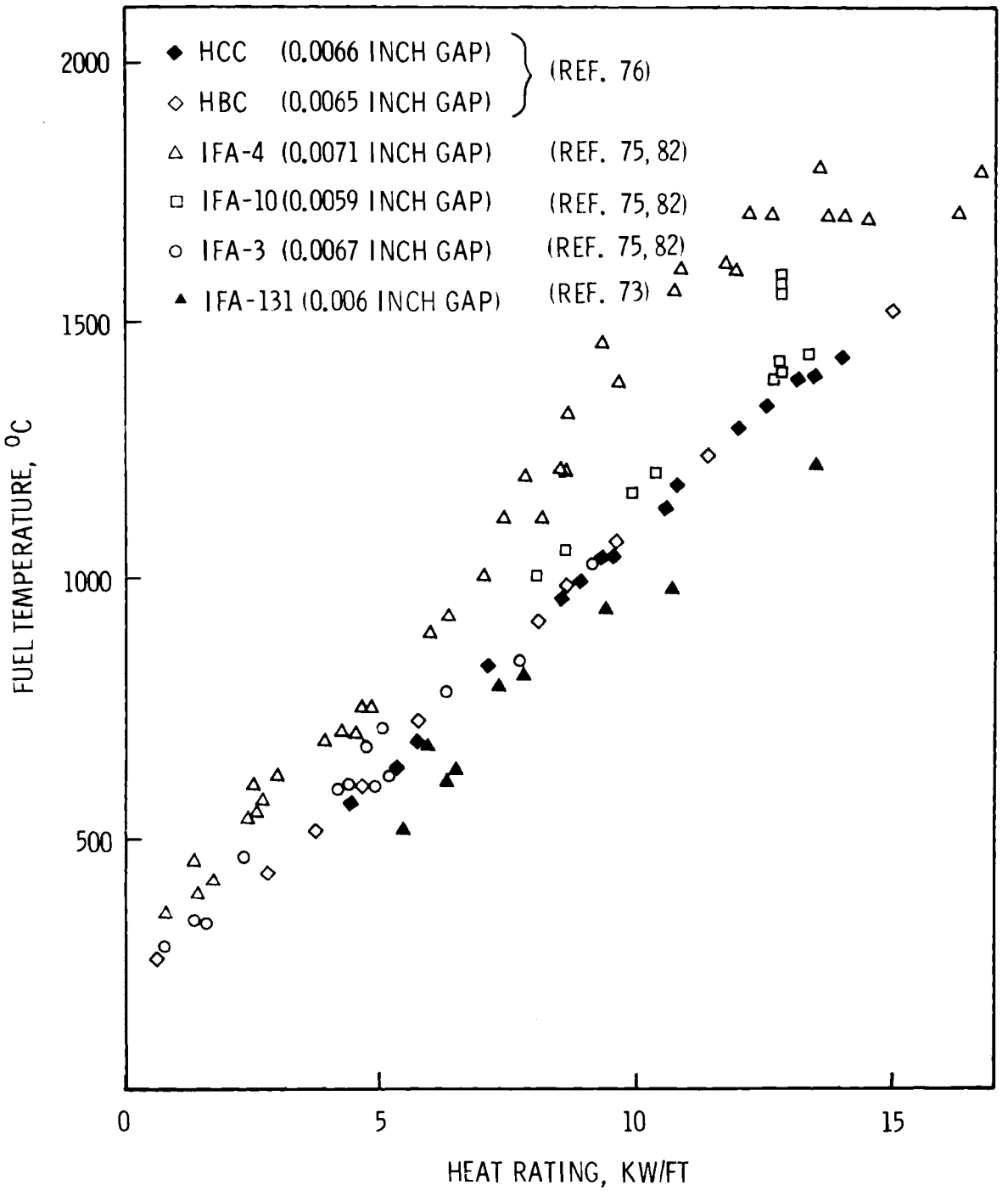

FIGURE 20. Fuel Temperatures Versus Heat Rating, Experimental Data From Various Irradiation Tests in Halden Reactor.

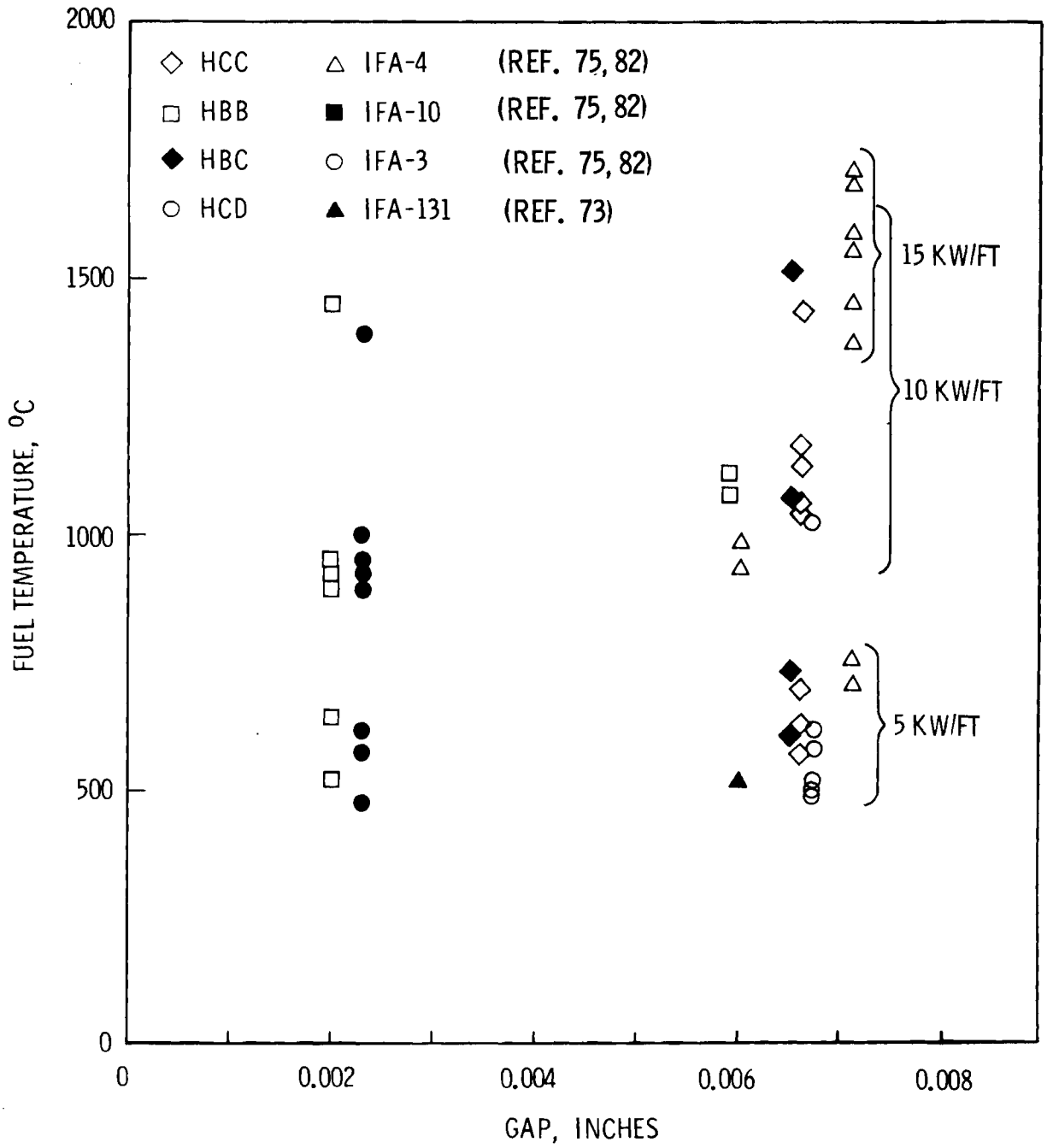

FIGURE 21. Fuel Temperatures Versus Fabricated Gap Size, Experimental Data From Various Irradiation Tests in Halden Reactor.

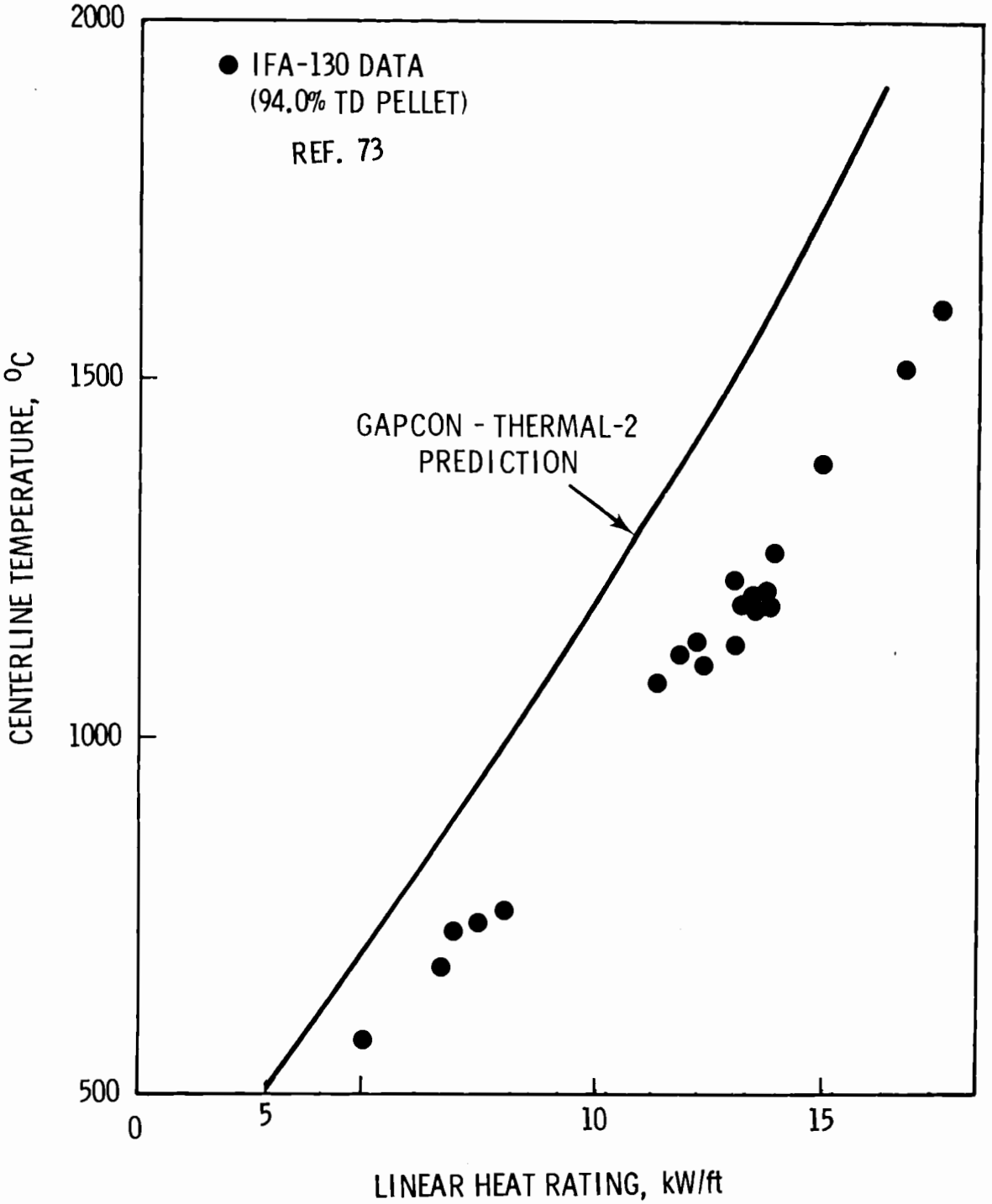

FIGURE 22. GAPCON-THERMAL-2 Predictions of IFA-130.

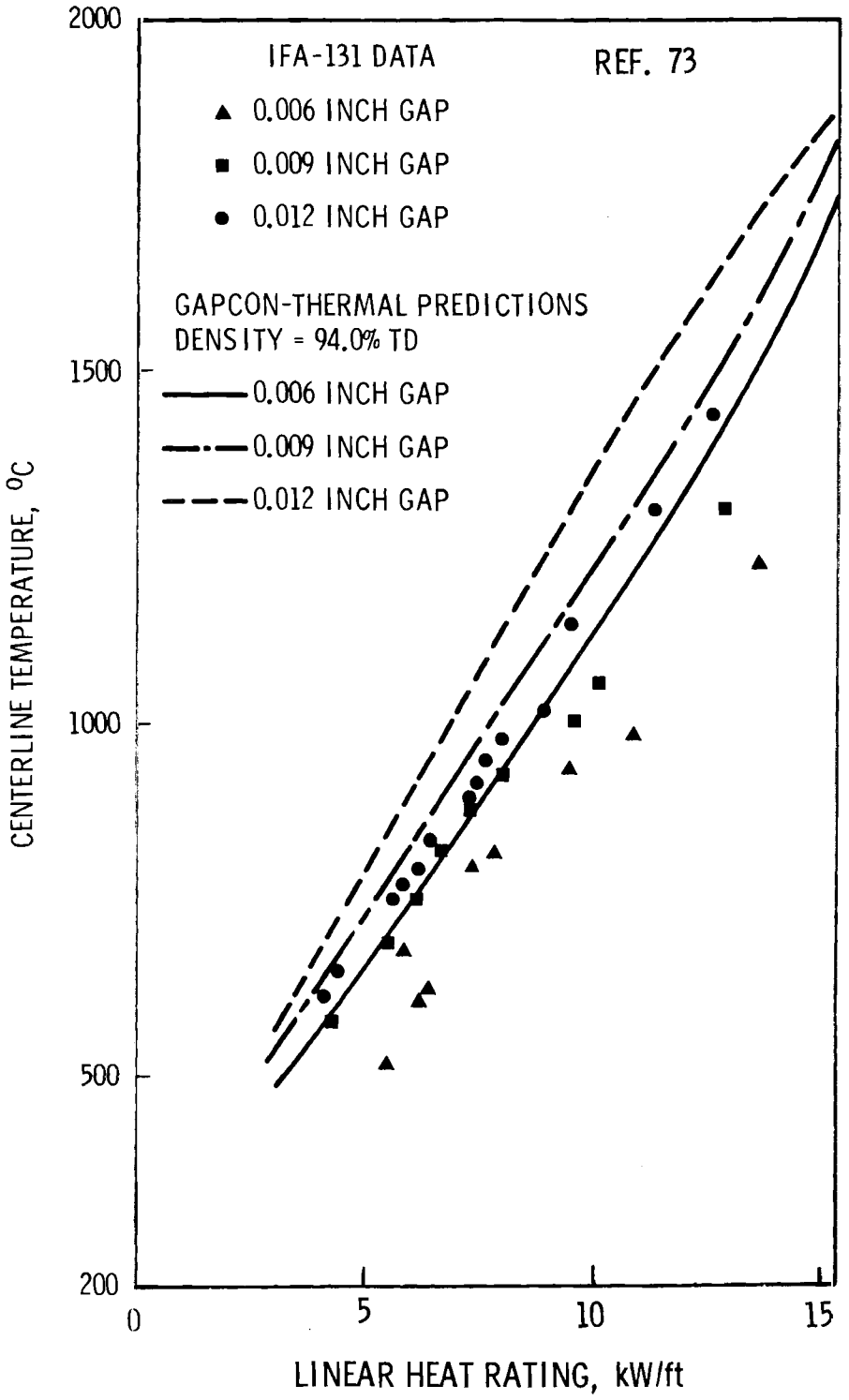

FIGURE 23. GAPCON-THERMAL-2 Predictions of IFA-131.

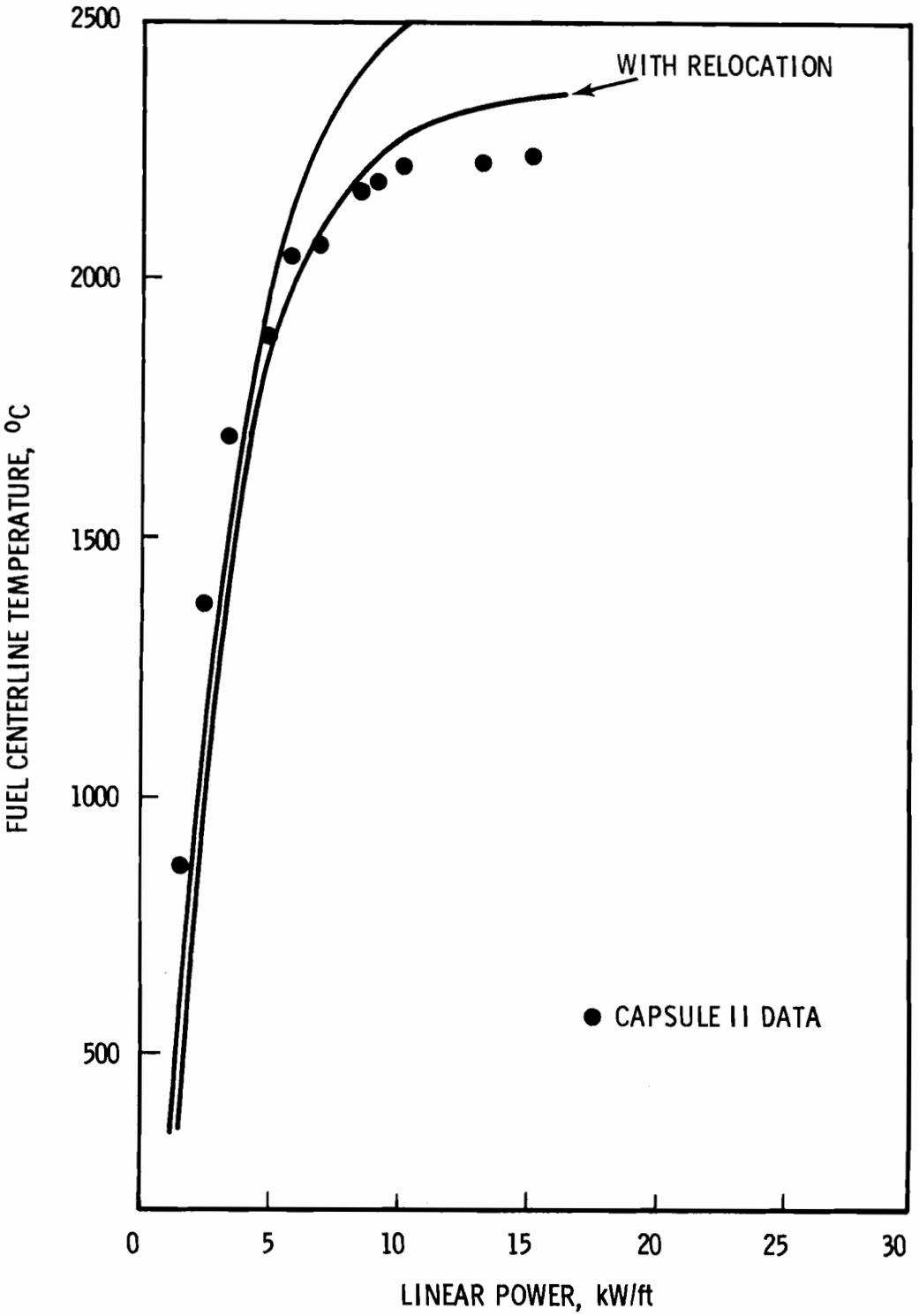

FIGURE 24. GAPCON-THERMAL-2 Predictions of Capsule II, WCAP 2923

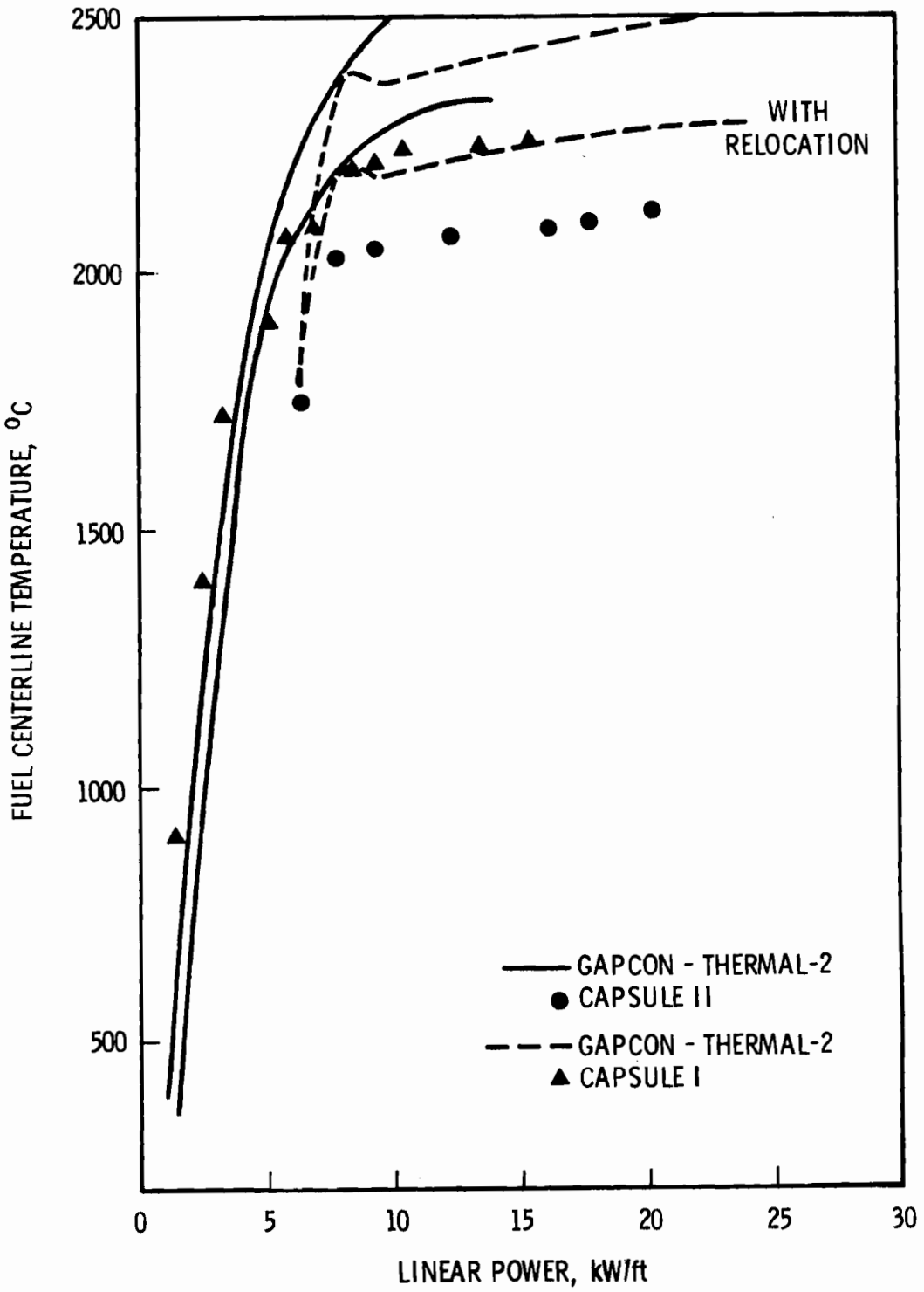

FIGURE 25. GAPCON-THERMAL-2 Predictions of Capsules I and II, WCAP 2923

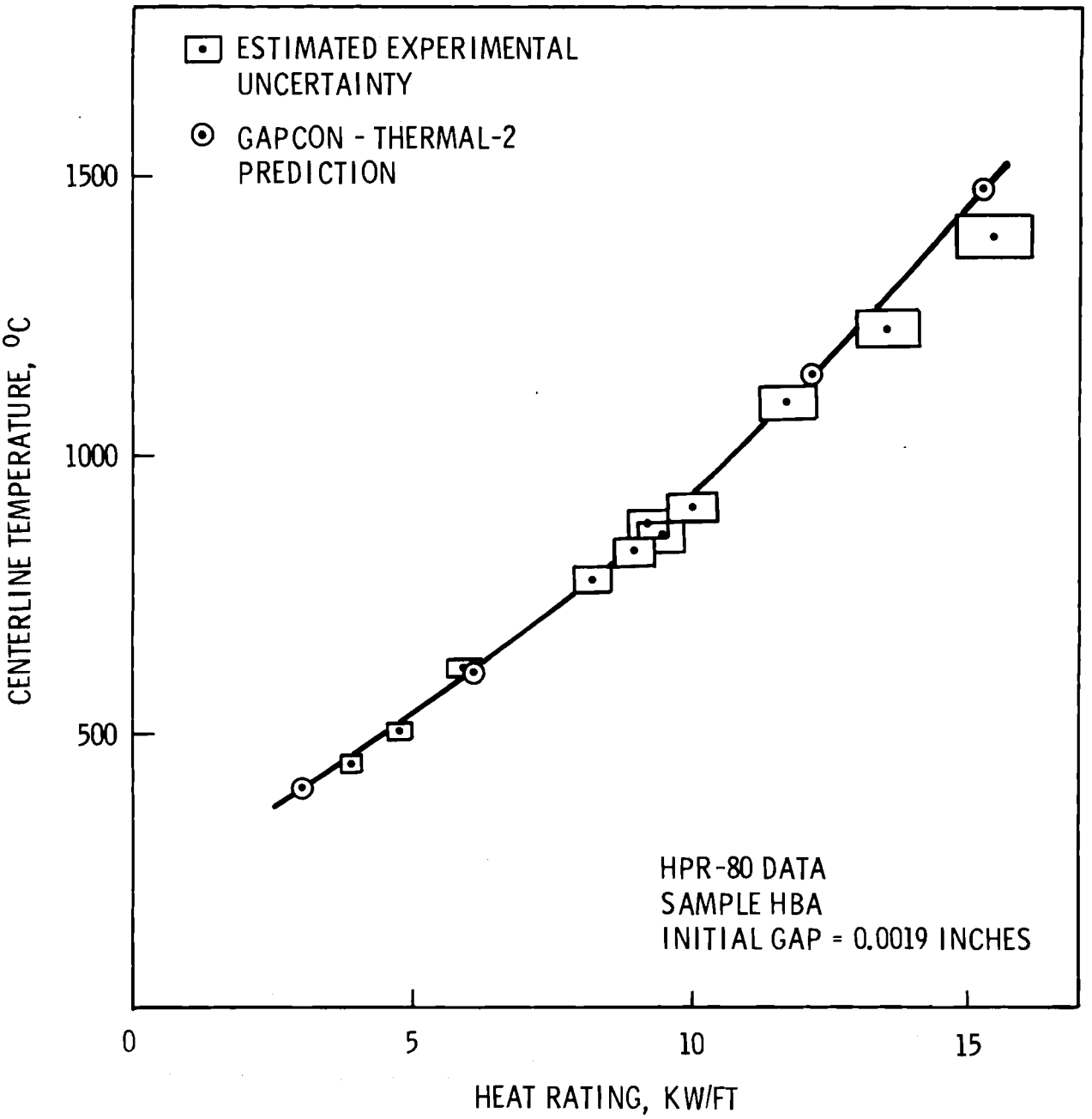

FIGURE 26. GAPCON-THERMAL-2 Prediction of Sample HBA, HPR-80.[76]

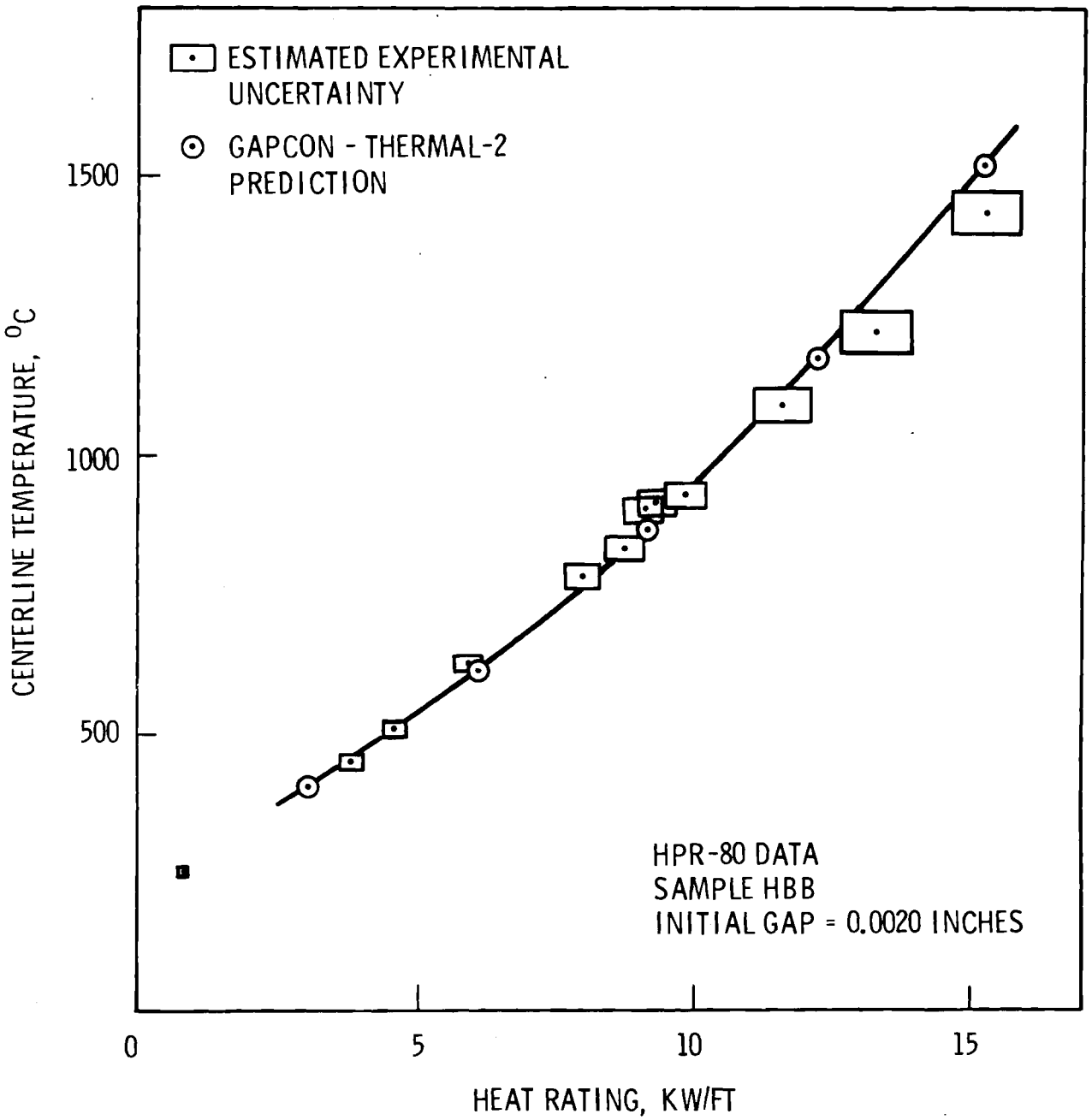

FIGURE 27. GAPCON-THERMAL-2 Prediction of Sample HBB, HPR-80.

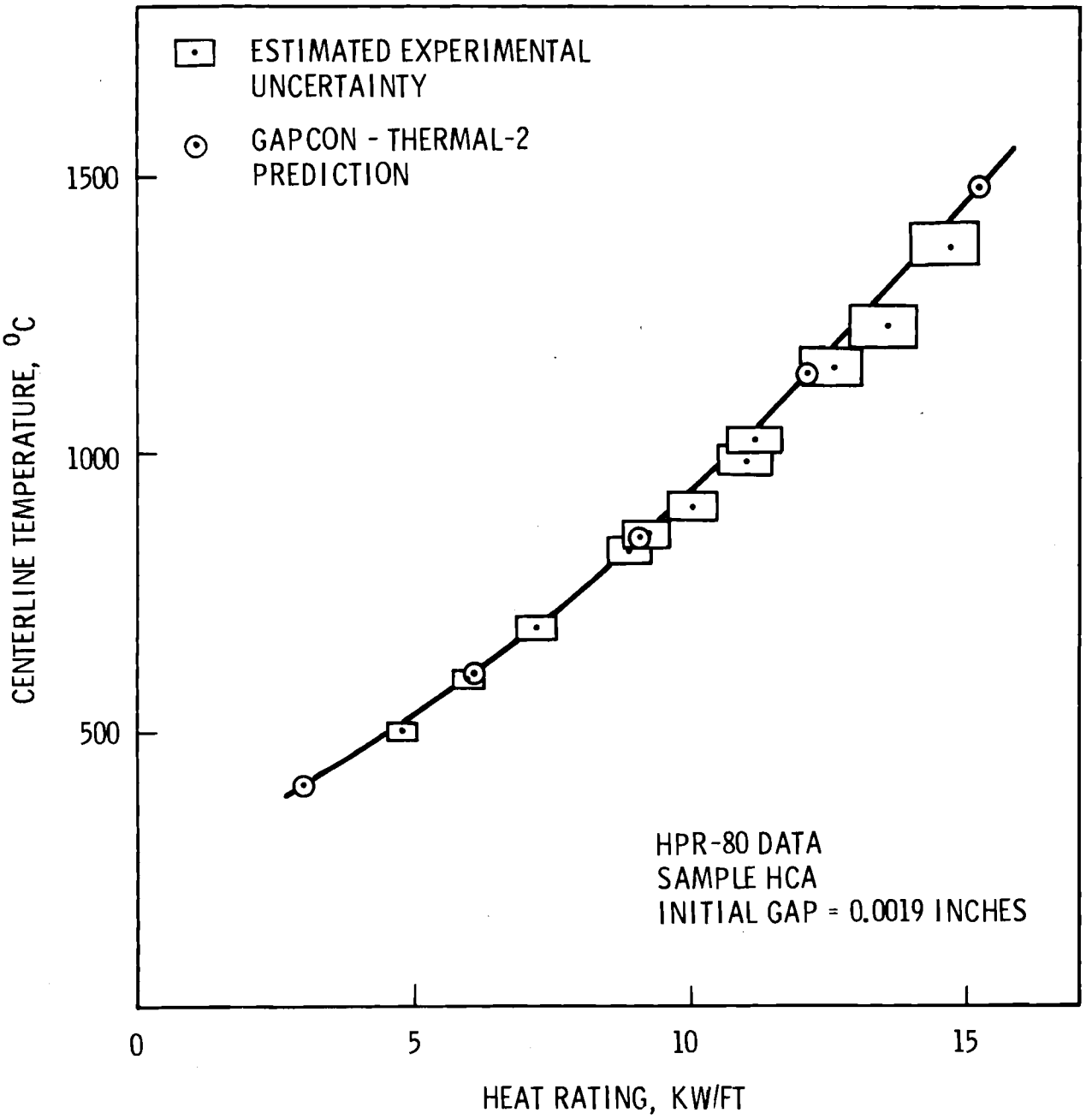

FIGURE 28. GAPCON-THERMAL-2 Prediction of Sample HCA, HPR-80.

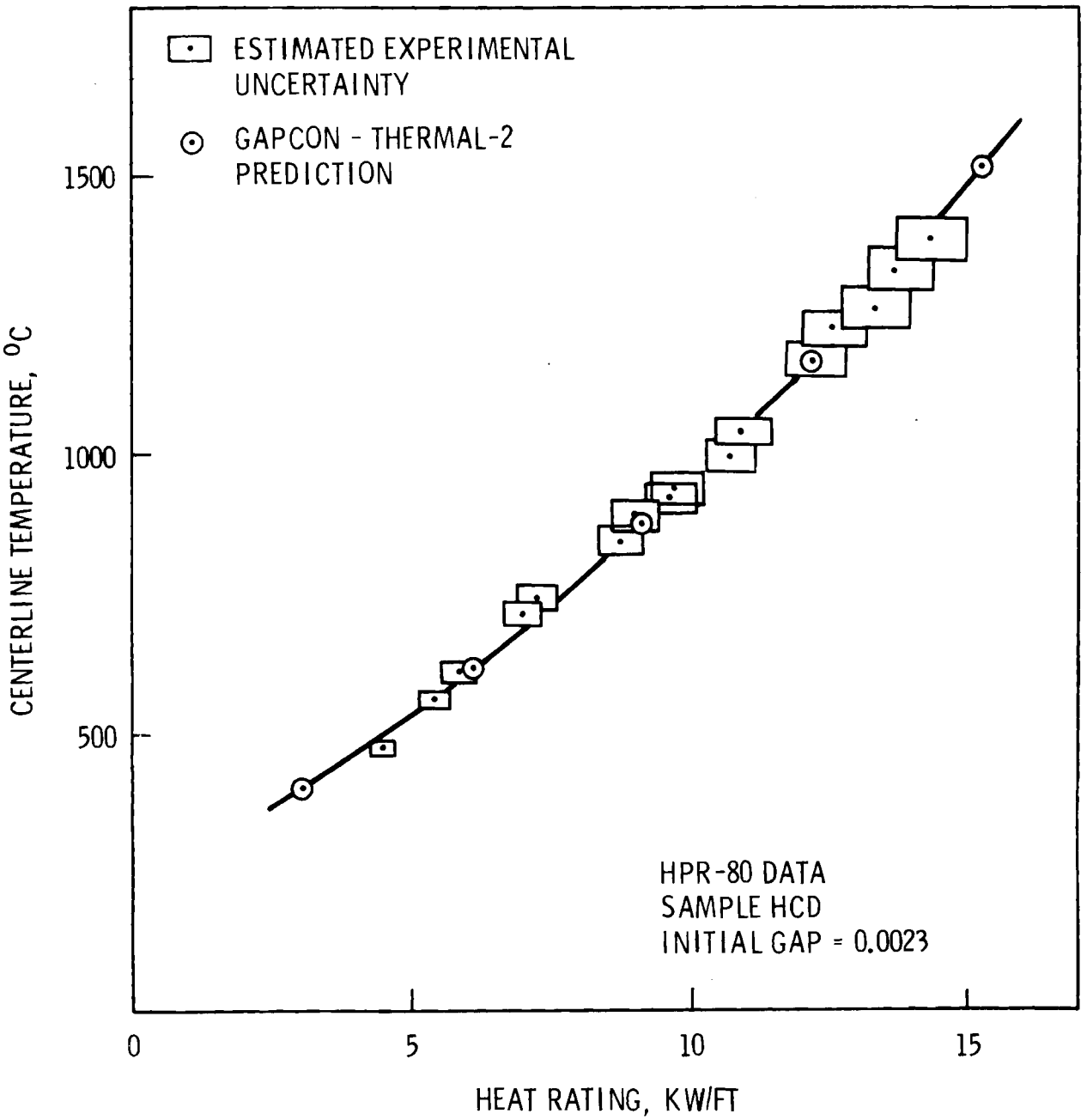

FIGURE 29. GAPCON-THERMAL-2 Prediction of Sample HCD, HPR-80.

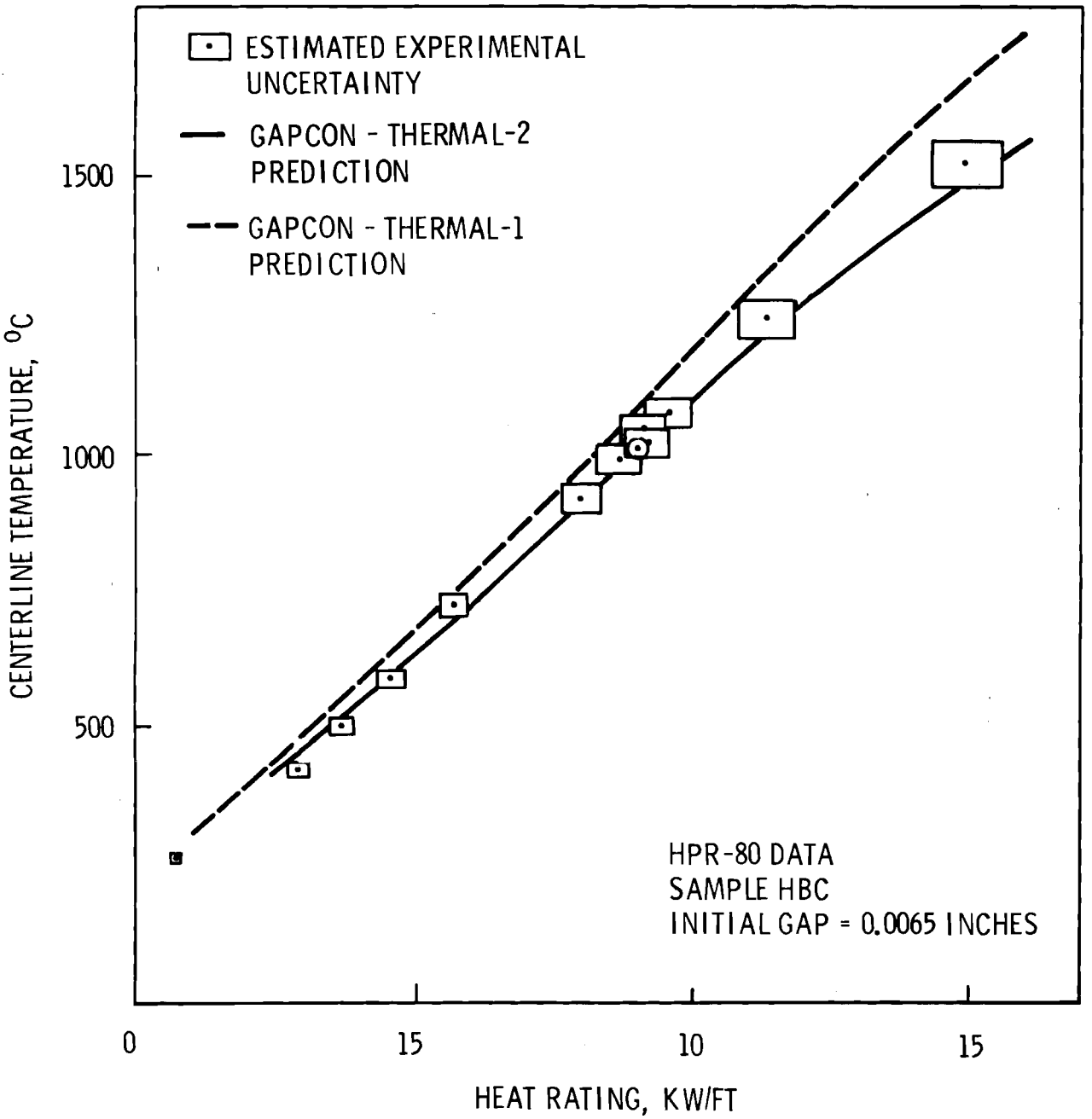

FIGURE 30. GAPCON-THERMAL-2 Prediction of Sample HBC, HPR-80.

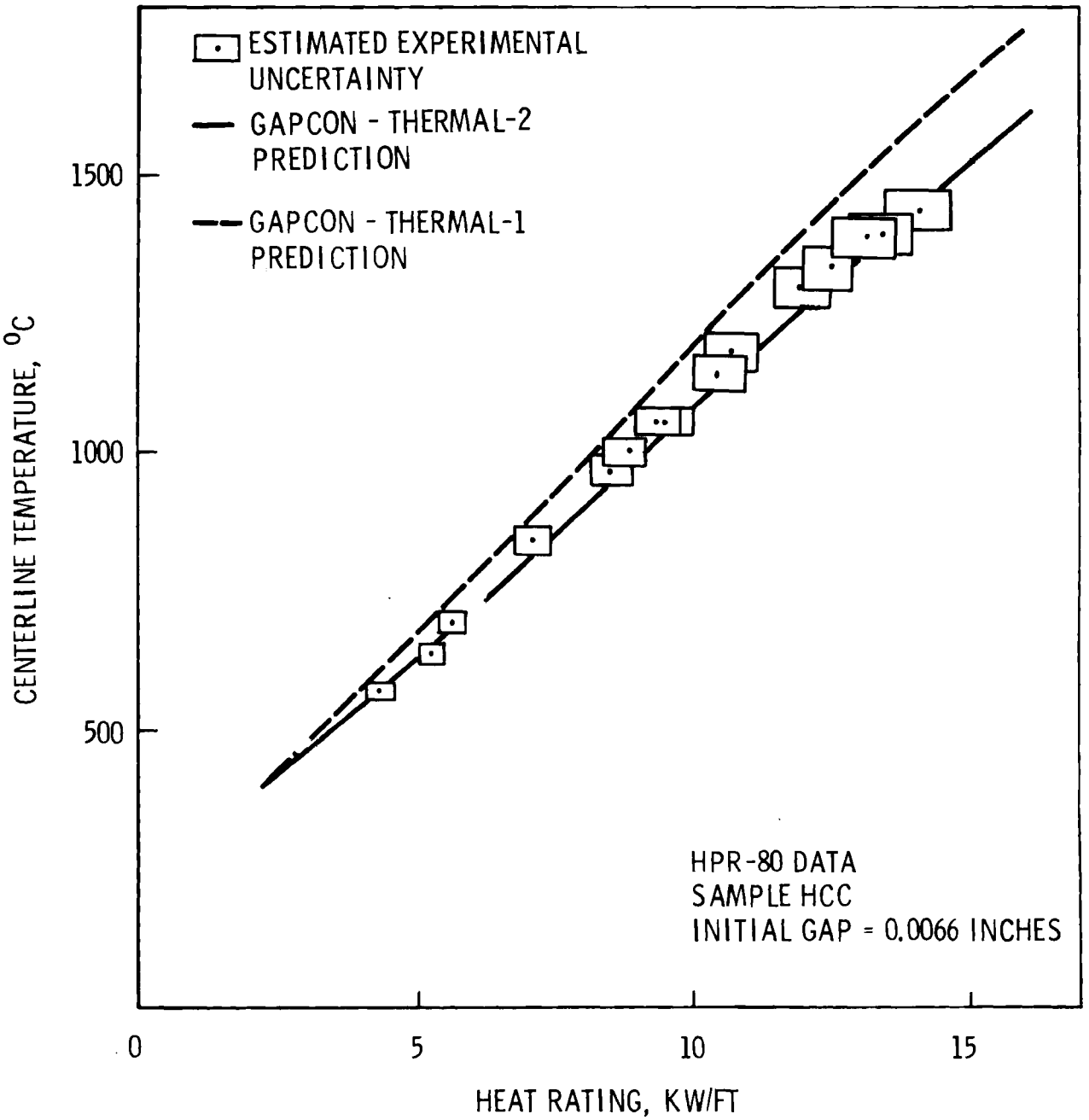

FIGURE 31. GAPCON-THERMAL-2 Prediction of Sample HCC, HPR-80.

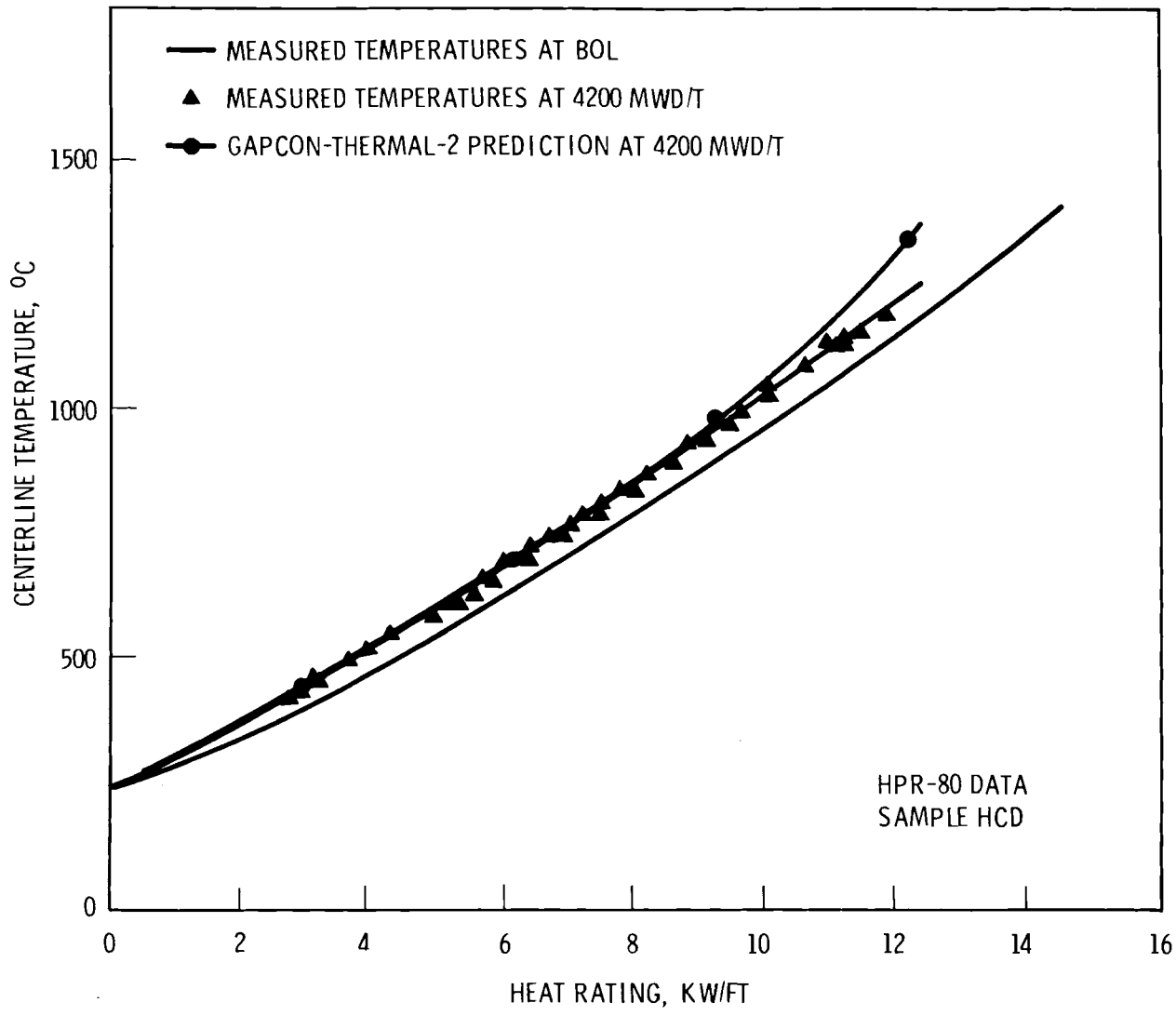

FIGURE 32. GAPCON-THERMAL-2 Prediction of Fuel Centerline Temperature Versus Linear Heat Rating for Sample HCD1, HPR-80.

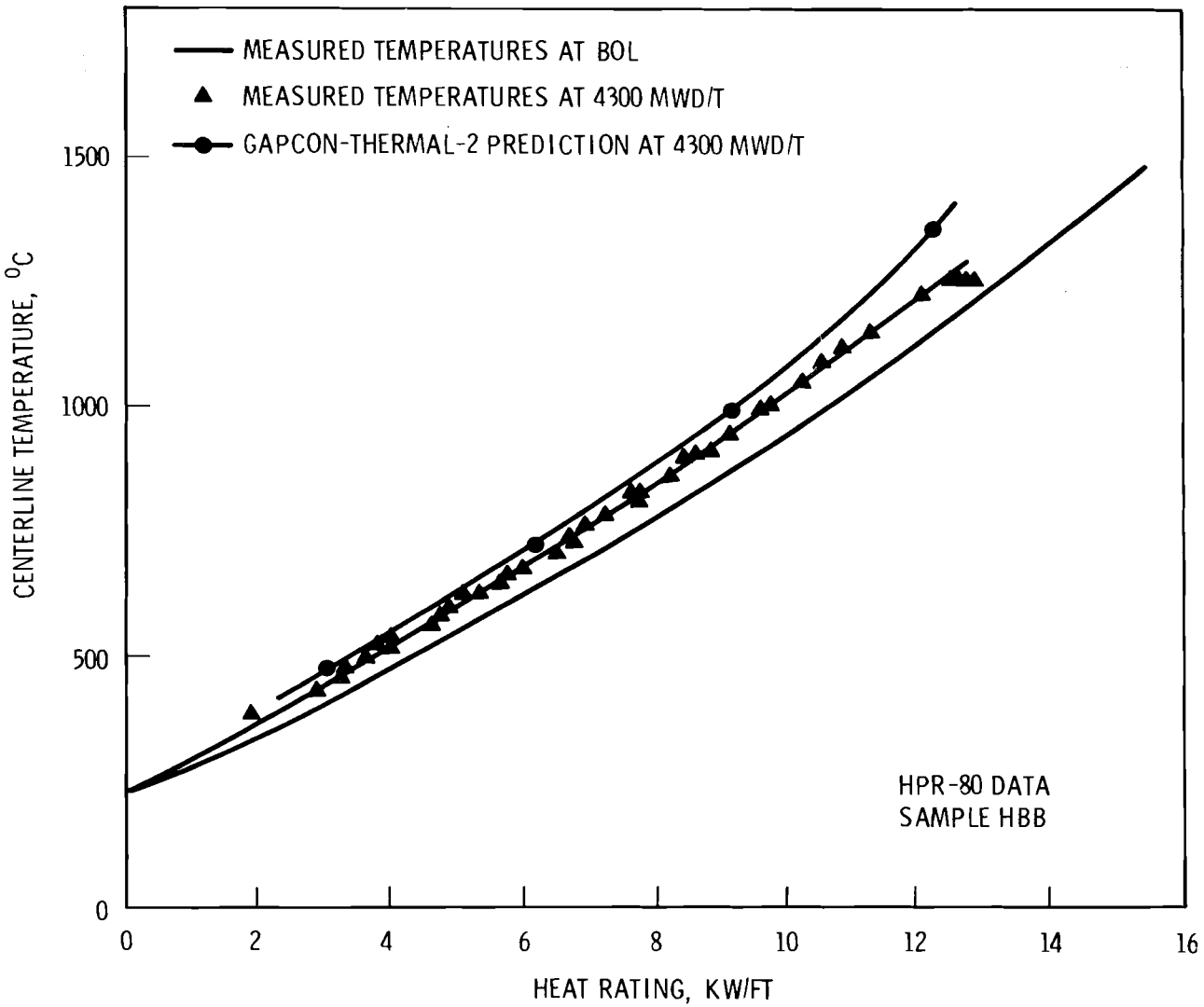

FIGURE 33. GAPCON-THERMAL-2 Prediction of Fuel Centerline Temperature Versus Heat Rating for Sample HBB, HPR-80.

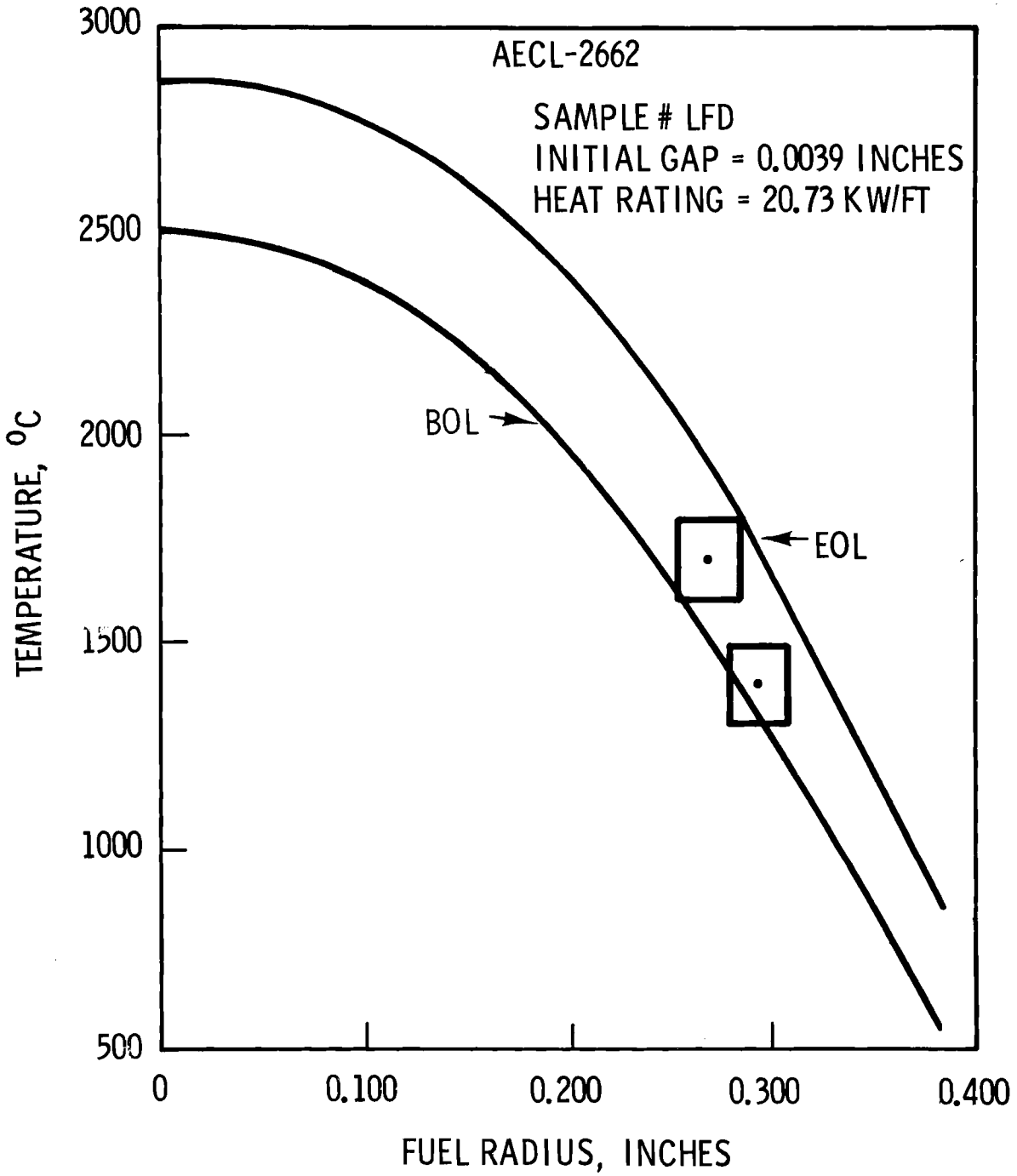

FIGURE 34. GAPCON-THERMAL-2 Prediction of Fuel Radial Temperature Profile for Sample LFD, AECL-2662.

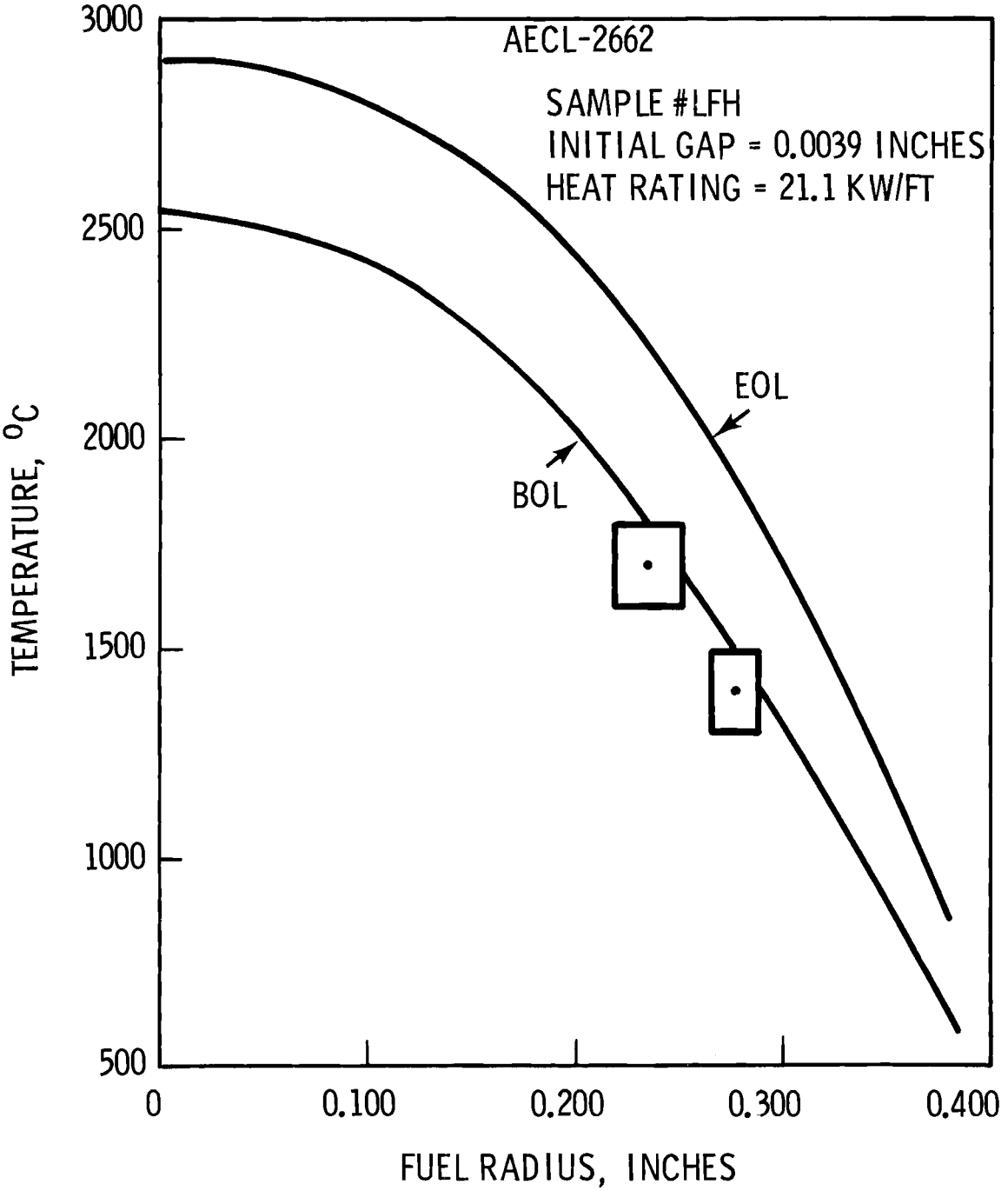

FIGURE 35. GAPCON-THERMAL-2 Prediction of Fuel Radial Temperature Profile for Sample LFH, AECL-2662.

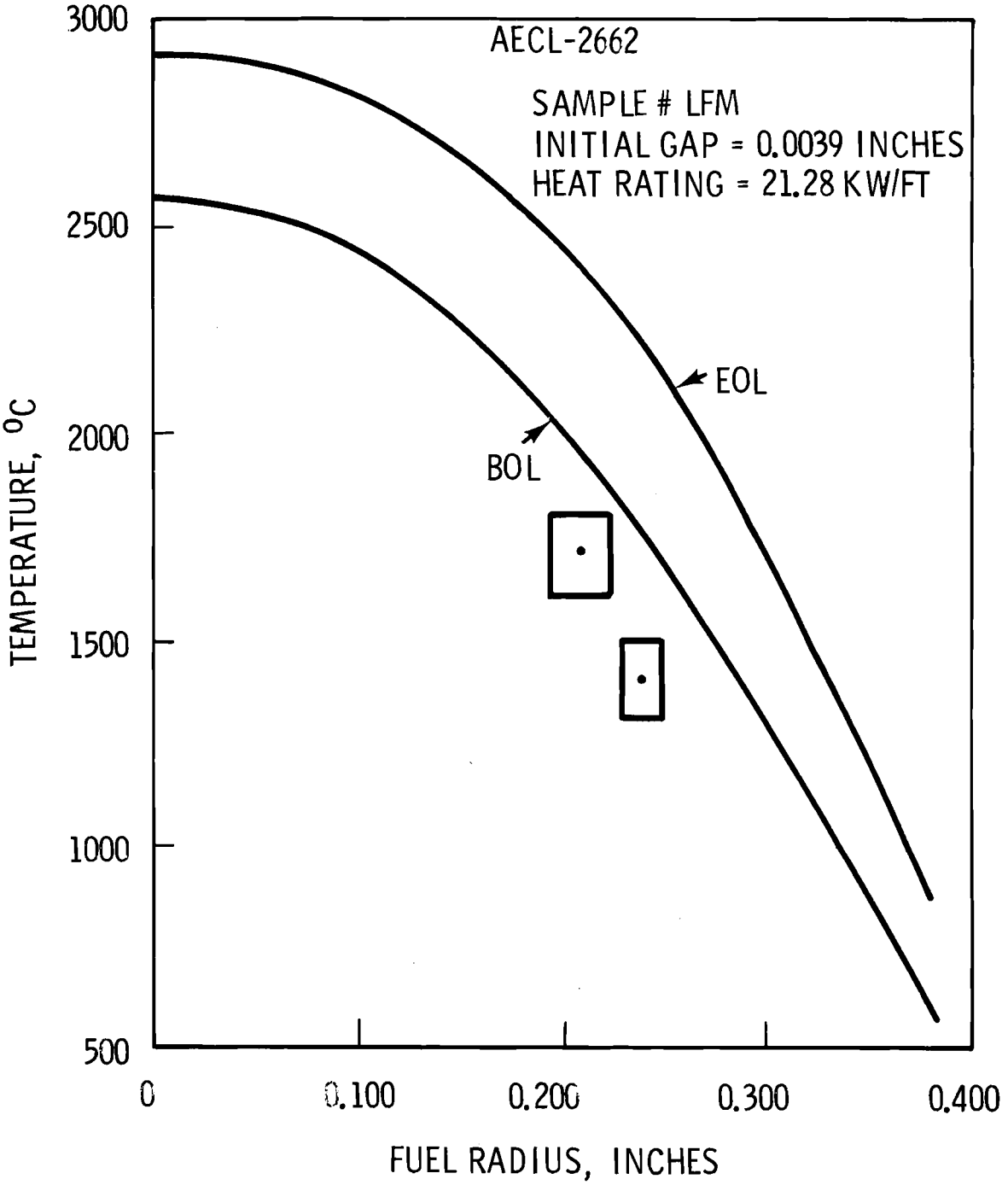

FIGURE 36. GAPCON-THERMAL-2 Prediction of Fuel Radial Temperature Profile for Sample LFM, AECL-2662.

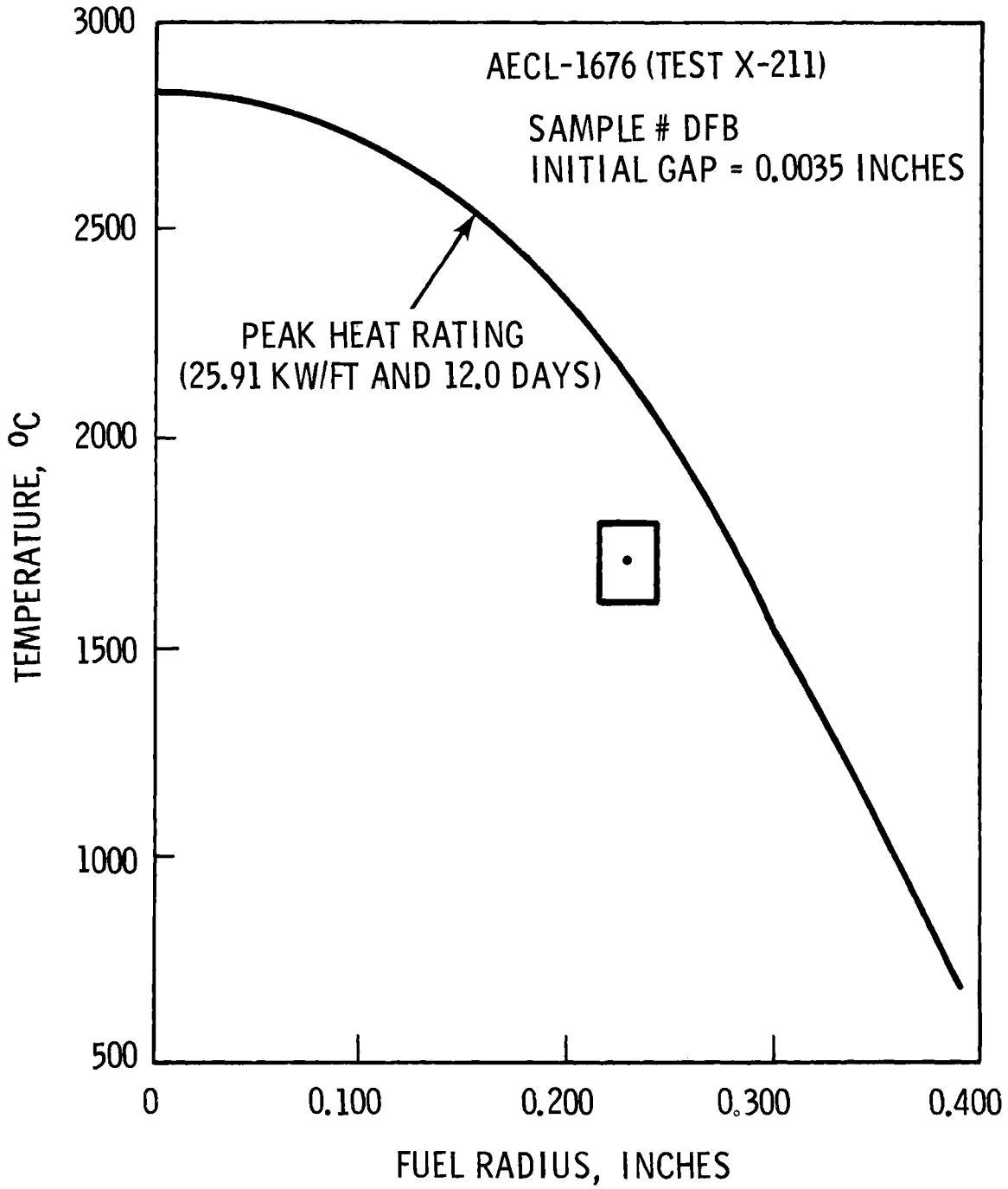

FIGURE 37. GAPCON-THERMAL-2 Prediction of Fuel Radial Temperature Profile for Sample DFB, AECL-1676.

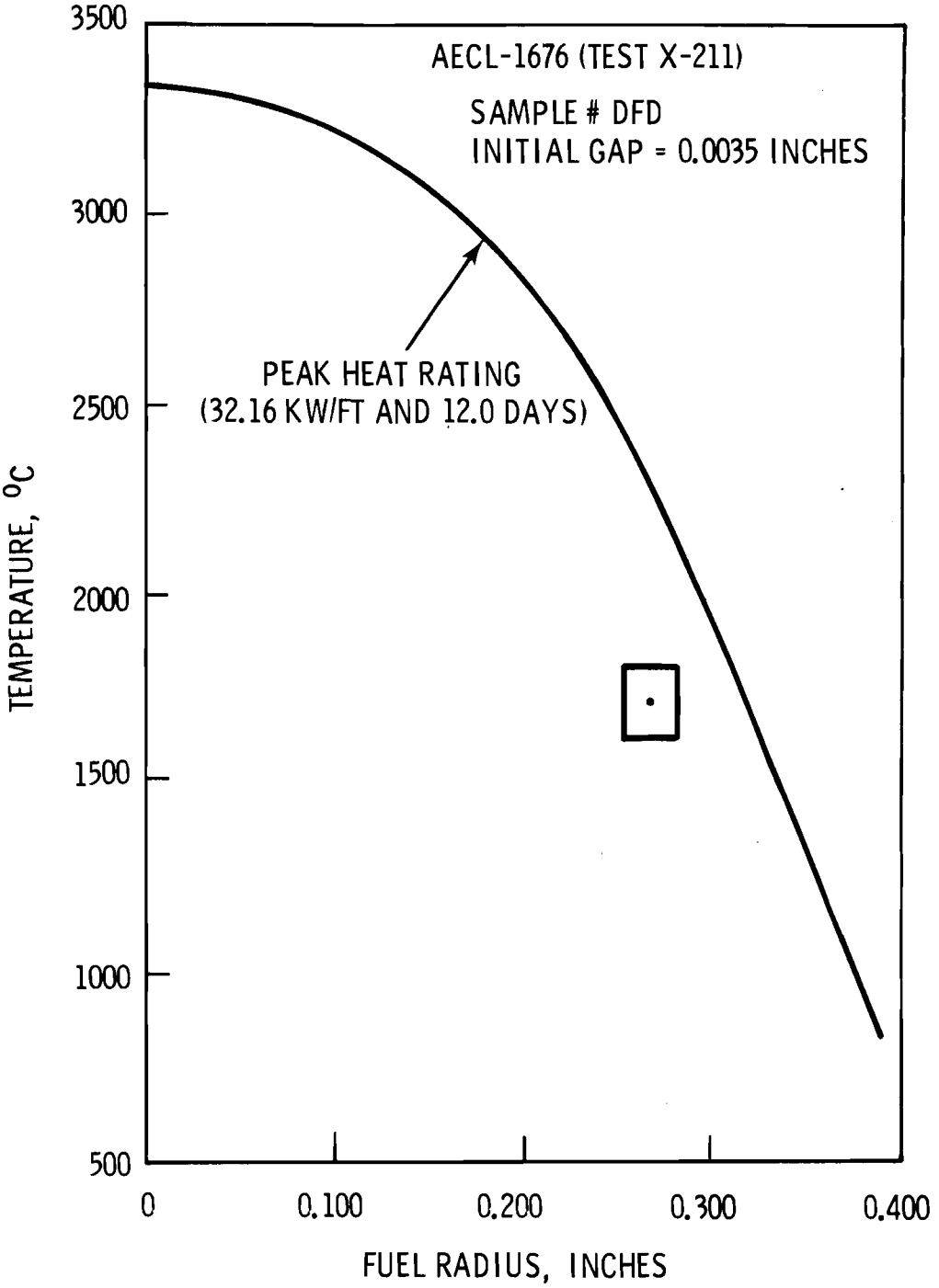

FIGURE 38. GAPCON-THERMAL-2 Prediction of Fuel Radial Temperature Profile for Sample DFD, AECL-1676.

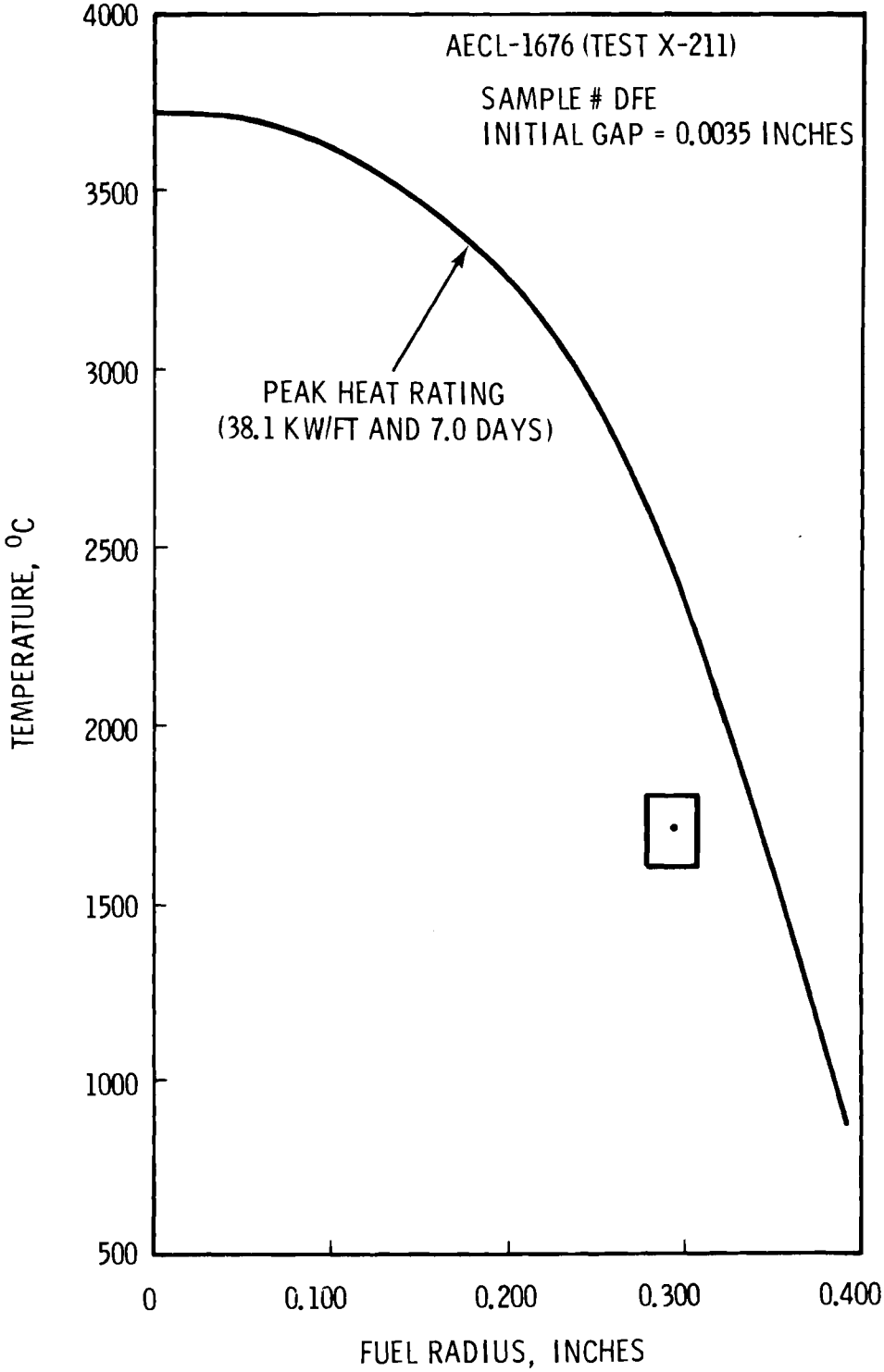

FIGURE 39. GAPCON-THERMAL-2 Prediction of Fuel Radial Temperature Profile for Sample DFE, AECL-1676.

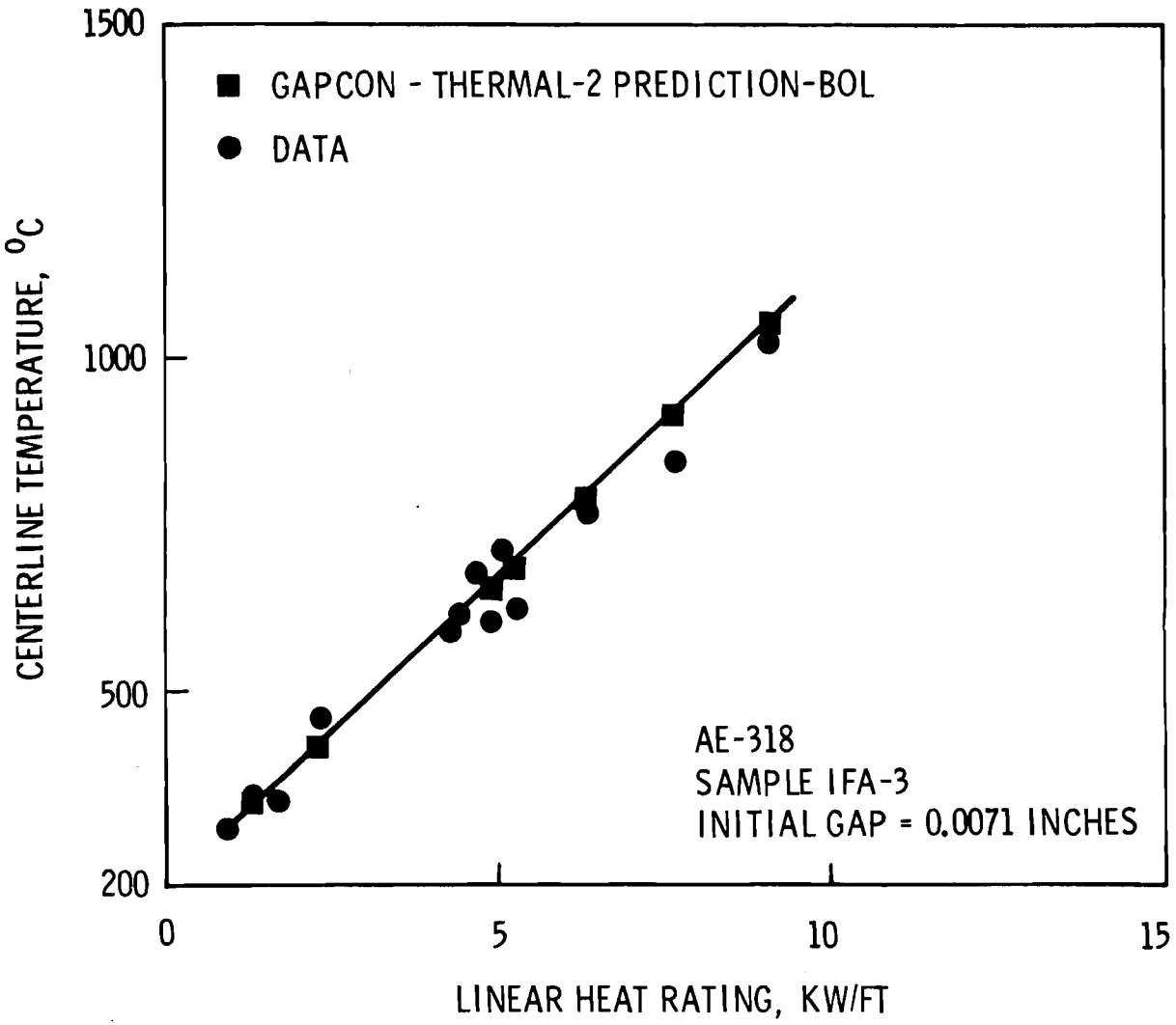

FIGURE 40. GAPCON-THERMAL-2 Prediction of Fuel Centerline Temperature Versus Linear Heat Rating for Sample IFA-3, AE-318.

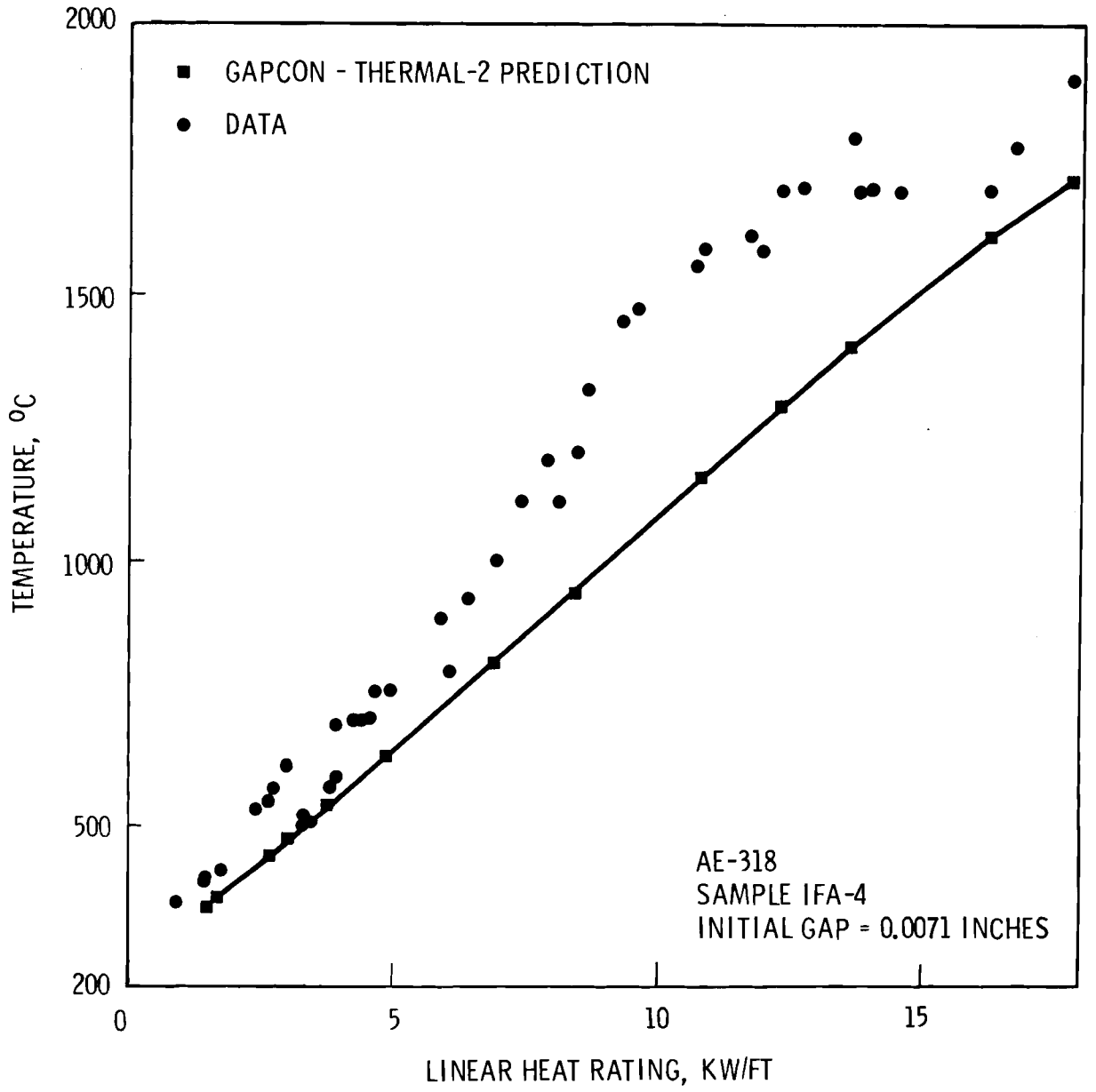

FIGURE 41. GAPCON-THERMAL-2 Prediction of Fuel Centerline Temperature Versus Linear Heat Rating for Sample IFA-4, AE-318.

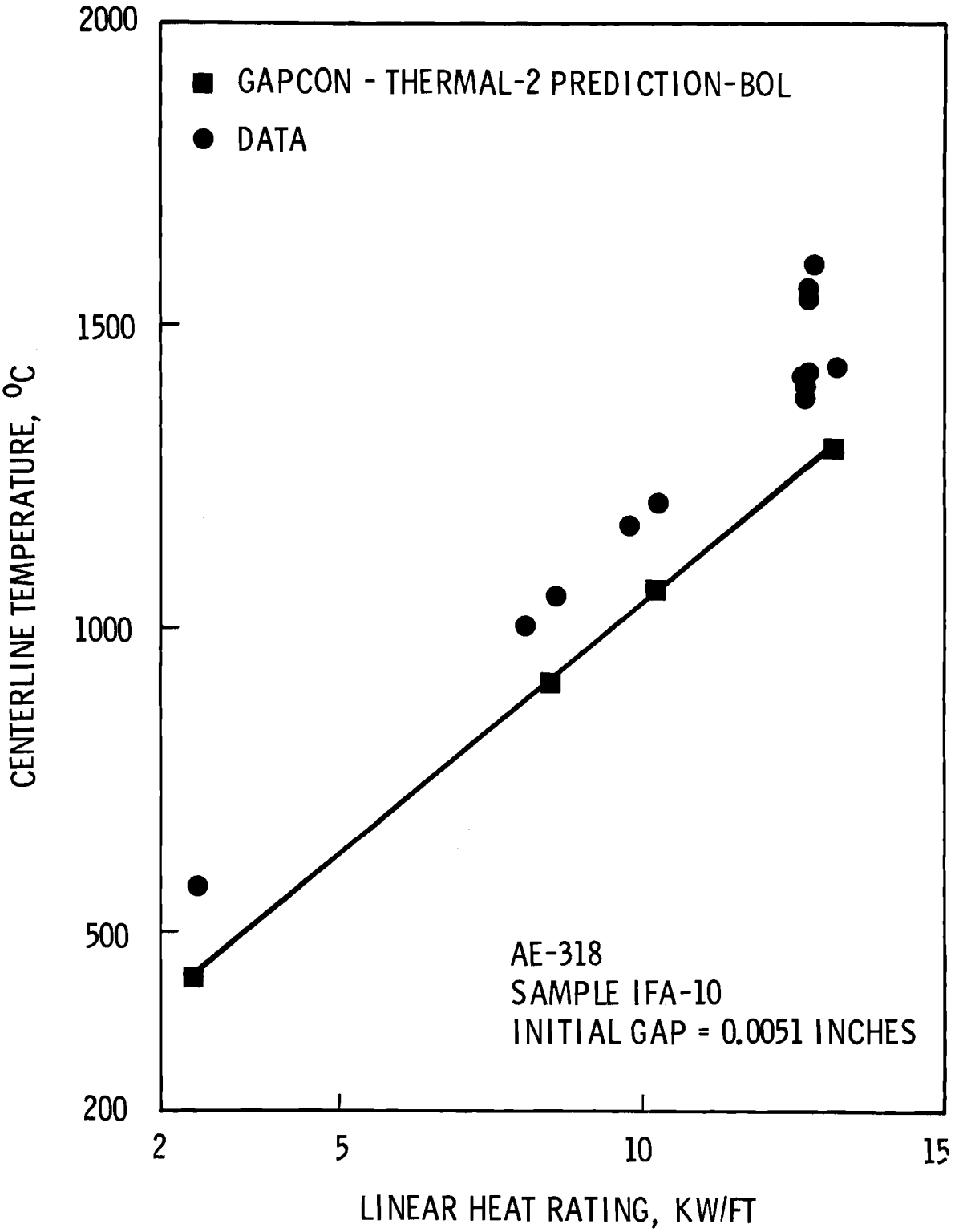

FIGURE 42. GAPCON-THERMAL-2 Prediction of Fuel Centerline Temperature Versus Linear Heat Rating for Sample IFA-10, AE-318.

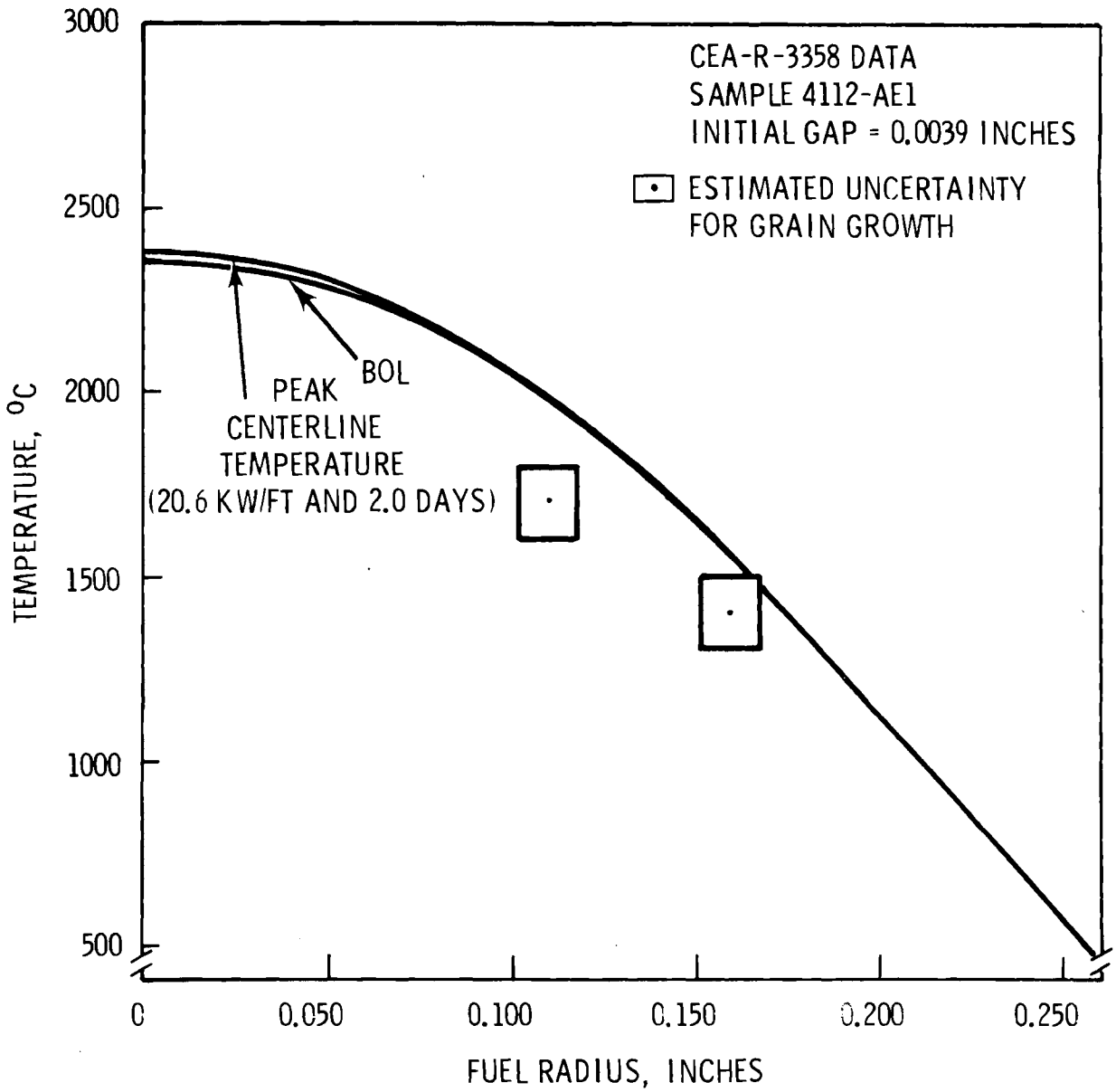

FIGURE 43. A Comparison of GAPCON-THERMAL-2 Predictions With Grain Growth Measurements from CEA-R-3358, Sample 4112-AE1.

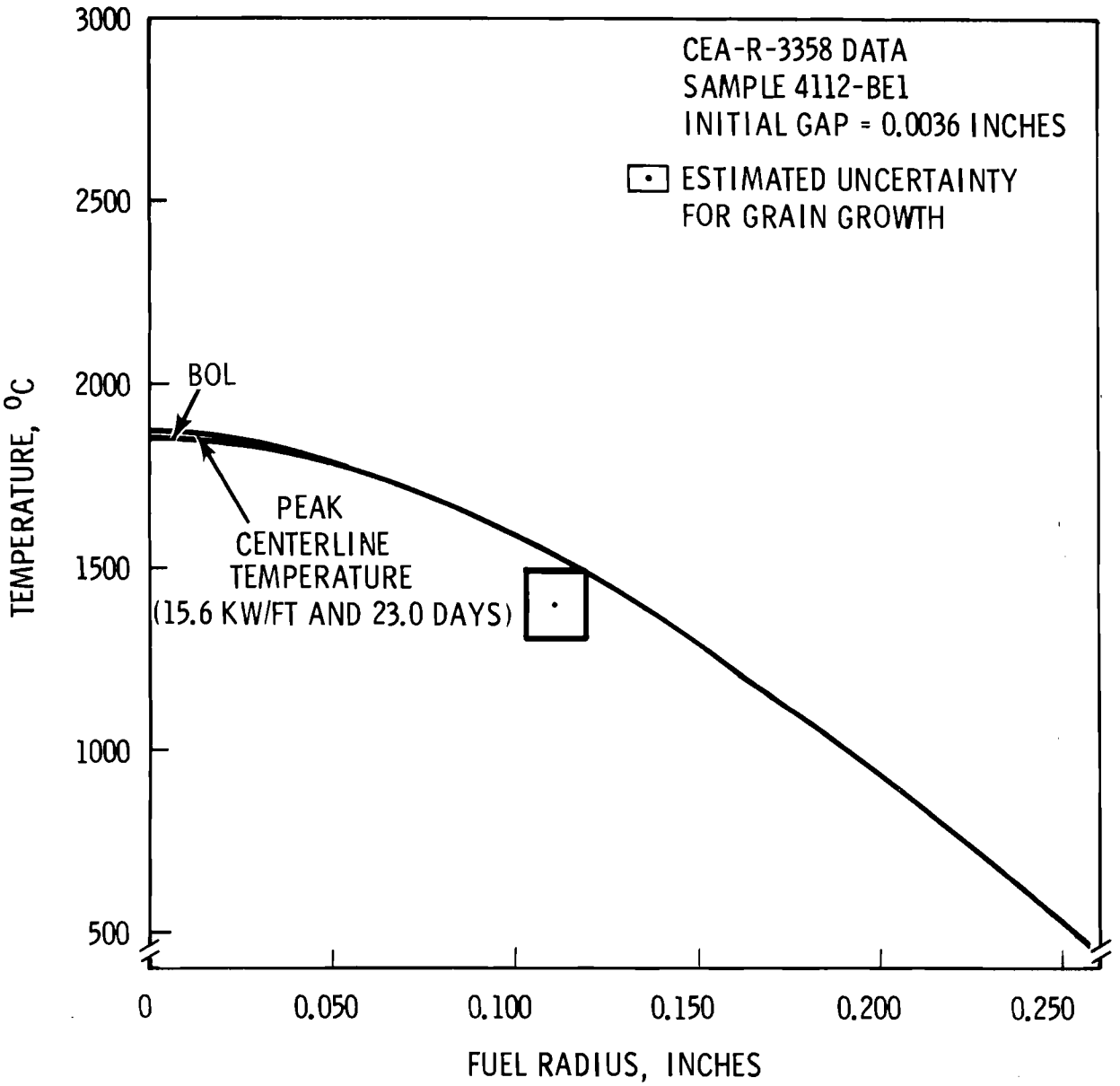

FIGURE 44. A Comparison of GAPCON-THERMAL-2 Predictions With Grain Growth Measurements from CEA-R-3358, Sample 4112-BE1.

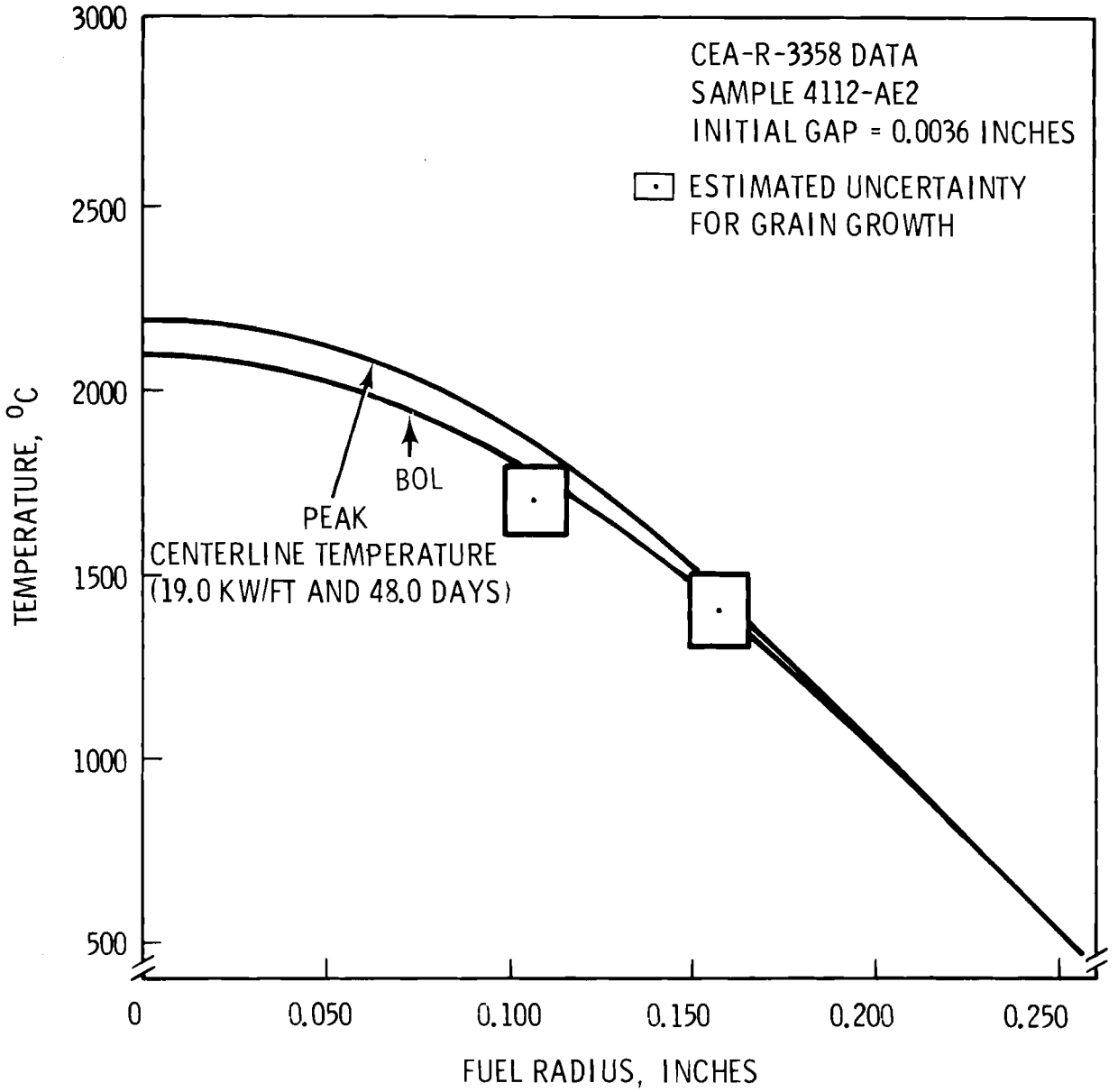

FIGURE 45. A Comparison of GAPCON-THERMAL-2 Predictions With Grain Growth Measurements from CEA-R-3358, Sample 4112-AE2

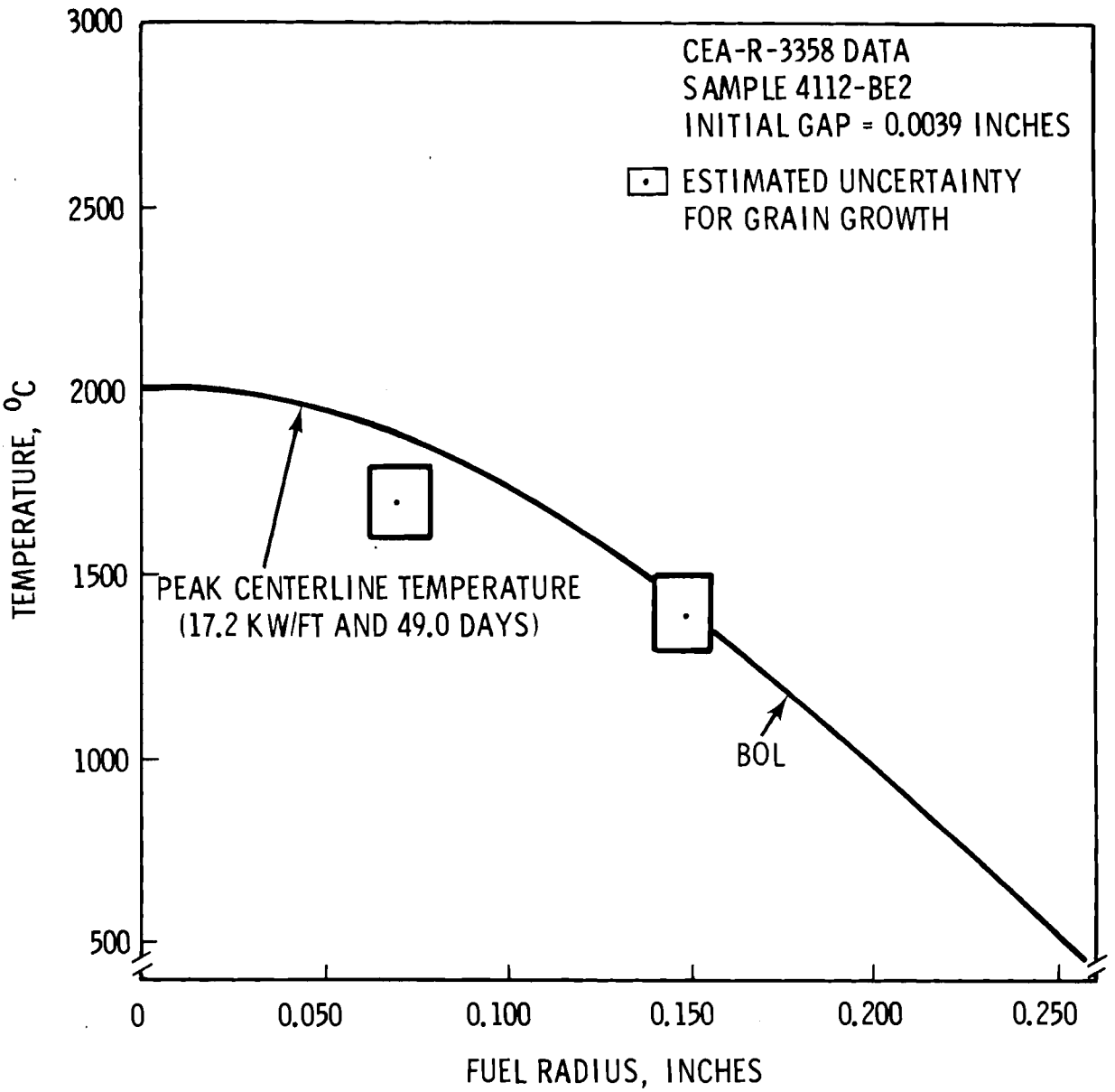

FIGURE 46. A Comparison of GAPCON-THERMAL-2 Predictions With Grain Growth Measurements from CEA-R-3358, Sample 4112-BE2

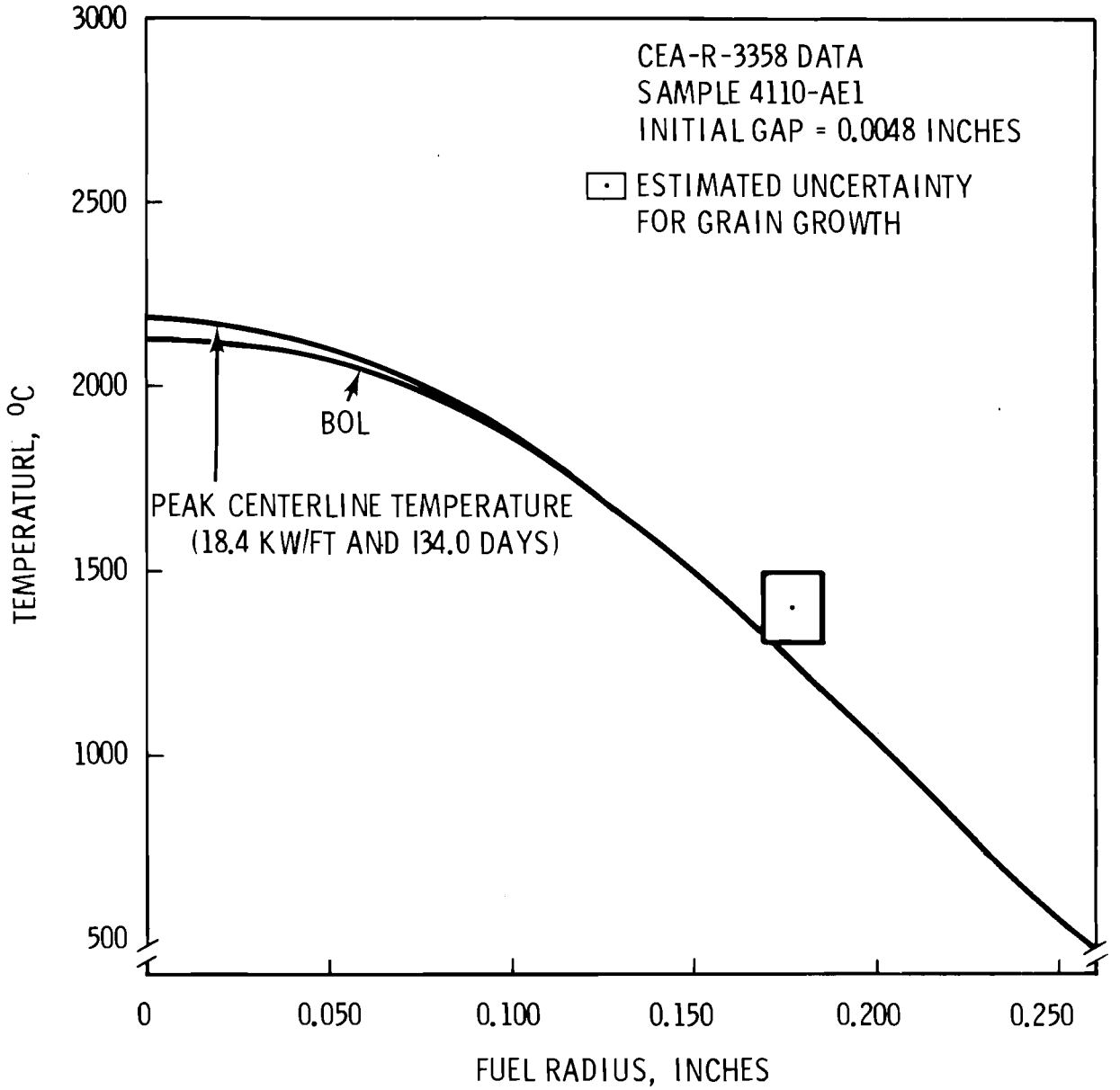

FIGURE 47. A Comparison of GAPCON-THERMAL-2 Predictions With Grain Growth Measurements from CEA-R-3358, Sample 4110-AE1

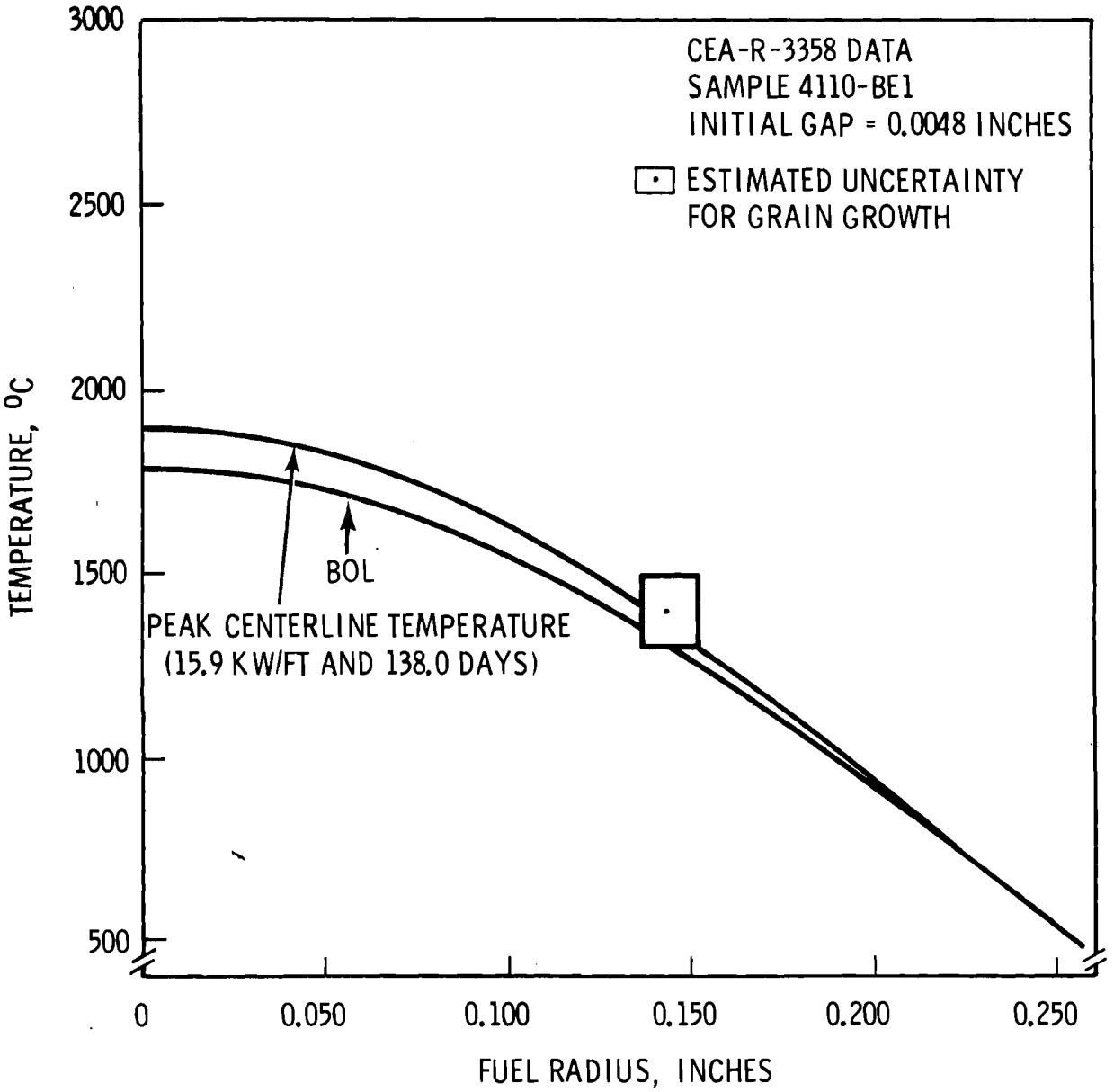

FIGURE 48. A Comparison of GAPCON-THERMAL-2 Predictions With Grain Growth Measurements from CEA-R-3358, Sample 4110-BE1

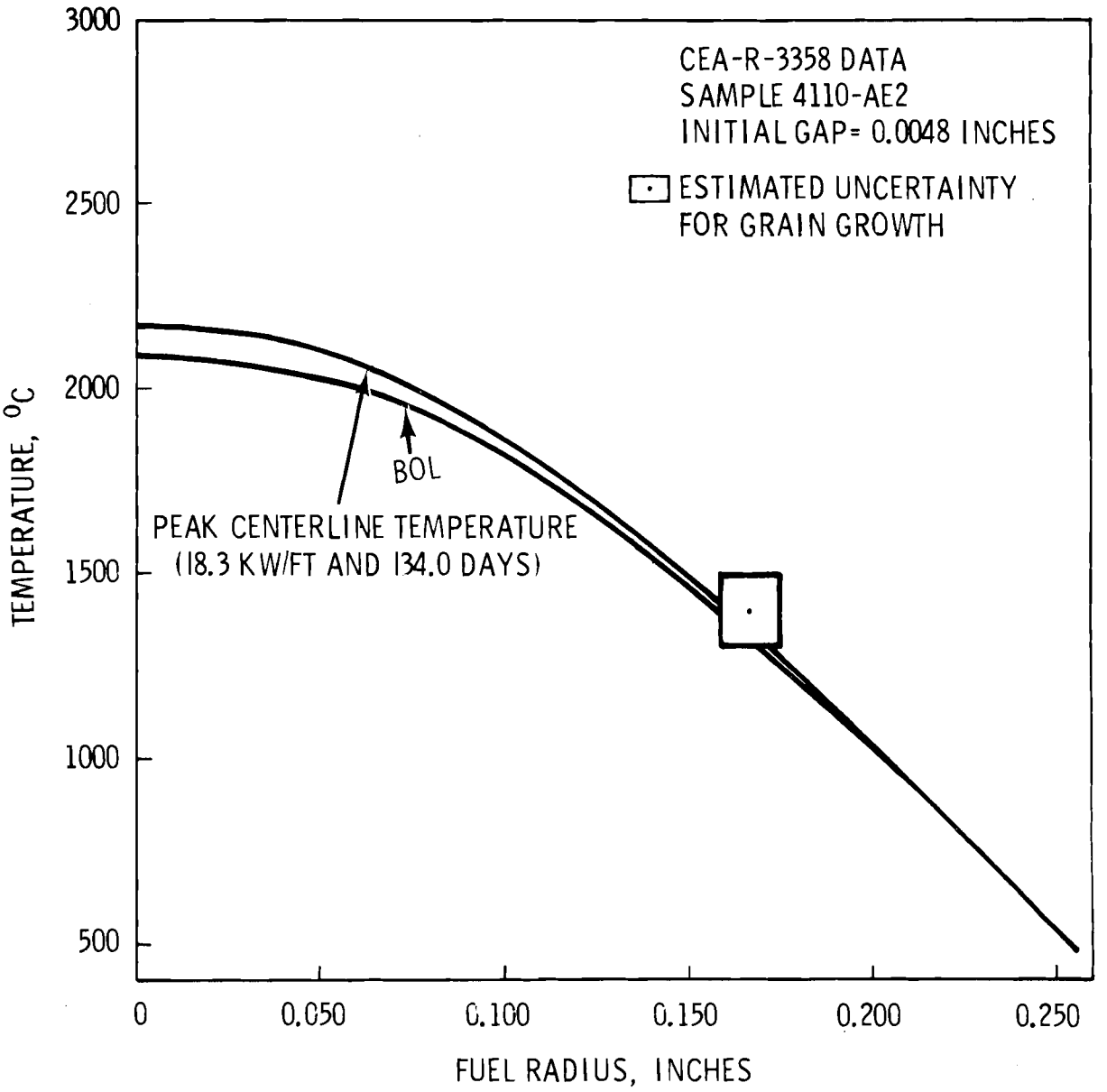

FIGURE 49. A Comparison of GAPCON-THERMAL-2 Predictions With Grain Growth Measurements from CEA-R-3358, Sample 4110-AE2

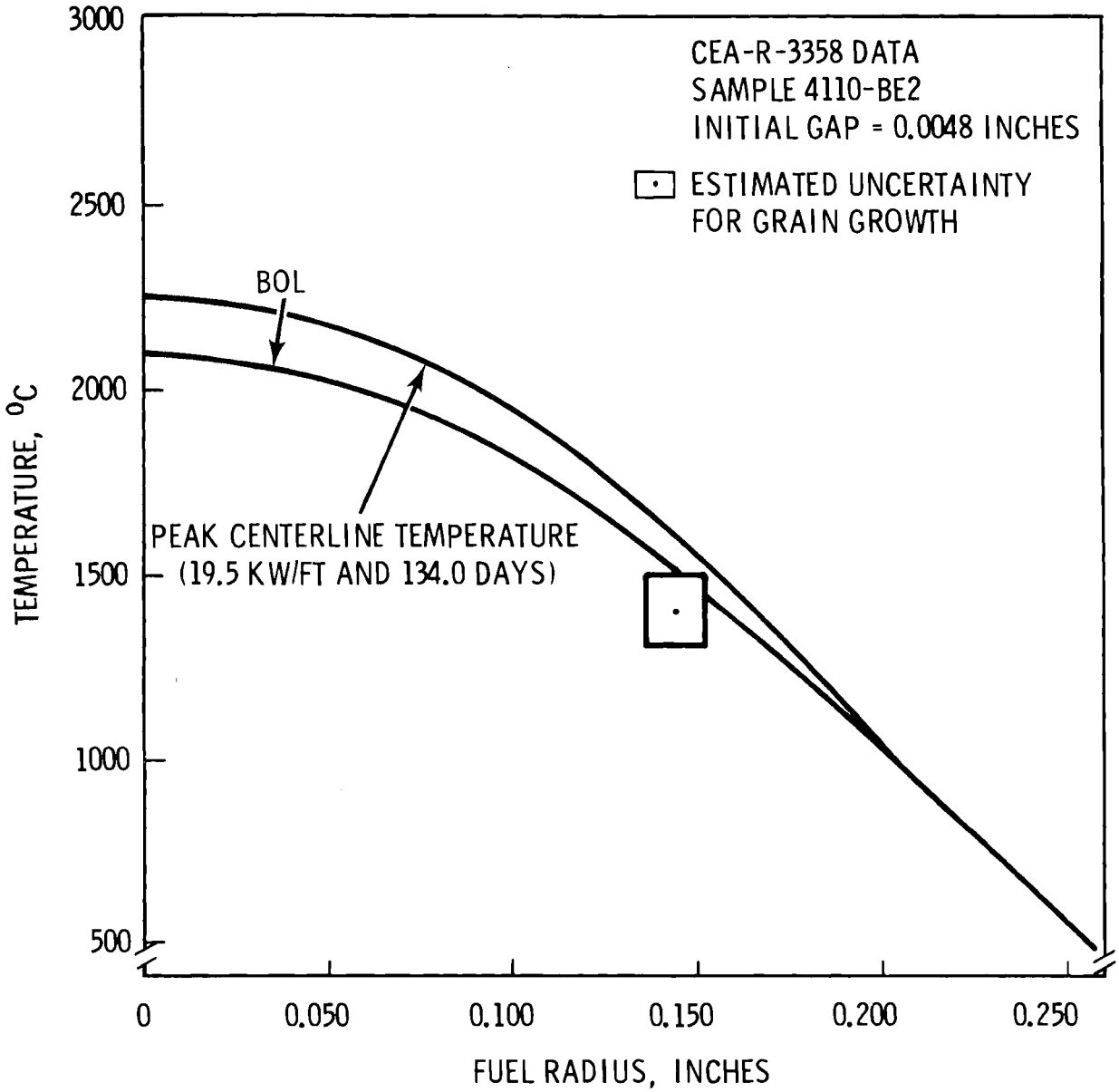

FIGURE 50. A Comparison of GAPCON-THERMAL-2 Predictions With Grain Growth Measurements from CEA-R-3358, Sample 4110-BE2

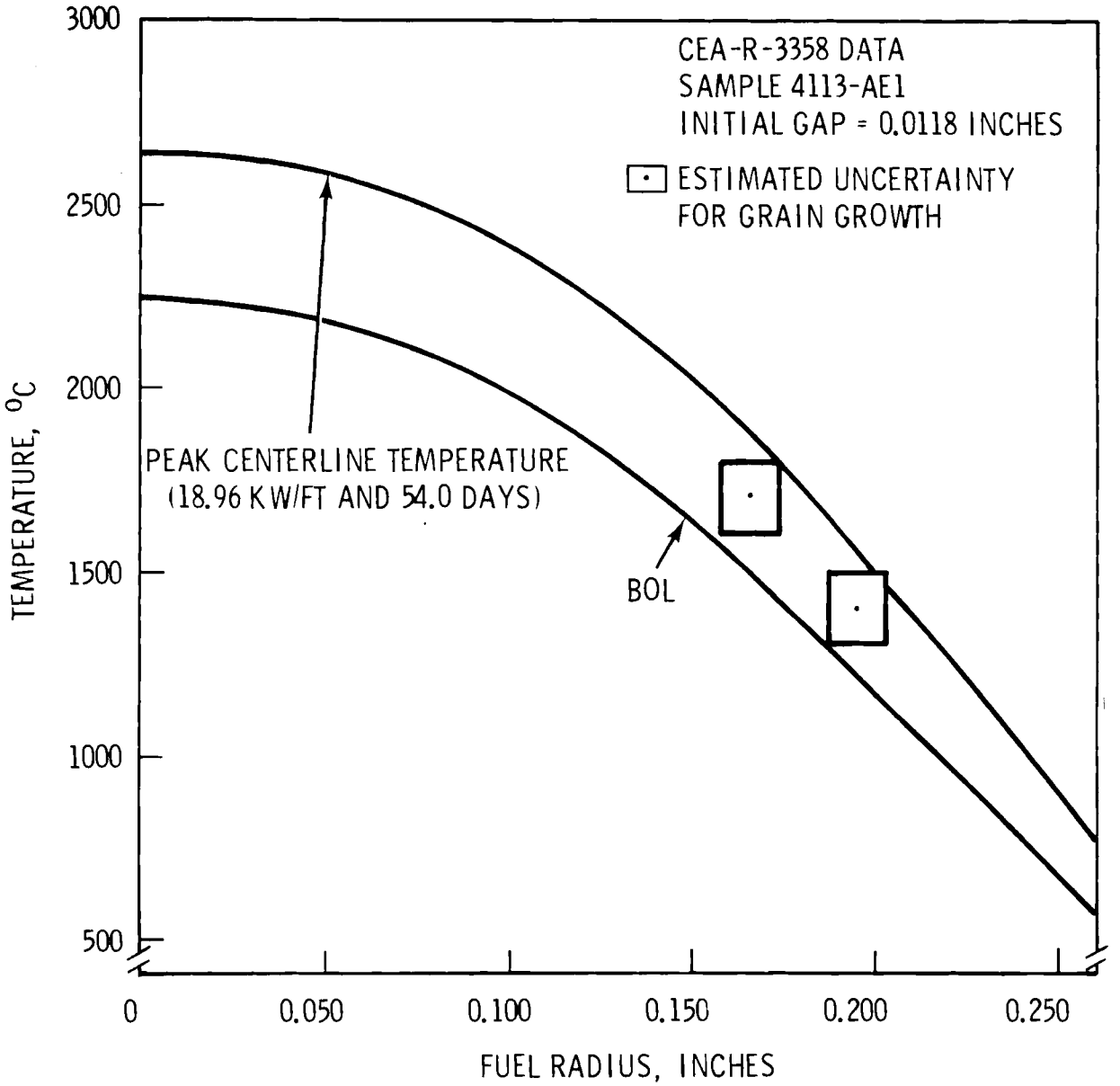

FIGURE 51. A Comparison of GAPCON-THERMAL-2 Predictions with Grain Growth Measurements from CEA-R-3358, Sample 4113-AE1

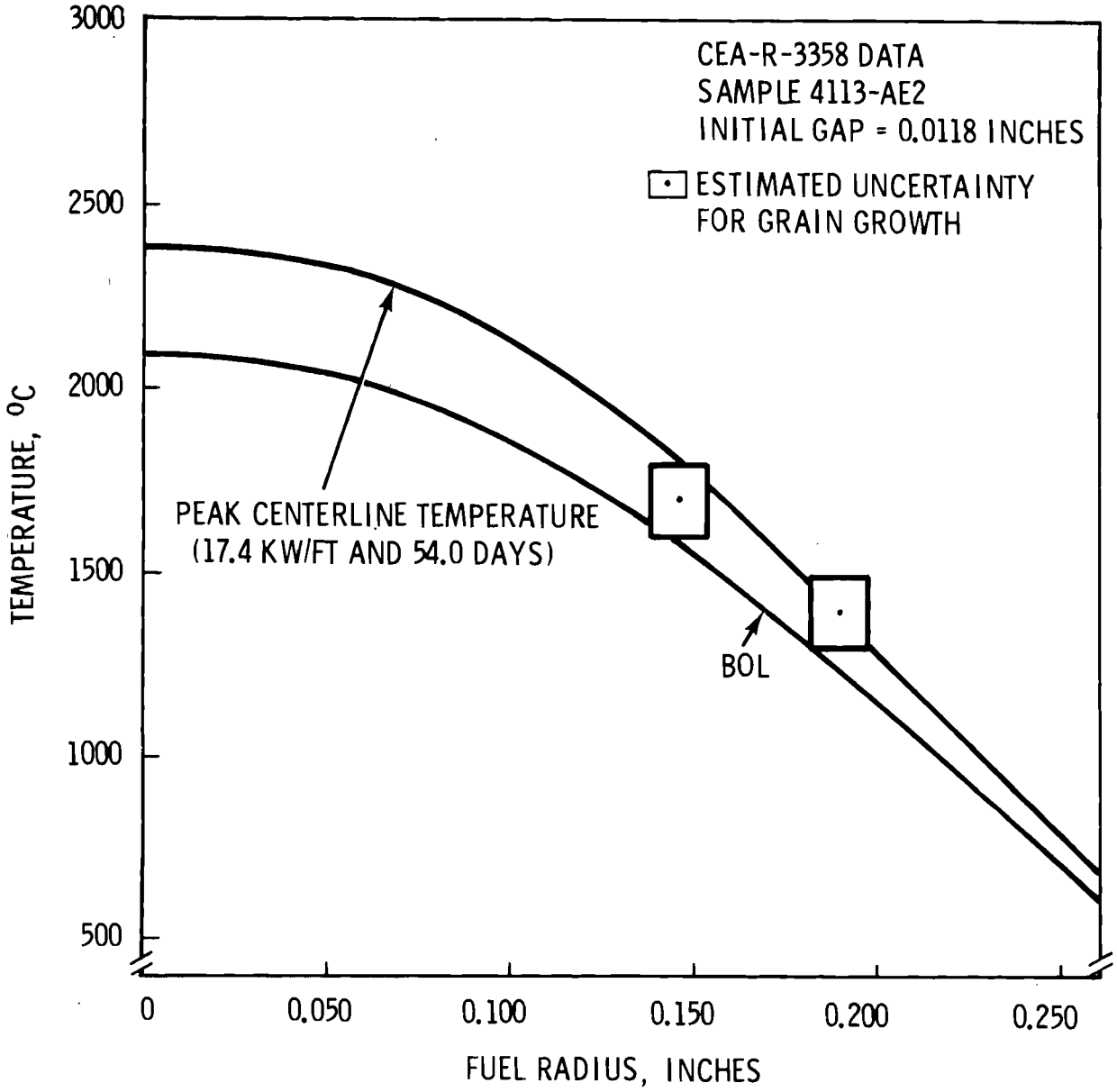

FIGURE 52. A Comparison of GAPCON-THERMAL -2 Predictions With Grain Growth Measurements from CEA-R-3358, Sample 4113-AE2

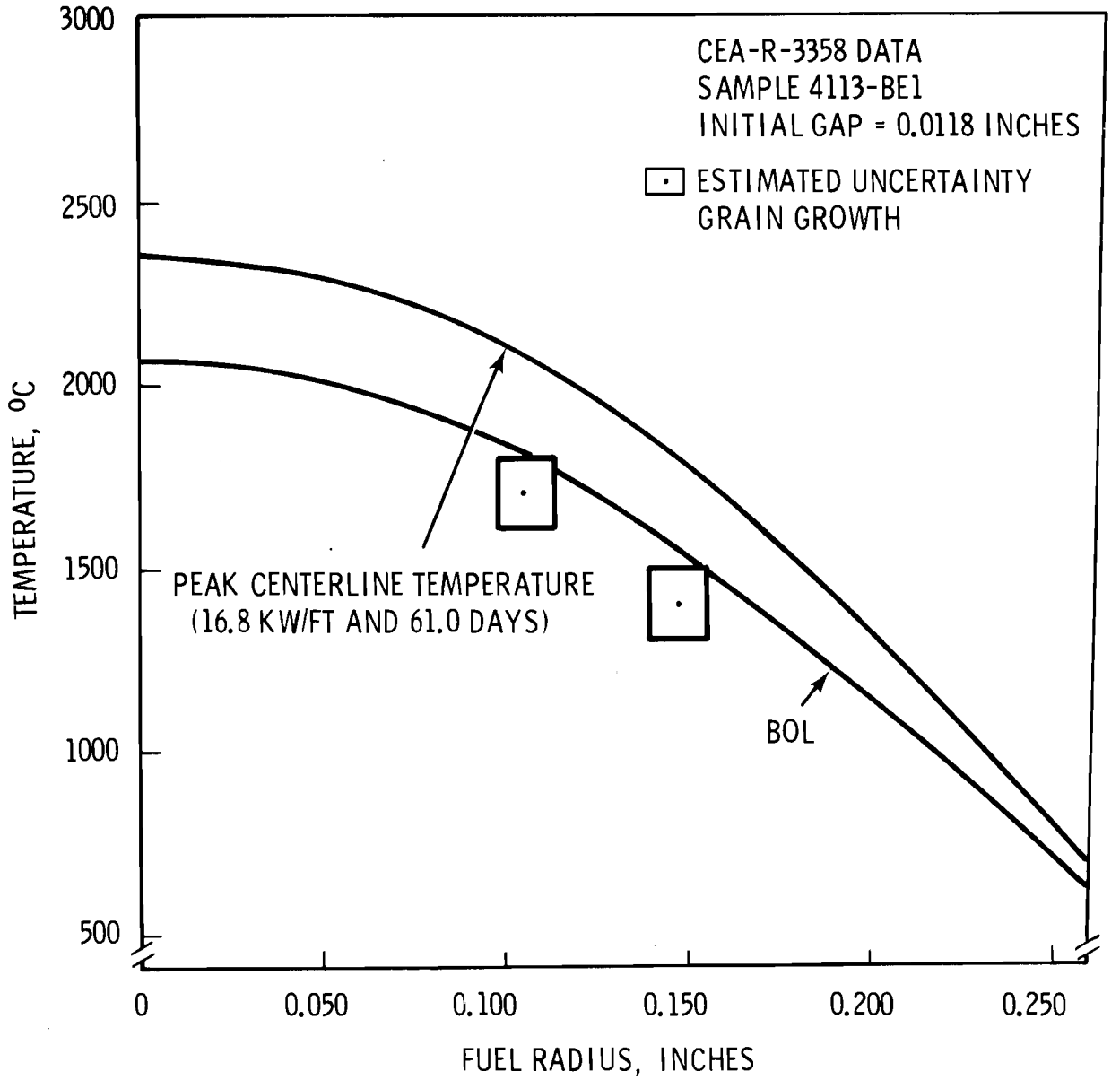

FIGURE 53. A Comparison of GAPCON-THERMAL -2 Predictions With Grain Growth Measurements from CEA-R-3358, Sample 4113-BE1

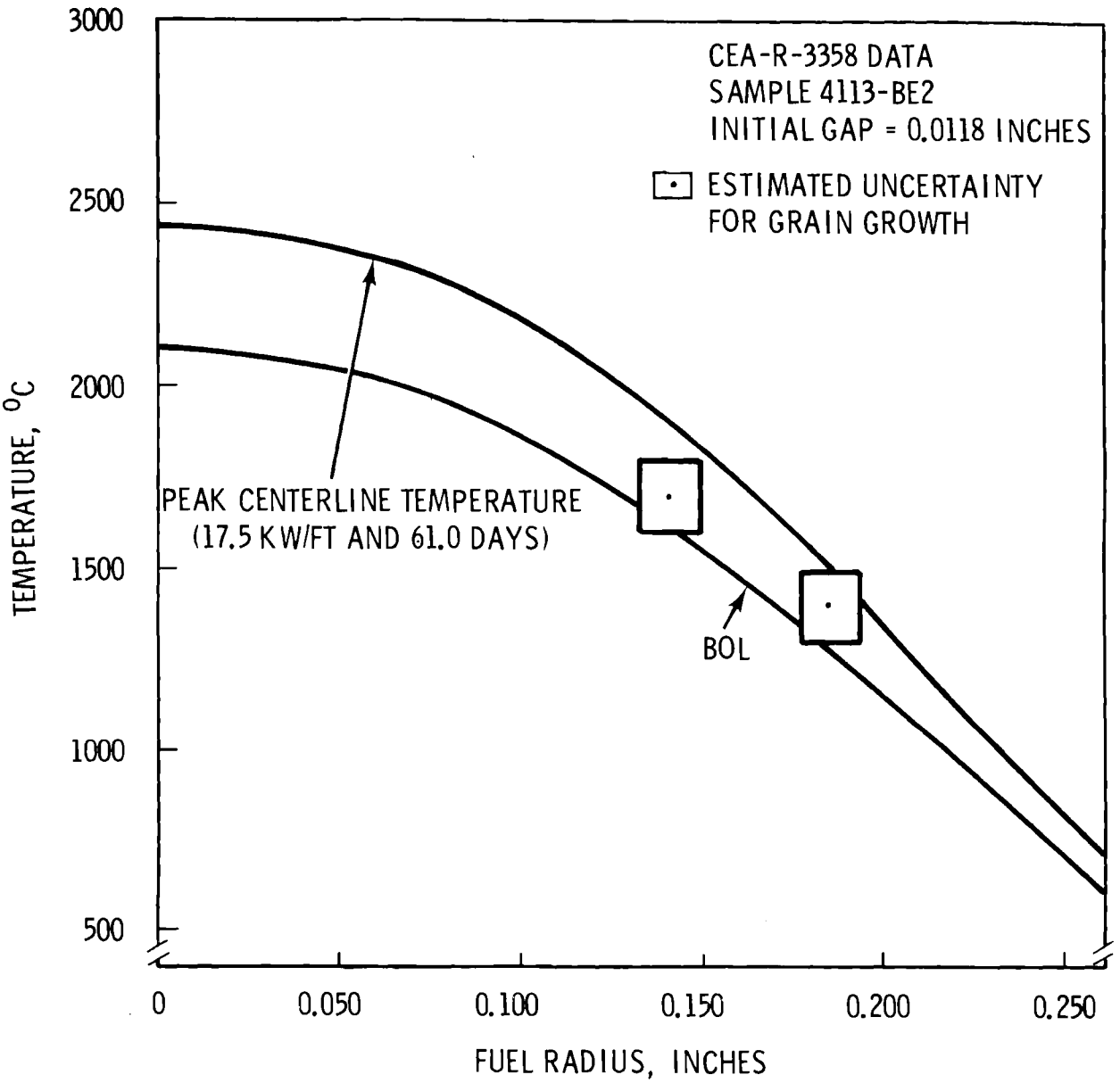

FIGURE 54. A Comparison of GAPCON-THERMAL-2 Predictions With Grain Growth Measurements from CEA-R-3358, Sample 4113-BE2

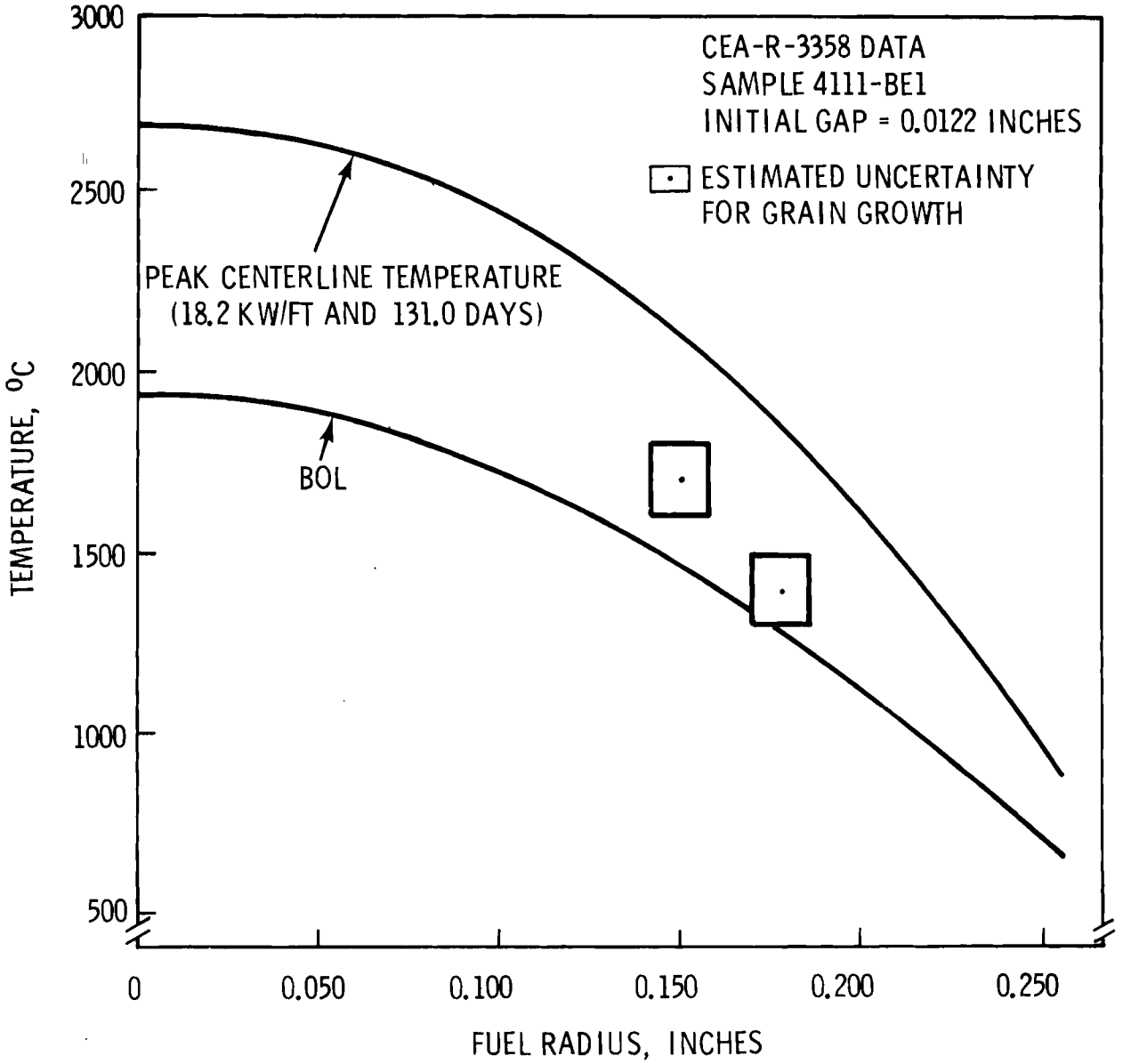

FIGURE 55. A Comparison of GAPCON-THERMAL-2 Predictions With Grain Growth Measurements from CEA-R-3358, Sample 4111-AE1

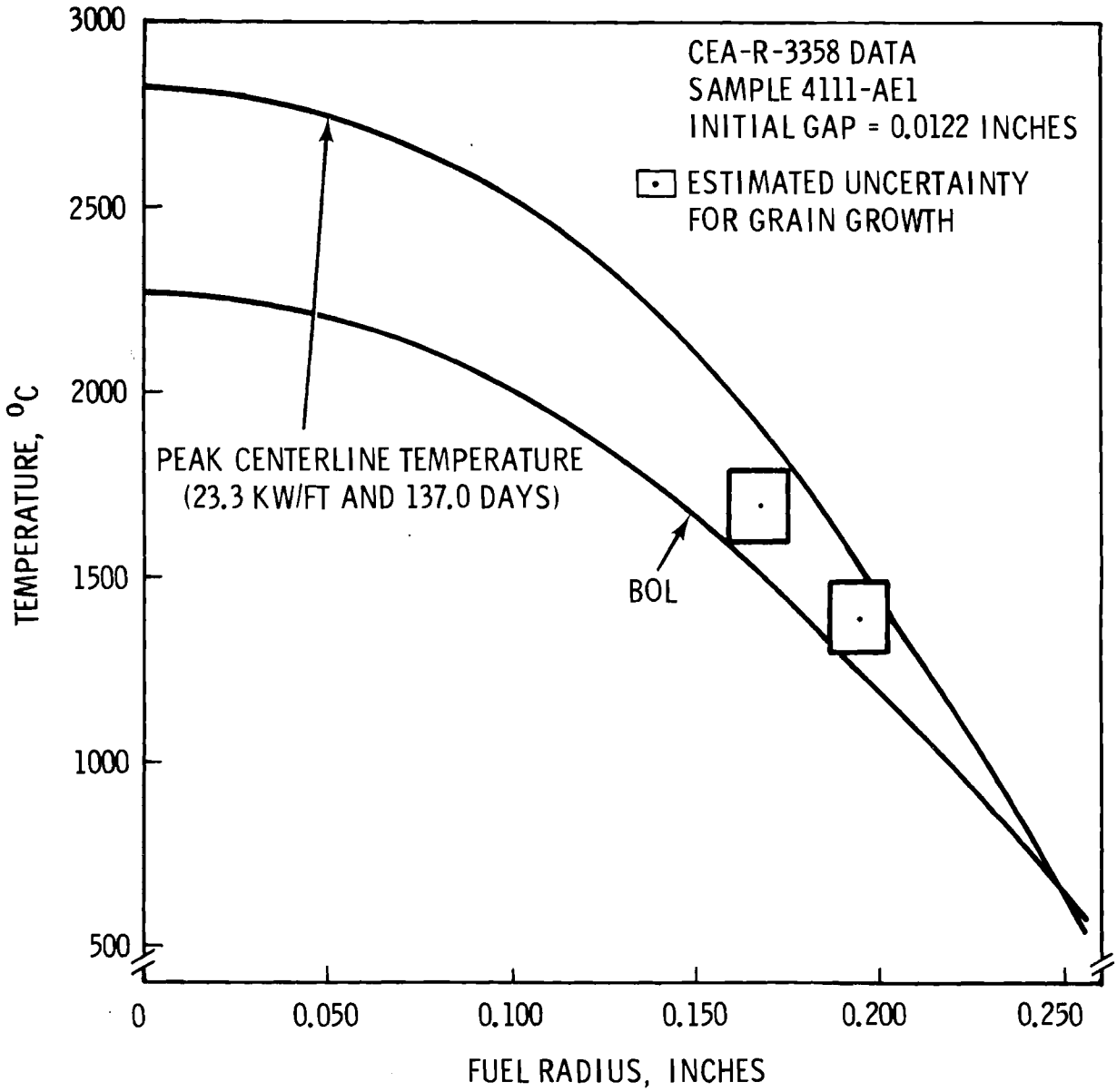

FIGURE 56. A Comparison of GAPCON-THERMAL-2 Predictions with Grain Growth Measurements from CEA-R-3358, Sample 4111-AE2

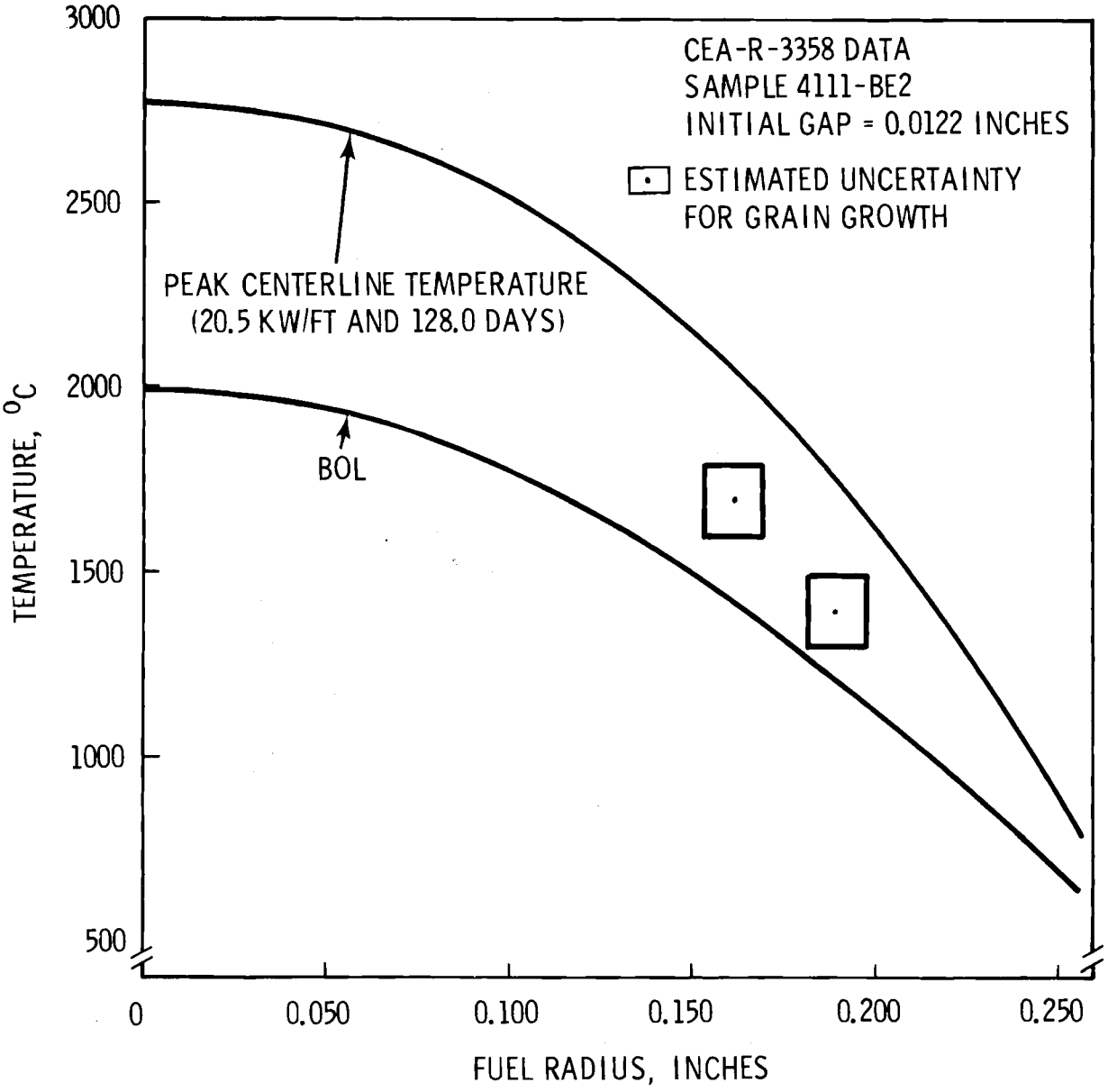

FIGURE 57. A Comparison of GAPCON-THERMAL-2 Predictions With Grain Growth Measurements from CEA-R-3358, Sample 4111-BE1

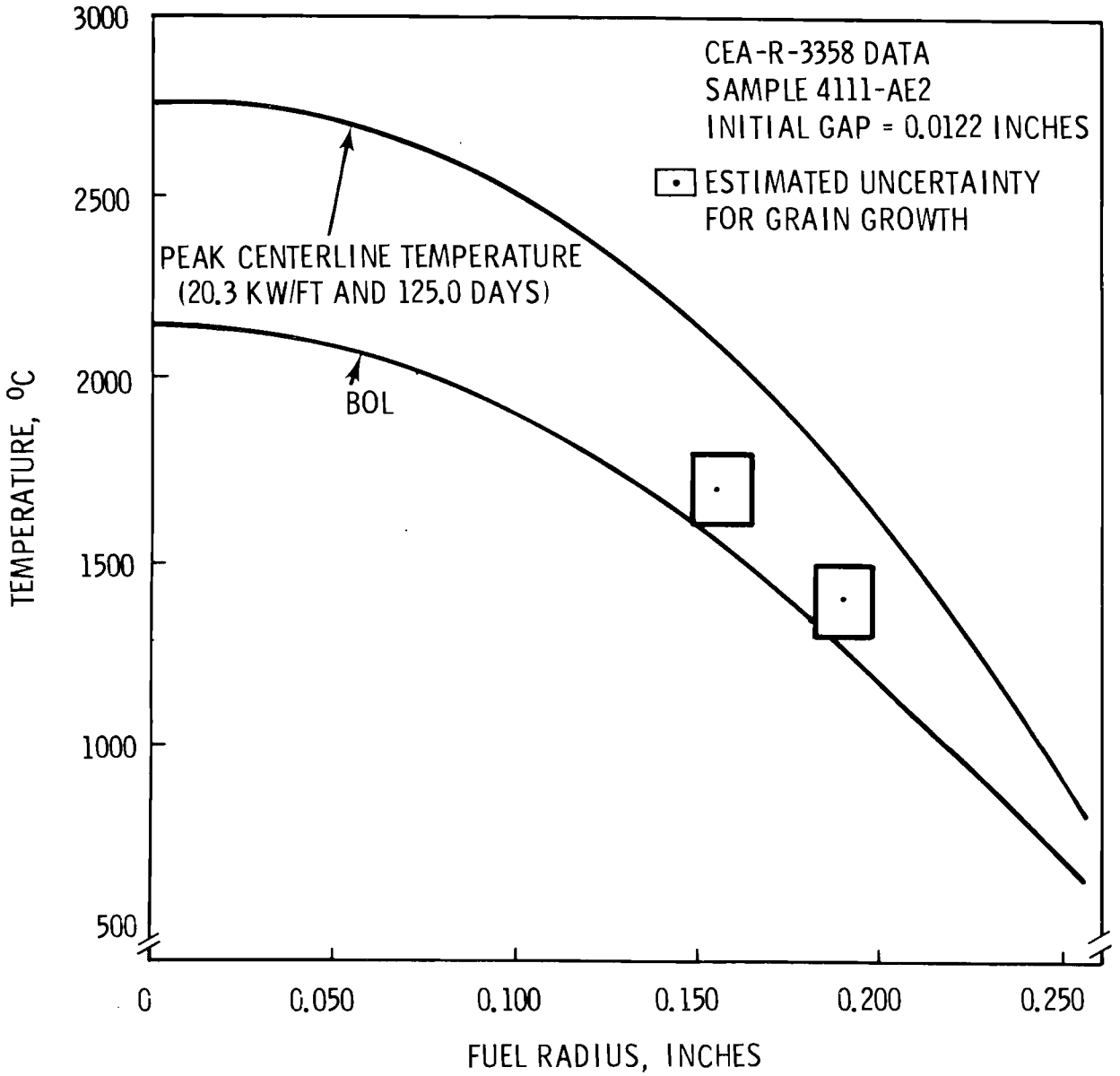

FIGURE 58. A Comparison of GAPCON-THERMAL-2 Predictions With Grain Growth Measurements from CEA-R-3358, Sample 4111-BE2

TABLE 1. Alphabetical Listing of INPUT Parameters for GAPCON-THERMAL-2

ATMOS	FR35	LVOIDZ	SIGHF
DBO	FR40	MINI	TIME
DCI	FR41	NCLAD	
DCO	HBC	NCON	TINLET (1,1)
DE	HGACEL	NFLX	TM 2790°C
DFS	ICDF	NFUEL	TPLAS 1200°C
DSINZ	ICREP	NOH	V
DTEMP 100°F	IDENSF	NPOW 10	VPLENZ
DVOIDZ	ICOR	NPRFIL 1	XCO
EXTP	IGAS	NTIME	XH
FRACAR	IPEAK	PRCDH	XN
FRACH	IRELOC	*PROFIL (1,1)	CRUDTH
FRACHE	IRELSE		
FRACKR	IRL	PSEUDO	
FRACN	ISTOR		
FRACXE	IT	RADS	
FRDEN	KB	ROUC	
FRPUO2	KOOL	ROUF	
FRSIN	LFUEL	S	

*PROFIL (1, 1) = 0.23, 0.63, 0.96, 1.21, 1.35, 1.41, 1.35, 1.21, 0.96, 0.63, 0.23

NOTE: ALL INPUT VARIABLES INITIALIZED TO ZERO EXCEPT AS SHOWN ABOVE.

TABLE 2. Fission Yields Used for Thermal Flux Irradiation

ISOTOPE	YIELDS (%) FROM FISSION OF: ^{235}U	^{238}U	^{239}Pu	^{241}Pu
^{83}Kr	0.52	--	0.29	0.208
^{84}Kr	0.97	--	0.47	0.341
$^{85}I_{Kr}$	1.30	--	0.535	0.30
^{85}Kr	0.0	--	0.0	0.0
^{86}Kr	1.93	--	0.75	0.40
$^{131}I_{Te}$	0.44	--	0.0	0.0
^{131}Te	2.52	--	3.7	3.01
^{131}I	0.0	--	0.09	0.0
^{131}Xe	0.0	--	0.0	0.0
^{132}Te	4.33	--	5.2	4.44
^{132}I	0.0	--	0.15	0.03
^{132}Xe	0.0	--	0.0	0.0
^{133}I	6.69	--	5.3	6.54
^{133}Xe	0.0	--	1.2	0.0
^{134}Xe	7.92	--	7.47	7.81
^{135}I	6.17	--	5.7	7.23
$^{135}I_{Xe}$	0.0	--	0.0	0.0
^{135}Xe	0.13	--	1.51	0.07
^{136}Xe	6.46	--	6.66	7.04

TABLE 3. Thermal Fission Cross Sections Used for the Heavy Metal Atoms

ISOTOPE	FISSION CROSS SECTION (barns)
^{235}U	535.
^{238}U	0
^{239}Pu	740.
^{241}Pu	0.
^{241}Pu	950.

TABLE 4. Data Base Used to Correlate Gas Release Model

REFERENCE	TEMPERATURE MEASUREMENT	HEAT RATINGS (kW/ft)	CENTERLINE TEMPERATURE (°C)	GAS RELEASE FRACTIONS	DATA POINTS
11	MS	12.5-15	1700-2200	0.044-0.232	6
28	TC*	10-14	1900-2050	0.11-0.15	2
29	TC	∿21	2000-2050	0.254-0.275	2
30	MS	17-25	1700-2700	0.057-0.498	10
31	MS	16.5-17.5	1850-2100	0.123-0.188	8
32	MS	19-36	1750-3250	0.0495-0.401	5
33	MS**	15-19.5	1700-2350	0.079-0.28	12

*THERMOCOUPLE
**MICROSTRUCTURE

TABLE 5. Base Input for Parametric Study

Fuel density	94% T.D.
Restructured density	96.5% T.D.
Densification density	97% T.D.
U-235 content	3%
Fuel diameter	0.4770 in.
Cladding inside diameter	0.4890 in.
Cladding outside diameter	0.5630 in.
Plenum volume	2.2 in^3
Coolant inlet temperature	533 °F
Coolant pressure	1050 psi
Fill gas pressure	1 atm
Fill gas composition	100% helium
Coolant temperature increase	20 F°
Coolant-cladding film coefficient	25000 Btu/hr-ft^2-°F
Fuel surface roughness	0.000039 in.
Cladding surface roughness	0.00002 in.
Fuel melting temperature	2790 °C
Fuel column length	144 in.
Number of axial nodes	10
Axial power profile	0.35, 0.86, 1.08, 1.175, 1.19, 1.19, 1.19, 1.17, 1.12, 0.78, 0.37

Power history	14.5	14.5	13.5	0.0	11.0	17.0	13.0	kW/ft
	0	60	120	180	240	300	360	days

All option signals set = 0--see listing of options page 34.

New axial power profile - 0.75, 0.80, 0.85, 0.90, 0.95, 1.0, 0.95, 0.90, 0.85, 0.80, 0.75

TABLE 6. Summary of Parametric Study

Parameter	Effect: Centerline Temperature °C	Effect: Internal Pressure psi	Reference Figure
Base case	-	-	13
Restructuring	-50°	+10	13
Constant power	-100	-50	13
Best estimate relocation	-800	-450	13
Conservative relocation	-400	250	14
Densification	+300	+110	14
Conservative gas release	+10	+150	14
Retard gas release	-50	-200	14
Cladding elastic deformation	-10	-10	15
Plastic fuel	none	-100	15
Rigid fuel	none	+10	15
Plenum volume doubled	-30	-350	15
Densification and best estimate relocation	+30	+10	16
Retard gas release, best estimate relocation, densification(1) ρ_f = 96.5% TD	-530	-420	16
Dished pellets volume = 2%	none	-30	16
Plenum volume halved	+15	+850	16
Sorbed gas, 0.01 cc/gm 1/4, 1/2, 1/4: H_2, N_2, CO	+170 BOL* none EOL	+30 BOL -10 EOL	17
Fill gas pressure 20 atmosphere	-440	+475	17
6% U^{235}	-90	-20	17
New axial power shape	none	+100	17

*BOL = Beginning of Life
EOL = End of Life

TABLE 7. IFA 116 and 117 Condensed Fuel Assembly Power History

IFA-116

Date	Power kW	Cumulative Irradiation Time Days
4/4/68	230	15
4/23	220	30
5/30	210	38
6/5	238	43
6/11	250	48
6/14	215	50
6/18	250	53
3/10/69	210	68
3/12	202	70
3/18	190	74
4/2	215	89
6/6	205	92

IFA-117

4/6/68	222	3
4/15	221	11
4/20	234	15
5/25	245	25
6/8	264	36
6/18	252	45
10/6	235	82
10/20	238	96
11/2	244	108
11/17	252	122
12/1	254	136
12/29	250	158

TABLE 8. GAPCON-THERMAL-2 HPR-129, IFA-116 Comparison

	Experimental Results IFA-116			GAPCON - THERMAL - 2 Predicitions			
	Average Burnup MWd/MT UO_2	Pressure psi	Temperature °C	Temperature °C	Pressure	Local Burnup	Heat Rating
PIN 1	646	33	1780	1711	52	647	19.98
	1277	23	1630	1682	57	1278	19.51
	1602	28	--	1626	60	1603	18.81
	1831	39	--	1943	85	1832	21.26
	2065	47	--	2030	100	2066	21.73
	2144	52	--	1685	98	2146	18.44
	2282	53	--	2012	105	2285	21.43
	2953	66	--	1949	119	2949	20.52
	3039	71	--	1869	120	3034	19.73
	3203	71	--	1796	121	3198	19.01
	3902	~95	--	2128	174	3898	21.65
	4036	~97	--	2075	178	4036	20.77

	Average Burnup	Pressure	Temperature	Temperature	Pressure	Temperature*	Pressure*	Local Burnup	Local Burnup*	Heat Rating	Heat Rating*
PIN 5	646	18	1740	1905	59	1835	59	686	665	19.98	19.36
	1277	42	1760	1891	70	1801	70	1358	1309	19.51	18.73
	1602	50	2000	1836	76	1732	74	1704	1623	18.88	18.18
	1831	71	1775	2152	107	2073	108	1947	1857	21.26	20.48
	2065	76	1850	2202	120	2155	121	2196	2109	21.73	21.05
	2144	85	~1850	1887	118	1844	120	2286	2192	18.44	18.05
	2282	90	2000	2186	128	2157	129	2428	2336	21.43	20.98
	2953	99	1950	2150	150	2086	152	3133	3013	20.52	19.69
	3039	~106	~1700	2094	152	2004	154	3223	3100	19.73	18.94
	3203	106	2050	2017	156	1920	158	3397	3237	19.01	18.31
	3902	146	2050	2261	202	2196	203	4142	3953	21.65	20.86
	4036	152	1950	2203	207	2141	208	4284	4091	20.77	20.00

*Input included time dependent axial power profile.

TABLE 9. GAPCON-THERMAL-2 HPR-129, IFA-117, Pins 1 and 3 Comparison

	Experimental Results IFA-117			GAPCON - THERMAL - 2 Predictions		
	Average Burnup MWd/MT UO_2	Pressure psi	Temperature °C	Temperature °C	Pressure	Heat Rating kW/ft
PIN 1	132	42	1850	1804	48	20.16
	489	39	1800	1892	56	20.74
	691	40	1840	2123	69	22.53
	1160	50	2100	2248	92	23.60
	1781	71	2106	2454	131	25.43
	2210	*	*	2334	149	23.96
	3744	128	1950	2050	193	19.48
	4345	142	1910	2131	224	20.17
	4844	170	2000	2149	246	20.23
	5478	199	1980	2198	281	21.04
	6079	213	1975	2206	309	21.05
	7148	213	1975	2211	356	20.72
PIN 3	121	48	1750	1561	53	17.57
	450	45	1600	1591	55	18.17
	637	45	1600	1775	61	19.81
	1071	51	1775	1906	72	20.74
	1642	64	2000	2134	100	22.34
	2040	*	*	2023	107	21.02
	3550	106	2200	2025	145	20.32
	4251	113	2150	2119	176	20.87
	4802	213	2200	2154	201	21.10
	5499	284	2180	2228	243	21.94
	6159	298	2025	2238	270	21.96
	7364	298	1975	2230	312	21.62

TABLE 10. GAPCON-THERMAL-2 HPR-129, IFA-117, Pins 5 and 6 Comparison

	Experimental Results IFA-117			GAPCON - THERMAL - 2 Predictions				
	Average Burnup MWd/MT UO_2	Internal Pressure psi	Peak Fuel Temperature °C	Peak Fuel Temperature °C	Internal Pressure psi	Local Burnup MWd/MT UO_2	Input Heat Rating kW/ft	
	122	46	1750	1688	47	122	17.57	
	456	38	1600	1733	52	454	18.17	
	644	41	1600	1991	61	644	19.81	
	1082	68	1775	2145	81	1083	20.74	
	1659	99	2000	2324	113	1664	22.35	
PIN 5	2060	*	*	2226	128	2065	21.02	
	3543	142	2200	2107	178	3770	18.89	
	4162	156	2150	2170	208	4432	19.42	
	4676	199	2200	2191	231	4986	19.61	
	5328	241	2180	2260	272	5690	20.41	
	5937	255	2025	2267	300	6358	20.41	
	7073	255	1975	2259	348	7546	00.10	
							Input	Local Peak
	111	34	1600	1738	44	134	15.83	20.07
	900	32	1575	1648	46	470	15.09	19.13
	551	32	1550	1692	48	650	15.40	19.52
	896	35	1700	1721	51	1050	15.53	19.69
	1347	32	1700	1913	61	1580	16.74	21.22
PIN 6	1663	*	*	1953	67	1973	16.90	21.42
	2867	43	1900	1783	80	3539	15.33	19.43
	3361	43	1875	1785	86	4127	15.23	19.31
	3771	57	2000	1908	97	4636	15.92	20.18
	4301	71	2025	2005	119	5272	16.28	20.64
	4804	85	2050	2061	140	5887	16.57	21.00
	5621	85	2050	2054	160	6978	16.31	20.67

TABLE 11. GAPCON-THERMAL-2 AECL-2662 and -1676 Gas Release Comparison

Reference	Sample No.	Initial Diametral Gap (in.)	Gas Release Fraction	
			Measured	Predicted
AECL-2662	LFD	0.004	0.458	0.487
	LFH	0.004	0.311	0.498
	LFM	0.004	0.155	0.500
AECL-1676	DFB	0.0035	0.179	0.368
	DFD	0.0035	0.330	0.546
	DFE	0.0035	0.401	0.652

TABLE 12. GAPCON-THERMAL-2 Other AECL Gas Release Comparisons

Sample Identification	Heat Rating, kW/ft First Period (15.5 Days)	Second Period (44.3 Days)	Third Period (16.2 Days)	Final Burnup (MWd/MTM)	Xenon Release %	Krypton Release %	GAPCON-THERMAL-2 Gas Release Prediction %
AZM	22.34	22.10	20.00	5265.	26.	23.	32.68
AZR	---	22.10	---	3120.	20.	18.	32.48
AZT	22.34	---	---	1110.	22.	18.	28.91
AZK	22.34	00000	---	1110.	33.	20.	28.91
AZB	12.58	13.00	20.00	3424.	25.	28.	25.53
AZC	12.58	13.00	20.00	3424.	22.	26.	25.53
AZD	12.58	13.00	11.80	3070.	3.	2.	0.15
AZE	12.58	13.00	11.80	3070.	4.	4.	0.15
AZJ	22.40	13.00	11.80	3555.	6.	10.	9.40

TABLE 13. GAPCON-THERMAL-2 Grain Growth Radii AECL-2588, X-23301 and X23303 Comparisons

Rod#	Pellet Diameter (in)	Initial Diametral Gap (in)	Pellet Density (% T.D.)	Rod Power (kW/ft)	Equiaxed Grain Growth Radius (%)*		
					Reported	GAP-1 Predicted (BOL)	GAP-2 Predicted (BOL)
FAN	.7047	.0142	95.7	21.46	72	79	80.0
FAD	.7047	.0142	95.8	16.86	67	76	78.8
FAP	.7047	.0142	95.5	19.92	70	76	78.7
FAT	.6902	.0291	95.9	18.01	84	100	90.7
FAW	.6902	.0291	95.5	19.92	83	100	88.0
FAZ	.6902	.0291	96.1	21.46	82	100	86.4
FAR	.7047	.0142	95.7	19.92	69	--	78.6
FAX	.6902	.0291	95.7	18.01	80	--	90.7
FAS	.7051	.0142	96.0	17.65	66	--	77.1

*Equiaxed Grain Growth Assumed to Occur at 1400°C

GAP-1 = GAPCON-THERMAL-1

GAP-2 = GAPCON-THERMAL-2

TABLE 14. GAPCON-THERMAL-2 CEA-R-3358 Gas Release Comparison

Sample No.	Initial Diametral Gap (in.)	Gas Release Fraction	
		Measured	Predicted
4110-AE1	0.0047	0.216	0.208
4110-AE2	0.0047	0.221	0.203
4110-BE1	0.0047	0.139	0.121
4110-BE2	0.0047	0.159	0.228
4112-AE1	0.0039	0.126	0.233
4112-AE2	0.0035	0.112	0.200
4112-BE1	0.0039	0.079	0.082
4112-BE2	0.0035	0.126	0.150
4111-AE1	0.0122	0.372	0.432
4111-AE2	0.0122	0.377	0.458
4111-BE1	0.0122	0.318	0.472
4111-BE2	0.0122	0.379	0.445
4113-AE1	0.0118	0.267	0.430
4113-AE2	0.0118	0.280	0.313
4113-BE1	0.0118	0.170	0.314
4113-BE2	0.0118	0.210	0.335

ACKNOWLEDGMENTS

This work was sponsored by the Core Performance Branch of the Nuclear Regulatory Commission. The authors acknowledge the guidance by R. M. Lobel and L. S. Rubenstein of the Core Performance Branch. We also acknowledge the following Battelle Northwest staff members: G. D. Seybold and Kent B. Stewart for their programming assistance; J. L. Carter for his work on FISGAS; W. J. Bailey and S. Goldsmith for their technical and administrative assistance, respectively.

REFERENCES

1. C. R. Hann, C. E. Beyer and L. J. Parchen, GAPCON-THERMAL-1: A Computer Program for Calculating the Gap Conductance in Oxide Fuel Pins, BWNL-1778, September 1973.

2. G. R. Horn, Babcock and Wilcox Company, Lynchburg, Virginia, 1973, Deceased September 25, 1975.

3. C. E. Beyer, C. R. Hann, D. D. Lanning, F. E. Panisko, and L. J. Parchen, User's Guide for GAPCON-THERMAL-2: A Computer Program for Calculating the Thermal Behavior of an Oxide Fuel Rod, BNWL-1897, November 1975.

4. D. D. Lanning and C. R. Hann, Review of Methods Applicable to the Calculation of Gap Conductance in Zircaloy-Clad Fuel Rods, BNWL-1894, April 1975.

5. A. M. Ross, R. L. Stoute, Heat Transfer Coefficients Between UO_2 and Zircaloy-2, CRFD-1075, June 1962 or AECL-1552.

6. W. R. Lloyd, D. P. Wilkins, and P. R. Hill, "Heat Transfer in Multi-component Gases in the Low, Intermediate and High Pressure Regime," (Nuclear Thermionics Conference, 1973).

7. N. Todreas and G. Jacobs, "Thermal Contact Conductance of Reactor Fuel Elements," Nuclear Science and Engineering 50, 1973, p. 283.

8. G. R. Horn, F. E. Panisko, User's Guide for GAPCON: A Computer Program to Predict Fuel-to-Cladding Heat Transfer Coefficients in Oxide Fuel Pins, HEDL-TME72-128, September 1972.

9. J. L. Carter BNWL Memo to C. R. Hann. "Revisions to FISGAS," November 12, 1973.

10. K. P. Galbraith, Pellet-to-Cladding Gap Closure from Pellet Cracking Data and Analysis, Exxon Nuclear Company, Inc. XN-73-17, August 1, 1973.

11. E. DeMeulemeester, et al., "Review of Work Carried out by BELGONCLEAIRE and CEA on the Improvement and Verification of the Computer Code with the Aid of In-Pile Experimental Results," British Nuclear Energy Society International Conference on Nuclear Fuel Performance, October 15-19, 1973.

12. Jean-Claude Janvier, et al., Irradiation of Uranium Dioxide in a Resistant Cladding Effects of Initial Diametral Gap on Overall Behavior CEA-P-3358, (October 1967).

13. D. S. Dutt, R. B. Baker and S. A. Chastain, Modeling of the Post-irradiation Fuel-Cladding Gap in Mixed-Oxide Fuels, HEDL-TME 74-19 April 1974 or Transactions ANS, 17, 1975, 1973.

14. R. O. Meyer, Private Communication, Nuclear Regulatory Commission, Washington, DC, April 1975.

15. R. B. Bird, W. F. Stewart, and E. N. Lightfoot, Transport Phenomena, John Wiley & Sons, New York, 1966.

16. A. Ullman, R. Acharya and D. R. Olander, "Thermal Accommodation Coefficients of Inert Gases on Stainless Steel and UO_2," Journal of Nuclear Materials 51, 1974, p. 277-279.

17. R. A. Dean, Thermal Contact Conductance Between UO_2 and Zircaloy-2, CVNA-127, 1962.

18. A. C. Rapier, T. M. Jones and J. E. McIntosh, "The Thermal Conductance of Uranium Dioxide/Stainless Steel Interfaces," International Journal of Heat and Mass Transfer, 6.(1963) p. 397.

19. W. B. Lewis, "Engineering for the Fission Gas in UO_2 Fuel," Nucl. Appl., 2, (1966) p. 171.

20. A. H. Booth, A Method of Calculating Fission Gas Diffusion from UO_2 Fuel and its Application to the X-2-f Loop Test, AECL-496 (September 1957).

21. G. W. Parker, et al., "Prompt Release of Fission Products from Zircaloy-Clad UO_2 Fuels," in Nuclear Safety Program Annual Progress Report for Period Ending December 31, 1967, ORNL-4228, Oak Ridge National Laboratory (April 1968).

22. D. L. Morrison, et al., An Evaluation of the Applicability of Existing Data to the Analytical Description of a Nuclear Reactor Accident, BMI-1779 (August 1966).

23. J. P. Hoffman and D. H. Coplin, The Release of Fission Gases from Uranium Dioxide Pellet Fuel Operated at High Temperatures, GEAP-4596 (September 1964).

24. V. F. Baston, et al., An Analytical Method for Calculating Steady-State Fission Gas Release--Fission Product Fuel Model (FPFM) Code, ANCR-1010, (September 1971).

25. H. R. Warner and F. A. Nichols, "A Statistical Fuel Swelling and Fission, Gas Release Model," Nucl. Appl. and Tech. vol. 9 (August 1970).

26. C. E. Beyer and C. R. Hann, Prediction of Fission Gas Release from UO_2 Fuel, BNWL 1875, November, 1974.

27. R. G. Bellamy and J. B. Rich, "Grain Boundary Gas Release and Swelling in High Burn-up Uranium Dioxide," J. Nucl. Mat. 33, 64-78, (1969).

28. J. P. Stora and P. Chenebault, Programme Cyrano-Mesure de l'intégrale de conductibilité thermique d' UO_2 fritté jusqu'a 2300°C - Evolution des gaz de fission a puissance constante, CEA-R-3618 (1968).

29. J. A. Ainsocugh, An Assessment of the IFA-116 and 117 Irradiations from Data Obtained from the In-Reactor Instrumentation, HPR-129, (April 1971).

30. M. J. F. Notley, R. Deshaies, et al., Measurements of the Fission Product Gas Pressures Developed in UO_2 Fuel Elements During Operation, AECL-2662 (1966).

31. M. J. F. Notley and J. R. MacEwan, The Effect of UO_2 Density of Fission Product Gas Release and Sheath Expansion, ORNL Report AECL-2230 (1965).

32. M. J. F. Notley, et al., Zircaloy Sheathed UO_2 Fuel Elements Irradiated at Values of $\int k d\Theta$ Between 40 and 83 w/cm, AECL-1676, (December 1962).

33. Jean-Claude Janvier, et al., Irradiation of Uranium Dioxide in a Resistant Cladding Effects of Initial Diametral Gap on Overall Behavior CEA-R-3358, (October 1967).

34. W. B. Lewis, et al., "Fission Gas Behavior in Uranium Dioxide Fuel," 3rd ICPUAE, p. 19 United Nations (1964).

35. W. B. Lewis, Uranium Dioxide: Properties and Nuclear Applications, ed. J. Belle (U.S. Govt., Washington, 1961) Section 9.4.2.

36. C. E. Beyer and C. R. Hann, Release of Indigenous Gases from LWR Fuel and Reaction Kinetics with Zircaloy Cladding, BNWL-1956, November 1975.

37. M. D. Freshley, Nuclear Technology, 15 (2), 125 (August 1972).

38. J. B. Conway, R. M. Fincel, Jr., and R. A. Hein, "The Thermal Expansion and Heat Capacity of UO_2 to 2200°C," Trans. Am. Nucl. Soc., vol. 6, no. 1, p. 153, 1963.

39. D. Geithoff, G. Karsten, and K. Bummerer, "Irradiation Performance of Fast Reactor Fuels," Presented at International Symposium on Plutonium Fuels Technology, AIME Symposium 1967; Nuclear Metallurgy, vol. 13, 1968.

40. U.S. Atomic Energy Commission, Generic Environmental Statements Mixed-Oxide Fuel, WASH-1327, vol. 3, Chapter IV c 3, August 1974.

41. M. F. Lyons, et al., UO_2 Pellet Thermal Conductivity From Irradiation with Central Melting, GEAP-4624, 1964.

42. S. Y. Ogawa, E. A. Lees, and M. F. Lyons, Power Reactor High Performance UO_2 Program, GEAP-5591, 1968.

43. J. A. Christensen, Thermal Expansion and Change in Volume on Melting for Uranium Dioxide, HW-75148, 1962.

44. J. A. Christensen, "Columnar Grain Growth in Oxide Fuels," Trans. Am. Nucl. Soc., vol. 15, no. 1, June 1972.

45. D. J. Bradley and C. R. Hann, An Evaluation of the Discrepancies Between Predicted and Experimental Effects of Xenon and Krypton in Nuclear Fuel Rods, BNWL-1955, November 1975.

46. B. H. Duane, Time-Variant Isotopic Transmutation GE-HL Program ALCHEMY, HW-80020 (Dec. 1963).

47. R. H. Holman and D. D. Matsomoto, ZODIAC-G: A Code for Multi-Group, Multi-Region Burnup Calculations, BNWL-1559, May 1971.

48. C. H. Westcott, Effective Cross Section Values for Well-Moderated Thermal Reactor Spectra, CRRP-960, Ed. 3 Rev. November 1960.

49. E. T. Merrill, ALTHAEA - A One Dimensional, Two Group Diffusion Code With an Effective Four Group Burnup, BNWL-462, May 1970.

50. C. A. Rohrmann, "Modified CHART of Nuclides," BNWL, May 6, 1969.

51. M. F. Lyons, et al., UO_2 Pellet Thermal Conductivity From Irradiation With Central Melting, GEAP-4624, 1964.

52. S. Y. Ogawa, E. A. Lees, and M. F. Lyons, Power Reactor High Performance UO_2 Program, GEAP-5591, 1968.

53. T. G. Godfrey, W. Fulkerson, T. G. Kollie, J. P. Moore, and D. L. McElroy, Thermal Conductivity of Uranium Dioxide and Armco Iron by an Improved Radial Heat Flow Technique, ORNL-3556, June 1964.

54. J. C. Maxwell, A Treatise on Electricity and Magnetism, vol. I, 3rd edition, Oxford University Press (1891), reprinted by Dover, New York (1954).

55. A. Eucken, "The Heat Conductivities of Ceramic Refractory, Calculations of Heat Conductivity from the Constituents," Forsch, Gebiete Ingenieurw, B3 Forschungsheft, no. 353, 1932.

56. J. Belle, R. M. Berman, W. F. Bourgeois, I. Cohen, R. C. Daniel, Thermal Conductivity of Bulk Oxide Fuels, WAPD-TM-586, 1967.

57. A. L. Loeb, "Thermal Conductivity: VIII, A Theory of Thermal Conductivity of Porous Materials," American Ceramic Society, 37, 1954.

58. Thermal Conductivity of Uranium Dioxide, IAEA Report No. 58, 1966.

59. Personal communication, J. B. Conway (Mar-Test Inc., Cincinnati, Ohio) to W. J. Bailey, Battelle-Pacific Northwest Laboratories, February 1973.

60. J. F. Kerrisk, D. G. Clifton, "Smoothed Values of the Enthalpy and Heat Capacity of UO_2," Nucl. Technology, vol. 16, 1972.

61. J. A. L. Robertson, $\int \kappa d\Theta$ in Fuel Irradiations, CRFD-835, April 1959.

62. G. R. Horn, HEDL, Private Communication. Richland, Washington March 1975.

63. D. B. Scott, Physical and Mechanical Properties of Zircaloy-2 and Zircaloy-4, WCAP-3629-41, May 1965.

64. Raymond J. Roark, Formulas for Stress and Strain, McGraw-Hill Book Co., New York City, New York, 4th edition, 1965.

65. P. J. Pankaskie, BUCKLE--An Analytical Computer Code for Calculating Creep Buckling of an Initially Oval Tube, BNWL-1784, May 1974.

66. C. L. Mohr, COVE-1, A Finite Difference Creep Collapse Code for Oval Fuel Pin Cladding, BNWL-1896, March 1975.

67. Han von Ubisch, "The Thermal Conductivities of Mixtures of Rare Gases at 29°C and 520°C," Arkiv for Fysik, Band 16, nr 7, June 1959.

68. W. L. Badger, W. L. McCabe, Elements of Chemical Engineering, p. 134, McGraw-Hill Book Co., New York, N. Y., 1936.

69. F. Kreith, Principles of Heat Transfer, p. 597, 2nd Ed., International Textbook Co., Scranton, PA., 1965.

70. J. E. Irvin, Chairman, Nuclear Systems Materials Handbook Advisory Group, HEDL, TID-26666, 1975.

71. Journal of Nuclear Materials, vol. 7, No. 2, p. 133, 1962.

72. J. A. Christensen, Thermal Expansion and Change in Volume on Melting for Uranium Dioxide, HW-75148, 1962.

73. G. Testa, et. al., "In-Pile Fuel Studies for Design Purposes," Nuclear Applications and Technology, vol. 7, December 1969.

74. M. G. Balfour, J. A. Christensen, and H. M. Ferrarri, In-Pile Measurement of UO_2 Thermal Conductivity, WCAP-2923, March 1966.

75. I. Devold, A Study of Temperature Distributions in UO_2 Reactor Fuel Elements, AE-318, 1968.

76. G. Kjaerheim, E. Rolstad, In-Pile Determination of UO_2 Thermal Conductivity, Density Effects and Gap Conductance, HPR-80, 1967.

77. M. J. F. Notley, "A Computer Program to Predict the Performance of UO_2 Fuel Elements Irradiated at High Power Outputs to a Burnup of 10,000 MWd/MTM," Nucl. Appl. vol. 9, p. 195 (August 1970).

78. A. S. Bain, Microscopic, Autoradiographic and Fuel/Sheath Heat Transfer Studies on UO_2 Fuel Elements, AECL-2588, June 1966.

79. A. S. Bain, Postirradiation Structures in UO_2 Quenched or Slowly Cooled From the Melt, AECL-2587, 1966.

80. R. D. MacDonald, Re-Irradiation of a High Burnup UO_2-Zircaloy Fuel Element at an Increased Heat Rating, AECL-2277, 1965.

81. J. R. MacEwan, J. Hayashi, "Grain Growth in UO_2: III - Some Factors Influencing Equiaxed Grain Growth," Presented at British Ceramic Society, AERE, Harwell, England, 1965.

82. I. Devold, Past, Present and Future Instrumented Fuel Assemblies at HBWR, HPR 35 1, section 2, 1964.

83. R. Soulhier and M. J. F. Notley, "Effect of Power Changes on Fission Product Gas Release from UO_2 Fuel," Nucl. Appl. vol. 5, p. 296.

84. D. O. Pickman, "Design of Fuel Elements," Nuclear Engineering and Design, vol. 21, no. 2, p. 308, 1972.

85. J. A. Dearien et al., Frap-S: A Computer Code for the Steady State of Oxide Fuel Rods, vol. 1, I-309-13.1, January 1975.

86. R. L. Miller et al., Frap-T: A Computer Code for the Transient Analysis of Oxide Fuel Rods, Matpro Materials Properties Subcode, vol. 2, ANC-I-243-2, January 15, 1975.

87. D. D. Lanning, C. R. Hann and E. S. Gilbert, Statistical Analysis and Modeling of Gap Conductance Data for Reactor Fuel Rods Containing UO_2 Pellets, BNWL-1832, August 1974.

88. D. R. Skeen and L. J. Page, Thermos/Battelle: The Battelle Version of the THERMOS Code, BNWL-516, September 1967.

APPENDIX A

INPUT VARIABLES FOR GAPCON-THERMAL-2

APPENDIX A

INPUT VARIABLES FOR GAPCON-THERMAL-2

Variable Name	Definition Comments and Units
DE	Equivalent diameter of the coolant passage (inches). Ignored if SIGHF is greater than zero.
EXTP	Coolant pressure (psi).
HBC	Heat transfer coefficient between basket and cladding (Btu/hr-ft^2-°F).
SIGHF	A signal to specify the type of coolant. If SIGHF < 0, coolant is water, a film coefficient will be calculated. If SIGHF > 0, coolant is unspecified and the film coefficient will be set to SIGHF.
V	Coolant velocity (ft/sec). Ignored if SIGHF is greater than zero.
CRUDTH	The thickness of crud on the cladding (inches). Assumed crud thermal conductivity is 0.23 Btu/hr-ft-°F.
ICOR	Signal for PWR (<3) or BWR (>3) Zr-coolant oxidation rate.
TINLET	Inlet coolant temperature (°F) - near axial node number 1. (In addition to the code that permits the user to input coolant temperature at each axial node. When TINLET (any axial code) = 0, then coolant temperature for that axial node is set equal to TINLET (1) - note DTEMP is not used when nodal TINLETS are used.
DTEMP	The axial ΔT across the core, (i.e. T outlet - T inlet), not used with nodal TINLET temperature.
KOOL	If a value (integer) greater than zero is assigned to KOOL, the cladding I.D. temperature is the same as the coolant temperature.
NCLAD	An integer signal to specify type of cladding. If NCLAD = 0, cladding is Zircaloy. If NCLAD < 0, cladding is 304 SS. If NCLAD > 0, cladding properties are input as described previously with the number of points (temperatures) input equal to NCLAD.
ZCLAD	An integer signal to specify Zr-2 or Zr-4 cladding. Material properties. If ZCLAD > 0, cladding is Zr-4. If ZCLAD < 0, cladding is Zr-2. NOTE: NCLAD must have a value of 0 to use ZCLAD.

Variable Name	Definition and Comments
ICDF	An integer signal that allows the user to include changes in the pellet-to-clad hot gap from elastic deflection of the clad due to differential internal and external pressures. If ICDF≠0, elastic clad deflection is taken into account. If ICDF=0, the option is not used. If a table of creepdown values (see ICREP) is input, this option should not be used.
ICREP	An integer signal to specify the number of cladding creepdown values to be input. If ICREP=0 it is assumed there is no time dependent cladding deformation. If ICREP>0 a table of time versus cladding creepdown values must be used. ICREP must equal the number of time values used in the table. Input format F10.0 and E10.0 (one set of values per card). (Limit of 20 values.)
DBθ	Outside diameter of a secondary cladding or basket (inches). If DBθ is omitted, no secondary cladding is assumed to exist.
KB	Thermal conductivity of the secondary cladding or basket (Btu/hr-ft°F).
DCI	Cladding inside diameter (inches).
DCθ	Cladding outside diameter (inches).
DFS	Fuel pellet diameter (inches).
DSINZ	Initial diameter of restructured fuel (normally equals 0.) (inches).
DVθIDZ	Diameter of initial central void in the fuel pellets (inches).
RθUC	Arithmetic mean cladding ID surface roughness (inches).
RθUF	Arithmetic mean fuel surface roughness (inches).
LFUEL	Length of fuel column (inches).
LVθIDZ	Length of initial central void in the fuel pellets (inches).
NPθW	Number of axial fuel segments. (limit of 20.)
FRDEN	Fractional density of the fuel pellet.
FRSIN	Fractional density of restructured fuel.
FR35	The weight fraction of the U which is ^{235}U (the remainder is assumed to be ^{238}U).

Variable Name	Definition and Comments
FR40	The weight fraction of the Pu which is ^{240}Pu.
FR41	The weight fraction of the Pu which is ^{241}Pu. The remaining fraction of Pu is assumed to be ^{239}Pu.
FRPUO2	The weight fraction of the fuel which is PuO_2 (the remainder is assumed to be UO_2).
NFUEL	An integer signal to specify the use of recycled UO_2-PuO_2; fuel thermal conductivity and melting temperature are changed accordingly. If NFUEL = 0 the thermal conductivity equation for UO_2 is used. If NFUEL · 0 the thermal conductivity equation for recycled UO_2-PuO_2 (PuO_2 additions up to 5 wt%) is used. If NFUEL · 0, a table of thermal conductivity values must be input.
TM	Melting temperature of the fuel (°C). If no value is input the code uses 2790°C.
TPLAS	The temperature at which the fuel becomes plastic. If no value is input the code uses 1200°C.
RADS	Radius of fuel pellet dish, inches.
PRCDH	Percent of fuel column volume that is dish volume (i.e., 100 x total dish volume/ total fuel column volume).

Variable	Definition and Comments
NFLX	An integer signal to specify flux depression values used. If NFLX = 0, flux depression values will be estimated in Subroutine DEPRES. NFLX should not be set to less than zero for fuel pins containing PuO_2 or for pins in which ^{235}U enrichment is greater than 4%. If NFLX < 0, it is assumed there is no flux depression. If NFLX > 0, a table of relative flux versus diameter is input as described previously with the number of points (diameters) equal to NFLX.
IRL	An integer to specify the output of flux depression values (from subroutine DEPRESS). If IRL = 0 eleven flux depression values and their respective pellet diameters will be printed out, with the first value given at the pellet centerline and the last at the pellet surface. If IRL >0 the subroutine DEPRESS will divide the fuel pellet into IRL equal nodes and print out the flux depression values and their appropriate diameters at the midplane of each node.
ISTØR	An integer to specify the calculation of stored energy in the fuel. If ISTØR = 0 no calculation is performed. If ISTØR ≠ 0 the calculation is performed.
IRELOC	A signal that allows the user to use the fuel relocation model developed for this code. If IRELOC = 0 change in fuel diameter due to relocation is 0, (i.e., relocation is not taken into account). If IRELOC > 0 the change in fuel radius due to relocation is taken into account by a best estimate value. If IRELOC < 0 the change in fuel radius due to relocation is taken into account by a conservative estimate i.e. gives less gap closure.
IDENSF	A signal that allows the user to include the effects of radial fuel shrinkage on the fuel-to-clad gap size due to isotropic densification. The code assumes the final density of the densified fuel to be 96.5% of theoretical. If IDENSF = 0 densification is not taken into account. If IDENSF ≠ 0 the change in fuel diameter due to densification is included. Fuel with a density greater than 96.5% will not swell to 96.5% T.D.
IT	A signal that allows the user to input the duration of the irradiation as burnup, MWd/MTM. These burnup values are read in through the namelist variable array TIME when IT ≠ 0. For regular input (days) set IT = 0 and use array TIME to read in the values.

Variable	Definition and Comments
IGAS	An integer signal to designate whether conservative or best estimate calculations are desired for gas release Set IGAS = 0 for best estimate ≠ 0 for conservative estimate (i.e., estimate is the 95% confidence boundary) - and yields more gas release
IRELSE	An integer signal to designate at which time the fission gas is to be released, during the time step (normal power operation) or after the time step (which would correspond to a reactor shut down or change in power). If IRELSE = 0 the gas is released during the time step. If IRELSE ≠ 0 the gas is released after the time step.
ATMOS	Initial fill gas pressure (atmospheres).
FRACHE	Fraction of initial fill gas which is helium.
FRACAR	Fraction of initial fill gas which is argon.
FRACH	Fraction of initial fill gas which is hydrogen.
FRACN	Fraction of initial fill gas which is nitrogen.
FRACKR	Fraction of initial fill gas which is krypton.
FRACXE	Fraction of initial fill gas which is xenon.
S	Fuel sorbed gas content (cc/g of fuel).
XCO	Fraction of sorbed gas that is carbon monoxide and carbon dioxide.
XH	Fraction of sorbed gas that is hydrogen and moisture.
XN	Fraction of sorbed gas that is nitrogen. Note: XCO + XH + XN should = 1.0 when S>0.
NOH	An integer signal to specify disposition of the hydrogen present in the sorbed gas. If NOH = 0, the hydrogen is assumed to react with the cladding. If NOH ≠ 0, the hydrogen is assumed to remain in the fuel pin as a gas.

Variable Name	Definition and Comments
VPLENZ	Volume of gas plenum included in the fuel pin (cubic inches).
TIME	A set of accumulative time increments (days) allows the user to follow a power history. NTIME values need to be input. LIMIT (15) values TIME (1) must = 0. Time (x) must be larger than previous time, time (x-1).
NTIME	Number of time increments. LIMIT (15)
PSEUDO	Power for each time step (kW/ft) allows the user to follow a power history. NTIME values need to be input. PSEUDO (1) and PSEUDO (2) may not = 0. (See IPEAK)
IPEAK	An integer to specify whether an average or peak power is to be input via PSEUDO. If IPEAK ≠ 0 an average power needs to be input, if IPEAK = 0 peak power needs to be input via PSEUDO.
PROFIL	A table that is used to input a normalized axial power profile for the pin. NPOW + 1 values for each profile needs to be input with the first and last values corresponding to the bottom and top of the fuel respectively. If more than one axial profile is to be used, then NPRFIL x (NPOW + 1) values have to be input in this table. If a power profile is not input a standard one in the code will be used.
NPRFIL	An integer signal to specify the number of axial power profiles, PROFIL, to be used for all time steps. If NPRFIL > 1, then NPRFIL = NTIME (i.e. an axial profile for each time step.
MINI	An integer signal to specify the output wanted. If MINI>0 a complete summary is given for each axial segment. If MINI=0 a complete summary is listed for the hottest segment of the pin and a short summary given for all the axial segments. MINI<0 only a short summary is given for the axial segments.

APPENDIX B

REVISIONS TO FISGAS

APPENDIX B

REVISIONS TO FISGAS[9]

The coding of the mathematical models in the FISGAS subroutine of GAPCON has been revised to improve the accuracy of the calculations. Several refinements have also been added. A description of the work follows.

The differential equations from the models in FISGAS for the concentrations of the krypton isotopes and of the xenon isotopes and their precursors were recoded in improved solutions which avoid an approximation used in a majority of the original equations. The mathematical model for these isotopes was otherwise unchanged. The number of equations for the model of the fuel isotopes was reduced from 15 to 6. The new solutions retain the assumption that the flux remains constant over a time step. However, an optional feature was added whereby the input time step can be subdivided into equal intervals over each of which the flux is constant. Provision in the coding was also made for two other modifications, though neither was implemented. One of these permits the energy per fission to depend on the isotope; the other permits the cross sections of both fuel and fission product isotopes to be a linear combination of the thermal and fast cross sections, rather than one or the other, as at present. This latter modification is an early attempt to correct for the inadequacy of the thermal cross sections.

The accuracy of the revisions was checked by comparison with solutions of the original equations found by ALCHEMY, a general purpose nuclear transmutation code.[46] The internal FISGAS isotope data and a flux typical of a commercial light-water power reactor were used in this comparison. Calculations were made at 17 time points, ranging from 4 hours to 1080 days. Solid agreement for the fission gas concentrations was obtained in the 8-figure answers, indicating that the coding logic errors were minimal and single precision arithmetic was adequate. The fast cross sections were not checked. For the fuel isotopes, the comparison was between the 15 equations in ALCHEMY and the 6 equations in FISGAS. The agreement is

considered adequate for FISGAS purposes; the solutions for U-235 and U-238 are exact and the solutions for the plutoniums agree to within a fraction of a percent for Pu-239 and to a few percent for Pu-240 and Pu-241 at the longer times. At the shorter times, where the neglect of the intermediate isotopes in the plutonium production chain in the shortened set of equations has its major effect, the concentrations of the plutoniums are too small to influence the results significantly. Two further tests were made with ALCHEMY alone, to check on the magnitude of two other reactions contributing to Pu-239 production via Pu-238. One of these is from U-235 capture, which was included in the 15 equations in the earlier FISGAS set, and the other is from the (n,2n) reaction in U-238, which was not. Both effects are a small fraction of a percent at the longer times and are considered negligible. Although these results were obtained with thermal cross sections that are considered inadequate, the conclusions should remain valid with more suitable cross sections.

Inadequacy in FISGAS and Recommended Revision

The thermal cross sections in FISGAS are inadequate, especially considering the relative sophistication of the mathematical model for the calculation of fuel and gaseous fission product concentrations. The fast cross sections have not been examined in detail; however, their adequacy is relatively unimportant in GAPCON-THERMAL. The inadequacy of these thermal cross sections was evident when the changes were tested which permitted time step subdivision with recalculation of the flux to maintain constant power. The flux rose unrealistically. For example, in one test in which the flux change per subdivision was restricted to 1% or less, so that frequent subdivisions were made, the flux at 90 days was almost double the original flux. In another test in which no subdivisions were made of the 17 input time steps, the flux at 90 days was only 25% greater than the original flux but the flux at 1080 days was 8 times the original flux.

These unrealistic numbers can be attributed principally to the cross section of U-238. Most of the plutonium production in light water reactors is due to the resonance absorption of neutrons in U-238. The U-238 cross

section in FISGAS is the 2200 m/sec value. Hence the plutonium production is seriously underestimated and, for the model to maintain constant power, the flux must be increased until the rapidly depleting U-235 can provide the fissions. The following table, which gives cross sections relative to U-235 absorption, illustrates the effect more quantitatively. The two sets of numbers are not strictly comparable because of the different fuels, but are close enough that the differences are mainly due to the neglect of epithermal cross sections in FISGAS. The U-238 absorption cross section is only about 1/5 of what it should be. The Pu-240 cross section is even more in error but its effect is smaller. The Pu-239 and Pu-241 cross sections are likewise in error, by about a factor of two.

	ZODIAC[47] - 3.0% U-235		FISGAS - 3.4% U-235	
Isotope	Absorption	Fission	Absorption	Fission
U-235	1.000	0.811	1.000	0.798
U-238	0.0192	0.0016	0.0039	0.0
Pu-239	3.316	2.108	1.602	1.068
Pu-240	4.060	0.010	0.418	0.0
Pu-241	2.922	2.195	1.948	1.371

The effect of these cross sections is serious enough that the option for subdividing the time step and recalculating the flux should not be used until the cross sections are changed. In addition, each time should be run as a separate case so that the yields of the fission products are calculated only with the original fuel composition. This procedure is effectively what was done with the flux and the yields in the previous version of FISGAS.

To remedy this situation, it is recommended that another cross section model, say the Westcott formalism, be inserted in FISGAS as soon as possible.[48] This is the model used in ALTHAEA, though a simplified version of the ALTHAEA[49] model would probably suffice. In the Westcott formalism, the effective cross section is written as

$$\hat{\sigma} = \sigma_0(g + rs)$$

where σ_0 is the 2200 m/sec value, g corrects for non-1/v and temperature effects in the thermal energy range, s corrects for epithermal effects, and r accounts for the epithermal/thermal flux ratio. This formalism has been widely used in burnup calculations, and a large amount of experience has accrued about its use. The major effort in inserting the formalism would be to provide tables of g and s for each isotope and reaction type, preferably as a function of temperature. The parameter r is the same for all isotopes.

This revision would apply only to the thermal cross sections in FISGAS. The fast cross sections may need an analogous revision, but probably not crucially at this time.

The Xenon Equations in FISGAS

The following 14 differential equations for the xenon isotopes and their precursors were deduced from the coding of the earlier version of FISGAS. The notation is principally that of FISGAS.

$$\frac{dN_{106}}{dt} = F_6 - X_{106} N_{106}$$

$X_{106} = \lambda_{106}$ Te 131 I (1)

$T_{106} = 1.2$ d

$$\frac{dN_{107}}{dt} = F_7 + A_6 X_{106} N_{106} - X_{107} N_{107}$$

$X_{107} = \lambda_{107}$ Te 131 (2)

$T_{107} = 25$ m.

$A_6 = .18$

$$\frac{dN_{108}}{dt} = F_8 + (1-A_6) X_{106} N_{106} + X_{107} N_{107} - X_{108} N_{108}$$

$X_{108} = \lambda_{108}$ I 131 (3)

$T_{108} = 8.05$ d

$$\frac{dN_{109}}{dt} = F_9 + X_{108}N_{108} - X_{109}N_{109}$$ $X_{109} = \sigma_{109}\phi$ Xe 131 (4)

$\sigma_{109} = 85$ b (0)

$$\frac{dN_{110}}{dt} = F_{10} - X_{110}N_{110}$$ $X_{110} = \lambda_{110}$ Te 132 (5)

$T_{110} = 78$ h.

$$\frac{dN_{111}}{dt} = F_{11} + X_{110}N_{110} - X_{111}N_{111}$$ $X_{111} = \lambda_{111}$ I 132 (6)

$T_{111} = 2.3$ h.

$$\frac{dN_{112}}{dt} = F_{12} + X_{109}N_{109} + X_{111}N_{111} - X_{112}N_{112}$$ $X_{112} = \sigma_{112}\phi$ Xe 132 (7)

$\sigma_{112} = 5$ b (0)

$$\frac{dN_{113}}{dt} = F_{13} - X_{113}N_{113}$$ $X_{113} = \lambda_{113}$ I 133 (8)

$T_{113} = 21$ h.

$$\frac{dN_{114}}{dt} = F_{14} + X_{113}N_{113} - X_{114}N_{114}$$ $X_{114} = \lambda_{114} + \sigma_{114}\phi$ Xe 133 (9)

$T_{114} = 5.27$ d.

$\sigma_{114} = 190$ b (0)

$$\frac{dN_{115}}{dt} = F_{15} + A_{14}X_{114}N_{114}$$ $A_{14} = \sigma_{114}\phi/X_{114}$ Xe 134 (10)

$$\frac{dN_{116}}{dt} = F_{16} - X_{116}N_{116}$$ $X_{116} = \lambda_{116}$ I 135 (11)

$T_{116} = 6.7$ h.

$$\frac{dN_{117}}{dt} = F_{17} + A_{16}X_{116}N_{116} - X_{117}N_{117}$$ $X_{117} = \lambda_{117}$ Xe 135 I (12)

$T_{117} = 16$ m.

$A_{16} = .3$

$$\frac{dN_{118}}{dt} = F_{18} + (1-A_{16})\, X_{116}N_{116} + X_{117}N_{117} - X_{118}N_{118} \qquad X_{118} = \lambda_{118}+\sigma_{118}\phi \quad \text{Xe 135} \qquad (13)$$

$$T_{118} = 9.2 \text{ h.}$$

$$\sigma_{118} = 2.7 \times 10^6 \text{ b (0)}$$

$$\frac{dN_{119}}{dt} = F_{19} + A_{18}X_{118}N_{118} \qquad A_{18} = \sigma_{118}\phi/X_{118} \quad \text{Xe 136} \qquad (14)$$

In these equations, F_i is the fission yield of isotope i, hereafter assumed constant over each time interval, and A_i in the equation for isotope j is the fraction of the transmutation rate X_iN_i of isotope i which results in isotope j. The half-life T_i given for i is taken from the BNW Chart of the Nuclides,[50] 1969, and does not correspond exactly with λ_i, the decay constant given in the FISGAS data. The σ_i is the thermal absorption cross sections in FISGAS. The numbers in parentheses by the thermal cross sections are the fast cross sections; these are seen to be set to zero for these isotopes in FISGAS.

Since the only xenon quantity transmitted to GAPCON from FISGAS is the total xenon concentration, the solution technique adapted in the recoding was to focus on calculating this total concentration rather than the concentrations of the individual isotopes. The solution is characterized by the presence of a term for each transmutation constant $X_i\Delta t$, where Δt is the time interval; the task is to determine algebraically the coefficient of each term in this solution. The algebra is straightforward but tedious, and only sketchy details will be given.

The first step in the procedure was to diagonalize the matrix representation of equations (1)-(14). That is, quantities C_j were determined as linear combinations of the N_i such that (1)-(14) could be replaced by an equivalent set of 14 equations, each of the form

$$\frac{dC_j}{dt} = Y_j - X_jC_j \qquad (15)$$

The Y_j in (15) are similarly linear combinations of the F_i. Expressions for these linear combinations will be given later. The advantage of expressing the solutions of (1)-(14) in terms of the C_j rather than the N_i is that the solution of each equation in the form of (15) can be written as

$$\Delta C_j = C_j - C_j^o = \left(\frac{Y_j}{X_j} - C_j^o\right)\left(1 - e^{-X_j \Delta t}\right) \tag{16}$$

That is, C_j depends on time only through the transmutation constant $X_j \Delta t$ In terms of the N_i, clearly for the time interval Δt

$$\Delta N_{Xe} = \Delta N_{109} + \Delta N_{112} + \Delta N_{114} + \Delta N_{115} + \Delta N_{117} + \Delta N_{118} + \Delta N_{119} \tag{17}$$

For reasons which will be explained later, the result will be written in terms of the change in xenon concentration, as

$$\begin{aligned}
\Delta N_{Xe} = {} & \Delta C_{115} + \Delta C_{119} - \frac{X_{112}}{X_{109}-X_{112}} \Delta C_{109} + \Delta C_{112} + (1-A_{18})\Delta C_{118} \\
& + (1-A_{14})\Delta C_{114} - (1-A_{18}) \frac{X_{118}}{X_{117}-X_{118}} \Delta C_{117} \\
& - \frac{X_{107}}{X_{107}-X_{108}} \frac{X_{108}}{X_{107}-X_{109}} \left(\frac{X_{109}}{X_{107}-X_{112}} - 1\right)\Delta C_{107} - \frac{X_{111}}{X_{111}-X_{112}} \Delta C_{111} \\
& - \left[A_{18} + (1-A_{18})\left\{\frac{X_{116}}{X_{116}-X_{118}}\left(1 - \frac{A_{16}X_{116}}{X_{116}-X_{117}}\right) + \frac{A_{16}\, X_{116}}{X_{116}-X_{117}}\right\}\right] \Delta C_{116} \\
& - \left[A_{14} + (1-A_{14}) \frac{X_{113}}{X_{113}-X_{114}}\right] \Delta C_{113} \\
& - \frac{X_{106}}{X_{106}-X_{108}} \frac{X_{108}}{X_{106}-X_{109}} \left(1 - \frac{A_6\, X_{106}}{X_{106}-X_{107}}\right)\left(\frac{X_{109}}{X_{106}-X_{112}} - 1\right) \Delta C_{106} \\
& + \frac{X_{110}}{X_{110}-X_{111}} \frac{X_{111}}{X_{110}-X_{112}} \Delta C_{110} + \frac{X_{108}}{X_{108}-X_{109}} \left(\frac{X_{109}}{X_{108}-X_{112}} - 1\right)\Delta C_{108}
\end{aligned} \tag{18}$$

where

$$\Delta C_{115} = \left[A_{14}\left(F_{13} + F_{14}\right) + F_{15}\right]\Delta t \tag{19}$$

$$\Delta C_{119} = \left[A_{18}\left(F_{16} + F_{17} + F_{18}\right) + F_{19}\right]\Delta t \tag{20}$$

$$\Delta C_{109} = \left[\frac{X_{106}}{X_{106}-X_{109}}\,\frac{X_{108}}{X_{108}-X_{109}}\left(1+\frac{A_6\,X_{109}}{X_{107}-X_{109}}\right)F_6 + \frac{X_{107}}{X_{107}-X_{109}}\,\frac{X_{108}}{X_{108}-X_{109}}\,F_7\right.$$

$$\left. + \frac{X_{108}}{X_{108}-X_{109}}\,F_8 + F_9 - X_{109}C^{o}_{109}\right]\left(\frac{1-e^{-X_{109}\Delta t}}{X_{109}}\right) \tag{21}$$

$$\Delta C_{112} = \left[\frac{X_{106}}{X_{106}-X_{112}}\,\frac{X_{108}}{X_{108}-X_{112}}\,\frac{X_{109}}{X_{109}-X_{112}}\left(1+\frac{A_6\,X_{112}}{X_{107}-X_{112}}\right)F_6\right.$$

$$+ \frac{X_{107}}{X_{107}-X_{112}}\,\frac{X_{108}}{X_{108}-X_{112}}\,\frac{X_{109}}{X_{109}-X_{112}}\,F_7 + \frac{X_{108}}{X_{108}-X_{112}}\,\frac{X_{109}}{X_{109}-X_{112}}\,F_8$$

$$+ \frac{X_{109}}{X_{109}-X_{112}}\,F_9 + \frac{X_{110}}{X_{110}-X_{112}}\,\frac{X_{111}}{X_{111}-X_{112}}\,F_{10} + \frac{X_{111}}{X_{111}-X_{112}}\,F_{11}$$

$$\left. + F_{12} - X_{112}C^{o}_{112}\right]\left(\frac{1-e^{-X_{112}\Delta t}}{X_{112}}\right) \tag{22}$$

$$\Delta C_{118} = \frac{X_{116}}{X_{116}-X_{118}}\left(1+\frac{A_{16}\,X_{116}}{X_{116}-X_{117}}\right)F_{16} + \frac{X_{117}}{X_{117}-X_{118}}\,F_{17} + F_{18}$$

$$\left. - X_{118}\,C^{o}_{118}\right]\left(\frac{1-e^{-X_{118}\Delta t}}{X_{118}}\right) \tag{23}$$

$$\Delta C_{114} = \left[\frac{X_{113}}{X_{113}-X_{114}} F_{13} + F_{14} - X_{114}\, C^{o}_{114} \right] \left(\frac{1 - e^{-X_{114}\Delta t}}{X_{114}} \right) \tag{24}$$

$$\Delta C_{117} = \left[\frac{A_{16}\, X_{116}}{X_{116}-X_{117}} F_{16} + F_{17} - X_{117}\, C^{o}_{117} \right] \left(\frac{1-e^{-X_{117}\Delta t}}{X_{117}} \right) \tag{25}$$

$$\Delta C_{107} = \left[\frac{A_{6}\, X_{106}}{X_{106}-X_{107}} F_{6} + F_{7} - X_{107}\, C^{o}_{107} \right] \left(\frac{1-e^{-X_{107}\Delta t}}{X_{107}} \right) \tag{26}$$

$$\Delta C_{111} = \left[\frac{X_{110}}{X_{110}-X_{111}} F_{10} + F_{11} - X_{111}\, C^{o}_{111} \right] \left(\frac{1-e^{-X_{111}\Delta t}}{X_{111}} \right) \tag{27}$$

$$\Delta C_{116} = \left[F_{16} - X_{116}\, C^{o}_{116} \right] \left(\frac{1-e^{-X_{116}\Delta t}}{X_{116}} \right) \tag{28}$$

$$\Delta C_{113} = \left[F_{13} - X_{113}\, C^{o}_{113} \right] \left(\frac{1-e^{-X_{113}\Delta t}}{X_{113}} \right) \tag{29}$$

$$\Delta C_{106} = \left[F_{6} - X_{106}\, C^{o}_{106} \right] \left(\frac{1-e^{-X_{106}\Delta t}}{X_{106}} \right) \tag{30}$$

$$\Delta C_{110} = \left[F_{10} - X_{110}\, C^{o}_{110} \right] \left(\frac{1-e^{-X_{110}\Delta t}}{X_{110}} \right) \tag{31}$$

$$\Delta C_{108} = \left[\frac{X_{106}}{X_{106}-X_{108}} \left(1 + \frac{A_6 X_{108}}{X_{107}-X_{108}} \right) F_6 + \frac{X_{107}}{X_{107}-X_{108}} F_7 + F_8 - X_{108} C^o_{108} \right] \left(\frac{1-e^{-X_{108}\Delta t}}{X_{108}} \right) \tag{32}$$

The C_i^o in these equations are the values of the C_i at the beginning of a time step; the $C_i^o + \Delta C_i$ for one time step are thus the C_i for the next time step. The order in which the ΔC_i are given is the order in which they are calculated in FISGAS. This order was chosen to simplify the calculation for multiple time steps. The first two, C_{115} and C_{119}, have contributions proportional to Δt because their X_i are zero; their contributions never vanish. The next two, C_{109} and C_{112}, have no radioactive decay and small cross sections; their contributions eventually vanish, but not for flux times of practical interest. The contributions of these four are thus always present for a time step. The remaining ten all decay radioactively fast enough that they approach an equilibrium value in times of practical interest; their ΔC_i will eventually vanish in a time step because the square bracket coefficient of the $1 - e^{-X_i \Delta t}$ becomes zero. The first of these last ten, C_{118} and C_{114}, have also nonzero cross sections and appear in order of vanishing of their contributions. The remaining eight have only radioactive decay and are arranged in order of vanishing of their contributions.

<u>The Krypton Equations in FISGAS</u>

$$\frac{dN_{101}}{dt} = F_1 - X_{101} N_{101} \qquad X_{101} = \sigma_{101}\phi \qquad \sigma_{101} = 180 \text{ b}(0) \qquad \text{Kr 83} \quad (1)$$

$$\frac{dN_{102}}{dt} = F_2 + X_{101} N_{101} \qquad \text{Kr 84} \quad (2)$$

$$\frac{dN_{103}}{dt} = F_3 - X_{103}\, N_{103} \qquad X_{103} = \lambda_{103} \qquad \text{Kr 85 I} \quad (3)$$

$$T_{103} = 4.4 \text{ h.}$$

$$\frac{dN_{104}}{dt} = F_4 + A_3\, X_{103}\, N_{103} - X_{104}\, N_{104} \qquad X_{104} = \lambda_{104} + \sigma_{104}\phi \qquad \text{Kr 85} \quad (4)$$

$$T_{104} = 10.76 \text{ y.}$$

$$\sigma_{104} = 15 \text{ b (0)}$$

$$A_3 = .21$$

$$\frac{dN_{105}}{dt} = F_5 + A_4\, X_{104}\, N_{104} \qquad A_4 = \sigma_{104}\phi / X_{104} \qquad \text{Kr 86} \quad (5)$$

The definitions of the quantities and the method of solution are the same as for the equations for the xenon isotopes and their precursors. The krypton equations are much simpler; however, they are fewer in number and no precursors are included. In addition, the facts that X_{102} and X_{105} are zero and that Kr-83 transmutes completely to Kr-84 make a further simplification possible: only C_{103} and C_{104} must be followed separately. The change in krypton concentration in a time interval Δt can be written as

$$\begin{aligned} \Delta N_{Kr} &= \Delta N_{101} + \Delta N_{102} + \Delta N_{103} + \Delta N_{104} + \Delta N_{105} \\ &= \left[F_1 + F_2 + A_3 A_4 F_3 + A_4 F_4 + F_5 \right] \Delta t \\ &+ \left[1 - A_3 A_4 - B_3\,(1-A_4) \right] \Delta C_{103} + (1-A_4)\, \Delta C_{104} \end{aligned} \qquad (6)$$

where

$$\Delta C_{103} = \left[F_3 - X_{103}\, C^o_{103} \right] \left(\frac{1-e^{-X_{103}\Delta t}}{X_{103}} \right) \qquad (7)$$

$$\Delta C_{104} = \left[B_3 F_3 + F_4 - X_{104} C^o_{104} \right] \left(\frac{1-e^{-X_{104}\Delta t}}{X_{104}} \right) \tag{8}$$

and

$$B_3 = \frac{A_3 \, X_{103}}{X_{103} - X_{104}} \tag{9}$$

The radioactive decay rate of C_{103} is such that C_{103} quickly reaches an equilibrium value and ΔC_{103} vanishes for subsequent time steps. Contributions from the other C_i are always present.

The Fuel Isotope Equations in FISGAS

The following 15 differential equations for the fuel isotopes and their precursors were deduced from the coding of the earlier version of FISGAS.

$$\frac{dN_1}{dt} = - X_1 N_1$$

$X_1 = \sigma_1 \phi$ U 238 (1)

$\sigma_1 = 2.7$ b (14)

$$\frac{dN_2}{dt} = A_1 X_1 N_1 - X_2 N_2$$

$X_2 = \lambda_2 + \sigma_2 \phi$ U 239 (2)

$T_2 = 23.5$ m

$\sigma_2 = 36$ b (0)

$A_1 = \sigma_{c1}/\sigma_1$

$\sigma_{c1} = 2.7$ b(0.1)

$$\frac{dN_3}{dt} = B_2 X_2 N_2 - X_3 N_3$$

$X_3 = \lambda_3 + \sigma_3 \phi$ Np 239 (3)

$T_3 = 2.35$ d.

$\sigma_3 = 60$ b (0)

$B_2 = \lambda_2 / X_2$

$$\frac{dN_4}{dt} = A_2 X_2 N_2 - X_4 N_4$$

$X_4 = \lambda_4$ U 240 (4)

$T_4 = 14.1$ h

$A_2 = \sigma_{c2} \phi / X_2$

$\sigma_{c2} = 22$ b (0)

$\frac{dN_5}{dt} = A_3X_3N_3 + X_4N_4 - X_5N_5$	$X_5 = \lambda_5$ $T_5 = 7.3$ m. $A_3 = \sigma_{c3}\phi/X_3$ $\sigma_{c3} = 60$ b (0)	Np 240 I	(5)
$\frac{dN_6}{dt} = X_5N_5 - X_6N_6$	$X_6 = \lambda_6$ $T_6 = 60$ m.	Np 240	(6)
$\frac{dN_{10}}{dt} = - X_{10}N_{10}$	$X_{10} = \sigma_{10}\phi$ $\sigma_{10} = 693$ b (6.6)	U 235	(7)
$\frac{dN_{11}}{dt} = A_{10}X_{10}N_{10} - X_{11}N11$	$X_{11} = \sigma_{11}\phi$ $\sigma_{11} = 6$ b (0.3) $A_{10} = \sigma_{c10}/\sigma_{10}$ $\sigma_{c10} = 140$ b (5.2)	U 236	(8)
$\frac{dN_{12}}{dt} = A_{11}X_{11}N_{11} - X_{12}N_{12}$	$X_{12} = \lambda_{12}$ $T_{12} = 6.75$ d. $A_{11} = \sigma_{c11}/\sigma_{11}$ $\sigma_{c11} = 6$ b (0.3)	U 237	(9)
$\frac{dN_{13}}{dt} = X_{12}N_{12} - X_{13}N_{13}$	$X_{13} = \sigma_{13}\phi$ $\sigma_{13} = 170$ b (13)	Np 237	(10)
$\frac{dN_{14}}{dt} = A_{13}X_{13}N_{13} - X_{14}N_{14}$	$X_{14} = \lambda_{14}+\sigma_{14}\phi$ $T_{14} = 2.10$ d. $\sigma_{14} = 1600$ b (0) $A_{13} = \sigma_{c13}/\sigma_{13}$ $\sigma_{c13} = 170$ b (13)	Np 238	(11)

$$\frac{dN_{15}}{dt} = B_{14}X_{14}N_{14} - X_{15}N_{15}$$

$X_{15} = \lambda_{15} + \sigma_{15}\phi$ Pu 238 (12)
$T_{15} = 89$ y.
$\sigma_{15} = 597$ b (2.6)
$B_{14} = \lambda_{14}/X_{14}$

$$\frac{dN_7}{dt} = B_3X_3N_3 + A_{15}X_{15}N_{15} - X_7N_7$$

$X_7 = \sigma_7\phi$ Pu 239 (13)
$\sigma_7 = 1110$ b (1.6)
$B_3 = \lambda_3/X_3$
$A_{15} = \sigma_{c15}\phi/X_{15}$
$\sigma_{c15} = 580$ b (0)

$$\frac{dN_8}{dt} = X_6N_6 + A_7X_7N_7 - X_8N_8$$

$X_8 = \sigma_8\phi$ Pu 240 (14)
$\sigma_8 = 290$ b (1.6)
$A_7 = \sigma_{c7}/\sigma_7$
$\sigma_{c7} = 370$ b (0)

$$\frac{dN_9}{dt} = A_8X_8N_8 - X_9N_9$$

$X_9 = \sigma_9\phi$ Pu 241 (15)
$\sigma_9 = 1350$ b (1.6)
$A_8 = \sigma_{c8}/\sigma_8$
$\sigma_{c8} = 290$ b (0)

These equations differ in form from the xenon and krypton equations in one important aspect: the fuel isotope equations have no external source terms. In addition, the concentrations of the fissioning isotopes are needed to determine the fission product yields and the flux to maintain a given power level. Consideration of these differences has led to use of a modification of the solution procedure used for the gaseous product equations: the N_i rather than the ΔC_i are calculated explicitly.

More significantly, further consideration of the uses of the fuel isotopes has also resulted in the elimination of 9 of the equations. This decision was made primarily on the basis of the following points: (1) The primary purpose of FISGAS calculations is to find the krypton and xenon concentrations, (2) only U-235, U-238, Pu-239, and Pu-241 fission yields are provided, and (3) fission energy release from only the principal fissioning isotopes is sufficient for determining the flux. In other words, the contributions of the neglected isotopes are negligible either because they are small at the longer times or occur at such short times that the xenon and krypton concentrations are small. The 6 equations retained are

$$\frac{dN_1}{dt} = - X_1 N_1 \qquad \text{U 238} \qquad (1)$$

$$\frac{dN_3}{dt} = B_2 A_1 X_1 N_1 - X_3 N_3 \qquad \text{Np 239} \qquad (3')$$

$$\frac{dN_{10}}{dt} = - X_{10} N_{10} \qquad \text{U 235} \qquad (7)$$

$$\frac{dN_7}{dt} = B_3 X_3 N_3 - X_7 N_7 \qquad \text{Pu 239} \qquad (13')$$

$$\frac{dN_8}{dt} = A_7 X_7 N_7 - X_8 N_8 \qquad \text{Pu 240} \qquad (14')$$

$$\frac{dN_9}{dt} = A_8 X_8 N_8 - X_9 N_9 \qquad \text{Pu 241} \qquad (15)$$

Note that three of these equations are slightly modified from the originals: the equation for Np-239 assumes that U-239 is always in equilibrium with U-238 and the equations for Pu-239 and Pu-240 have each dropped a term as negligible.

The solutions of these equations can be written

$$N_1 = N_1^o \, e^{-X_1 \Delta t} \tag{16}$$

$$C_3 = C_3^o \, e^{-X_2 \Delta t} \tag{17}$$

$$C_7 = C_7^o \, e^{-X_7 \Delta t} \tag{18}$$

$$N_7 = C_7 - \frac{A_1 X_1}{X_1 - X_2} \frac{B_2 X_2}{X_1 - X_3} \frac{B_3 X_3}{X_1 - X_7} N_1 - \frac{B_3 X_3}{X_3 - X_7} C_3 \tag{19}$$

$$C_8 = C_8^o \, e^{-X_8 \Delta t} \tag{20}$$

$$N_8 = C_8 + \frac{A_1 X_1}{X_1 - X_2} \frac{B_2 X_2}{X_1 - X_3} \frac{B_3 X_3}{X_1 - X_7} \frac{A_7 X_7}{X_1 - X_8} N_1 + \frac{B_3 X_3}{X_3 - X_7} \frac{A_7 X_7}{X_3 - X_8} C_3 - \frac{A_7 X_7}{X_7 - X_8} C_7 \tag{21}$$

$$C_9 = C_9^o \, e^{-X_9 \Delta t} \tag{22}$$

$$N_9 = C_9 - \frac{A_1 X_1}{X_1 - X_2} \frac{B_2 X_2}{X_1 - X_3} \frac{B_3 X_3}{X_1 - X_7} \frac{A_7 X_7}{X_1 - X_8} \frac{A_8 X_8}{X_1 - X_9} N_1 - \frac{B_3 X_3}{X_3 - X_7} \frac{A_7 X_7}{X_3 - X_8} \frac{A_8 X_8}{X_3 - X_9} C_3 + \frac{A_7 X_7}{X_7 - X_8} \frac{A_8 X_8}{X_7 - X_9} C_7 - \frac{A_8 X_8}{X_8 - X_9} C_8 \tag{23}$$

The Earlier FISGAS Approximation

The approximation made in the earlier version of FISGAS in solving the equation for the concentration of a daughter isotope can be illustrated by the following typical equation. Let

$$\frac{dN_i(t)}{dt} = A_{i-1}\, X_{i-1}\, N_{i-1}(t) - X_i N_i(t) \tag{1}$$

where $X_j = \sigma_{aj}\phi + \lambda_j$, and A_{i-1} is the fraction of the transmutations, $X_{i-1}\, N_{i-1}$ of isotope i-1 which result in isotope i; both A_{i-1} and the X_j are assumed constant. The formal solution to (1) can be written as

$$N_i(t) = N_i(0)e^{-X_i t} + A_{i-1}X_{i-1}\int_0^t e^{-X_i(t'-t)}\, N_{i-1}(t')dt' \tag{2}$$

The earlier FISGAS approximation was to assume

$$N_{i-1}(t') \doteq N_{i-1}(t)$$

so that (2) became

$$N_i(t) \doteq N_i(o)e^{-X_i t} + A_{i-1}\, X_{i-1}\, N_{i-1}(t)\left(\frac{1-e^{-X_i t}}{X_i}\right) \tag{3}$$

This approximation is not as accurate as the improved method described earlier.

APPENDIX C

MODELS AND DATA UNALTERED FROM GAPCON-THERMAL-1

APPENDIX C

MODELS AND DATA UNALTERED FROM GAPCON-THERMAL-1

The following models are unaltered from the previous version of GAPCON-THERMAL and the descriptions are repeated in this section.

UO_2 Thermal Conductivity
Porosity Correction
Fuel Thermal Expansion
Restructuring
Fission Product Swelling
Stored Thermal Energy - HCAP and CARL
Flux Depression - DEPRES
Properties of Zr and Stainless Steel*
Cladding Elastic Deflection
Cladding Creep
Gas Properties
Internal Gas Pressure Model
Power and Coolant Temperature Profiles - POWDIS
Axial Segments for Analyzing Power Profiles
Radiation Heat Transfer
Radial Temperature Calculations - RTEMP
Water-to-Cladding Heat Transfer Coefficient - HTCW
Linear Interpolation - TERP and TEPP

---

* See note bottom of page C-9.

UO_2 Thermal Conductivity Equation

The code utilizes the thermal conductivity equation derived by Lyons, et al.[51,52] for 95% TD UO_2

$$K = \frac{38.24}{402.4 + T} + 6.1256\times10^{-13}(T + 273)^3 \qquad [1]$$

K = Thermal conductivity (W/cm-°C)

T = Temperature (°C)

Equation 1 yields an integral-to-melt value of 93 W/cm, is a best estimate of the data, and replaces Equation 2 below which is based on extrapolation of Godfreys, et al.[53] data from 1100°C to the melting point

$$K = \frac{45.1}{135 + T} + 4.79\times10^{-13}T^3 \qquad [2]$$

K = Thermal conductivity (W/cm-°C)

T = Temperature (°K)

Porosity Correction Factor for UO_2 Thermal Conductivity

The Maxwell-Eucken[54,55] relationship, Equation 3, is used to account for effects of porosity on UO_2 thermal conductivity

$$Kp = k_{100}\frac{(1 - P)}{(1 + \beta P)} \qquad [3]$$

Kp = thermal conductivity of UO_2 with porosity, P

k_{100} = thermal conductivity of 100% dense UO_2

P = volume fraction of porosity

β = porosity coefficient (β = 0.5 is used for fuel densities greater than 90% TD)

The value of 0.5 for beta is based on recommendations of Belle, et al.[56]

Equation 3 is used as a multiplier to the UO_2 thermal conductivity equation:

$$\frac{1.025}{0.95}\left[\frac{F}{1 + (1 - F)\ 0.5}\right] \qquad [4]$$

F = fraction of theoretical density

The Maxwell-Eucken relationship replaces the Loeb[57] correction (Equation 5) used originally in GAPCON[8]

$$Kp = k_{100}\left(1 - \alpha\right)\left(\frac{\rho_{100} - \rho}{\rho_{100}}\right) = k_{100}(1 - \alpha P) \qquad [5]$$

ρ = density

P = volume fraction of porosity

α = porosity coefficient (α = 2.5 in GAPCON)

The Loeb equation was a recommendation of the IAEA Panel on Thermal Conductivity[58] wherein the value of alpha ranged from 1 to 4. The use of the Maxwell-Eucken relationship reduces some of the conservation in fuel temperatures for low density fuel.

Thermal Expansion of UO_2 - Subroutine EXPAND

We use an equation developed by Conway, Fincel, and Hein[38] to calculate thermal expansion for UO_2. It is the best available for UO_2.

$$\frac{\Delta L}{L} = 2.896\text{x}10^{-9}T^2 + 6.797\text{x}10^{-6}T - 1.723\text{x}10^{-4} \qquad [6]$$

Note: The equation often appears with a positive $1.723\text{x}10^{-4}$ which is a typographical error[59]

An average alpha is calculated with Equation 7.

$$\alpha = \frac{\Delta L/L}{\Delta T} = (T^2 - 625)2.896\text{x}10^{-9} + (T - 25)6.797\text{x}10^{-6}\ \frac{1}{(T - 25)} \qquad [7]$$

EXPAND calculates the increase in fuel radius caused by thermal expansion of the fuel as follows. The fuel pellet is divided into 50 equally spaced radial increments. Each annular ring formed is assumed to be a free body at its average temperature T. The increase in radius of each ring due to thermal expansion in the circumferential direction is calculated from:

$$\Delta R_c = \alpha R_{avg} (T - T_r) \qquad [8]$$

where ΔR_c = increase in radius due to expansion in the circumferential direction

α = linear coefficient of thermal expansion

R_{avg} = average radius of the increment

T = average temperature of the increment (°C)

T_r = room temperature (25°C).

The code then finds that node in which the maximum increase in radius occurs, and it is assumed that all the thermal expansion that occurs inside that increment is accounted for by the radius increase of that increment. EXPAND then calculates the increase in thickness of each node outside the node of maximum circumferential expansion from

$$\Delta t_i = \alpha t (T - T_r) \qquad [9]$$

where Δt_i = increase in thickness of increment i due to thermal expansion in the radial direction.

t = initial thickness of node i.

The total increase in fuel radius due to thermal expansion is then assumed to be:

$$\Delta R = (\Delta R_c)_{max} + \left(\sum_{i=1}^{L} \Delta t_i \right) - \frac{\Delta t_i}{2} \qquad [10]$$

where ΔR = total increase in fuel radius due to thermal expansion

L = the number of the increment immediately outside that increment in which $(\Delta R_c)_{max}$ occurs (numbering starts with the outermost increment being 1).

Fuel Restructuring

Fuel restructuring is assumed to occur to some temperature that is dependent on time at power. The relationship used in GAPCON was derived from data presented by Christensen:[44]

$$1/T_{RS} = 0.00001367 \log_{10} (t) + 0.000480 \qquad [11]$$

where T_{RS} = temperature to which restructuring occurs (°K)

t = time at power (hr).

As Christensen indicated, a unique restructuring temperature-time relationship should be used for each combination of burnup (xenon content of the pores) and thermal gradient. The above relationship was derived to represent an average over the life of a fuel pin.

A restructured fuel radius and center hole radius are calculated based on the above restructuring temperature and the (input) density of restructured fuel. The temperature distribution calculations are then repeated for the restructured fuel pin.

Fuel Fission Product Swelling

Expansion due to fuel swelling is calculated from the relationship proposed by Geithoff,[39] et al.:

$$\Delta V_B = [(h_f)\ (V_f)\ (f) + (h_c)\ (V_c)]\ \frac{BU}{10{,}000} - (1-f)\ (0.8V_h + 0.5V_v + 0.3V_\ell) \qquad [12]$$

where ΔV_B = change in volume due to burnup (fission product swelling)

f = fractional density

h_f = swelling rate for entire fuel rod, presumed to be 1.6% $\Delta V/V$ per 10,000 MWd/MTM

V_f = volume of fuel per unit length

h_c = additional swelling in fuel between 1300 and 1700°C, presumed to be 0.4% $\Delta V/V$ per 10,000 MWd/MTM

V_c = volume of fuel between 1300 and 1700°C

BU = Burnup, MWd/MTM

V_h = volume of fuel, above 1700°C

V_ℓ = volume of fuel below 1300°C.

It is assumed that 1/3 of the volume increase is longitudinal; therefore;

$$\Delta r_b = \frac{2/3\ (\Delta V_B)}{2\pi r} . \qquad [13]$$

Stored Thermal Energy - Subroutines HCAP and CARL

An option for calculating stored energy of the fuel was added to GAPCON-THERMAL because stored energy is the main parameter in a safety evaluation of the fuel system. Some accident codes use steady-state codes to initialize temperature profiles; some index on a volumetric average temperature profiles; some index on a volumetric average temperature; others may use the stored energy per unit volume or mass of fuel. All of the above parameters are included as output of the code.

Two methods are available for calculating stored energy for each axial segment from the heat capacity and temperature of the fuel. One method approach approximates the stored energy by using the volume average temperature of an axial segment multiplied by the enthalpy for that temperature. However, due to the nonlinearity of heat capacity in certain temperature regimes this approximation can be off as much as 20%. The second method is more exact in that the pellet is divided into 50 concentric annular rings of unit length and the stored energy contribution of each ring is summed.

$$E\ (\text{cal/g} - UO_2) = \left[\frac{\sum_{i=1}^{N} m_i \int_{298}^{T_i} C_p\ (T)\ dT}{m}\right] \frac{1}{270\ \text{g/mole} - UO_2} \qquad [14]$$

m_i = mass of segment (i), grams
T_i = temperature of segment (i),
C_p (t) = heat capacity, cal/mole-°k
E = stored energy

$$\bar{E}\ (\text{cal/g} - UO_2) = \left[\int_{298}^{\bar{T}} C_p\ (T)\ dT\right] \frac{1}{270\ \text{g/mole} - UO_2} \qquad [15]$$

$\bar{E}$ = stored energy at volumetric average temperature $\bar{T}$

The relationship used in the code to describe heat capacity of UO_2 as a function of temperature is taken from Kerrisk and Clifton.[60]

Flux Depression - Subroutine DEPRES

DEPRES is a subroutine which estimates the radial flux depression profile for irradiations conducted in a thermal flux. These calculations are modified slightly to use the as-fabricated fuel density instead of theoretical density on the flux depression calculation.

The model used in the flux depression calculation is based on a report by Robertson.[61] The modified Bessel function is approximated by the first four terms of its infinite series expansion.[62] DEPRES should not be used with mixed oxide nor with UO_2 above ~4% U^{235}. DEPRES does not calculate a flux depression burnup dependence.

PROPERTIES OF ZIRCALOY

Temp. (°F)	Thermal Conductivity[63] (Btu/hr-ft °F) Zr-2	Zr-4	Yield Strength (psi)	Young's Modulus (psi)	Poisson's Ratio	Alpha* (in./in.°F)	Meyer Hardness** (kg/cm^2)
75	—	—	44,800	13.8×10^6	0.370	3.24×10^{-6}	9,470
212	7.74	7.86	34,800	13.0 c 10^6	0.400	3.47×10^{-6}	7,360
392	8.38	8.27	23,800	12.1×10^6	0.446	3.70×10^{-6}	5,030
572	9.02	8.79	15,800	11.1×10^6	0.492	3.87×10^{-6}	3,340
752	9.83	9.48	12,100	13.1×10^6	0.492	3.99×10^{-6}	2,560
932	10.64	10.40	10,000	9.1×10^6	0.492	4.08×10^{-6}	2,110

* ALPHA = Linear coefficient of thermal expansion
**Meyer Hardness is assumed to be equal to 3x Yield Strength

PROPERTIES OF 304 SS

Temp. (°F)	Thermal Conductivity (Btu/hr-ft °F)	Yield Strength(1) (psi)	Young's Modulus (psi)	Poisson's Ratio	Alpha(2) (in./in.°F)	Meyer Hardness(3) (kg/cm^2)
100	8.50	30,000	28.1×10^6	0.267	9.15×10^{-6}	6,340
200	8.93	25,300	27.7	0.266	9.33	5,350
300	9.36	22,500	27.2	0.271	9.48	4,760
400	9.80	30,700	26.6	0.276	9.60	4,360
500	10.24	19,300	26.0	0.280	9.71	4,080
600	10.68	18,200	25.4	0.285	9.82	3,850
700	11.12	17,500	24.7	0.290	9.95	3,700
800	11.56	16,900	24.1	0.295	10.08	3,520
900	12.00	16,200	23.4	0.300	10.19	3,420
1000	12.44	15,600	22.6	0.304	10.30	3,300
1100	12.87	14,900	21.8	0.309	10.40	3,150
1200	13.32	14,200	20.9	0.314	10.46	3,000

(1) Alpha = Linear coefficient of thermal expansion
(2) Meyer Hardness is assumed to be equal to 3X Yield Strength
(3) NOTE: Annealed values, user should supply yield strengths for specific cladding if cold worked.

Cladding Elastic Deflection

Since the wall thickness for most commercial fuel cladding is greater than one-tenth the radius,[64] we used the thick-wall vessel formulas in an elastic deflection option for GAPCON-THERMAL. The option should not be used if the cladding diameters are obtained from a creep collapse code because a double correction may be inadvertently provided.

The general tangential and radial stress relations (Lamé's equations) are:[65]

$$S_t = \frac{\left[\left(r_1^2 p_1 - r_2^2 p_2\right) + \left(p_1 - p_2\right) r_1^2 r_2^2 / r^2\right]}{\left(r_2^2 - r_1^2\right)} \qquad [16]$$

$$S_r = \frac{\left[\left(r_1^2 p_1 - r_2^2 p_1\right) - \left(p_1 - p_2\right) r_1^2 r_2^2 / r^2\right]}{\left(r_2^2 - r_1^2\right)} \qquad [17]$$

where S_t = tangential stress, (psi)

S_r = radial stress, (psi)

p_1 = uniform internal pressure, (psi)

p_2 = uniform external pressure, (psi)

r_1 = cladding inner radius, (in.)

r_2 = cladding outer radius, (in.)

$r_2 \geq r \geq r_1$

Now at the inner boundary (i.e., $r = r_1$), the tangential elongation is:[64]

$$\varepsilon_t = (S_t - \mu S_r)/E \qquad [18]$$

where ε_t = tangential elongation, (in./in.)

μ = Poisson's Ratio

E = Young's Modulus, (psi)

As a result, the change in cladding inner radius, Δr_1, due to internal and external pressure is:

$$(E)(\varepsilon_t) = S_t - \mu S_r \qquad [19]$$

$$(E)\left(\frac{2\pi\Delta r_1}{2\pi r_1}\right) = S_t - \mu S_r \qquad [20]$$

$$\Delta r_1 = \frac{r_1}{E\left(r_2^2 - r_1^2\right)}\left[\left(r_1^2 p_1 - r_2^2 p_2\right)\left(1 - \mu\right) + \left(p_1 - p_2\right)\left(r_2^2\right)\left(1 + \mu\right)\right] \qquad [21]$$

where =

Δr_1 = change in cladding inner radius, (in.)

Substituting values for PWR cladding data into Equation 15 and using $\mu = 0.492$ and $E = 11.1 \times 10^6$ psi, we obtained these values:

Case 1

With $P_1 = 0$ and $P_2 = 2250$ psi, $\Delta r_1 = -0.000349$ in.

Case 2

With $P_1 = 600$ psi and $p_2 = 2250$ psi, $\Delta r_1 = -0.000261$ in.

Cladding Creep

Creep of the cladding will contribute to gap closure and thus lower fuel temperatures. Creepdown is currently a user option (see section on input instructions) in that a table of cladding diameters as a function of time must be supplied. The option has been used to simulate various gap closure data. Cladding diameters can also be obtained from the output of BUCKLE[65] and COVE[66] which contain uniform creepdown rates.

Internal Gas Properties

The thermal conductivity of a mixture of gases at low density is calculated from:[15]

$$k_{mix} = \sum_{i=1}^{n} \frac{X_i k_i}{\sum_{j=1}^{n} X_j \Phi_{ij}} \qquad [22]$$

where the X_i and X_j are mole fractions, and the k_i is the thermal conductivity of the pure components. The coefficients Φ_{ij} are computed from:[15]

$$\Phi_{ij} = \frac{1}{\sqrt{8}} \left(1 + \frac{M_i}{M_j}\right)^{-1/2} \left[1 + \left(\frac{\mu_i}{\mu_j}\right)^{1/2} \left(\frac{M_j}{M_i}\right)^{1/4}\right]^2 \qquad [23]$$

where the M_i and M_j are molecular weights of the pure components, and the μ_i and μ_j are viscosities of the pure components. Viscosities of the pure gases are estimated from:[15]

$$\mu_i = 2.67 \times 10^{-5} \frac{(M_i T)^{1/2}}{\sigma_i^2 \Omega_i} \qquad [24]$$

where T is temperature in °K, σ_i is the characteristic diameter of the molecule and Ω_i is a function of $(\kappa/\varepsilon)T$(κ is the Boltzman constant and ε is a characteristic energy of interaction between molecules of a pure gas). Values of σ and (ε/κ) for various gases and a table of Ω as a function of $(\kappa/\varepsilon)T$ are tabulated in Reference 15.

For monatomic gases, thermal conductivity of the pure gas is calculated from:[15]

$$k_i = 1.989 \times 10^{-4} \frac{(T/M_i)^{1/2}}{\sigma_i^2 \Omega_i} \text{ (cal/cm-sec-°C).} \qquad [25]$$

For nitrogen and hydrogen, thermal conductivity is estimated from:

$$k_i = (C_p + \frac{5}{4} R) \frac{\mu_i}{M_i} \qquad [26]$$

where C_p is heat capacity at constant pressure, and R is the gas constant (1.987 cal/gmole/°K).

This calculational technique was checked against gas-mixture thermal conductivity data reported by von Ubisch.[67] For ternary mixtures of helium, krypton, and xenon covering extremes of composition and temperatures from 29 to 520°C, calculated gas thermal conductivities were in all cases within 10% of the values reported by von Ubisch and in most cases were within 5% of the reported value.

Gas Pressures*

Fuel rod gas pressures are calculated in the code with the following relationship:

$$P = \frac{M^T}{\frac{V^P}{T^P} + \sum_{i=1}^{i=N} \left(\frac{Vi^v}{Ti^v} + \frac{V_1^g}{T_1^g} \right)} \qquad [27]$$

where

N = number of axial segments

M^T = total moles of gas in the free volume of the fuel rod

Vi^v = volume of center void of segment i

Ti^v = temperature of the center void of segment i

V^P = plenum volume of the fuel rod

T^P = temperature of the plenum, assumed to be equal to the outlet coolant temperature +10°F

Vi^g = volume of the pellet-to-clad gap of segment i

Ti^g = the average temperature between the fuel surface temperature and inside clad temperature at segment i.

*Modified slightly to include fuel axial expansion into fission gas plenum; previous versions used the input value for plenum volume.

Power and Coolant Temperature Profile - Subroutine POWDIS*

A power profile which is normalized to average pin power can be input to the code as described in the Table of Input Variables. The normalized power profile when plotted versus X/L integrates to 1.0 with the peak of the profile being equal to the peak power/average power ratio for that pin. The profile has to contain values which bound each axial segment along the pin since power is linearly interpolated from the points that bound each axial segment. Thus the number of input values for the power profile has to be equal to N + 1, N being number of segments. For example, if the first two values entered for the normalized power profile were 0.2 and 0.5, 0.35 would be used for the first segment.

The axial temperature profile of the coolant is calculated from the power profile, the temperature gradient of the coolant across the core, and the inlet coolant temperature. A reasonable approximation of the coolant temperature profile can be made by assuming a direct correlation between integrated fraction of power along the pin to the coolant temperature gradient. A power fraction is calculated for each axial segment by integrating the power from the bottom of the pin to each axial segment and dividing that power by the total power of the pin (i.e., the integrated power fraction for the axial segment at the top edge of the fuel is 1.0). Thus, if 70% of the power of a pin was located in the lower half of the pin, the axial segment at the middle of the pin would have a coolant temperature equal to $T_{inlet} + 0.7\ \Delta T_{core}$. Considering the intended use of the code and its accuracy (which is limited by other areas of the code), the additional computer time required to perform a more extensive hydraulics calculation is not justified.

Axial Segments

The code considers a specified number with a limit of 20 of axial segments. Each equal length axial segment has its own fuel, fission gas inventory, heat rating, coolant temperature and pellet-to-clad gap. Since only

* When nodal TINLETS are used the coolant temperature increase, ΔTEMP, across the core is not used.

radial heat flow is considered, the temperature profile of each axial segment is calculated at the center of the segment using the heat rating and coolant temperature associated with the mid-point of the axial segment (see section on the power and coolant temperature profile). One radial temperature profile describes the thermal conditions of the entire axial segment. Thus, a more accurate axial temperature profile is obtained the greater the number of segments, but ten axial segments are usually sufficient.

Heat Transfer by Radiation

The radiant heat transfer coefficient, h_r, is determined from:

$$h_r = \frac{(q_r/A_1)}{(T_1 - T_2)} \qquad [28]$$

but,

$$\left(q_r/A_1\right) = \sigma_{sB}\left[\frac{1}{f_1} + \frac{A_1}{A_2}\left(\frac{1}{f_2} - 1\right)\right]^{-1}\left[T_1^{\,4} - T_2^{\,4}\right] \qquad [29]$$

therefore,

$$h_r = \sigma_{sB}\left[\frac{1}{\varepsilon_1} + \frac{A_1}{A_2}\left(\frac{1}{\varepsilon_2} - 1\right)\right]^{-1}\left[T_1^{\,2} + T_2^{\,2}\right]\left[T_1 + T_2\right] \qquad [30]$$

where σ_{sB} is the Steffan-Boltzman constant, ε_1 and ε_2 are emissivities of the fuel surface and cladding surface respectively, A_1 and A_2 are the fuel and cladding surface areas, respectively, and T_1 and T_2 are temperatures of the fuel and cladding surfaces, respectively.

Radial Temperature Calculations Subroutine RTEMP

The temperature drop through the fuel is calculated by dividing the fuel region into 50 radial increments, then calculating the temperature

drop across each increment assuming that thermal conductivity and volumetric heat generation rate is constant within each increment. The calculation proceeds as follows: the heat generated within an increment is determined from the total heat generation rate, increment volume, and the flux depression table provided previously; an average temperature of the increment is assumed; and appropriate thermal conductivity value is assigned; temperature drop across the increment and, therefore, average temperature is calculated; and the calculated average temperature is compared to the assumed value. If the assumed and calculated values do not agree, a new value is assumed and the process is repeated. The temperature drop across each increment is calculated from:

$$\Delta T_i = \frac{q'''}{2\pi k}\left[\frac{1}{2} - \left(\frac{r_i^2}{r_o^2 - r_i^2} - \frac{q_i}{q'''}\right)\ln\frac{r_o}{r_i}\right] \qquad [31]$$

where ΔT = temperature drop across increment i

q''' = heat generated in increment i

k = fuel thermal conductivity

r_i = inside radius of increment i

r_o = outside radius of increment i

q_i = heat transferred into increment i.

Water-to-Cladding Heat Transfer Coefficient Subroutine HTCW

HTCW is a subroutine used to calculate the cladding-to-coolant heat transfer coefficient if the coolant is water (if SIGHF is less than zero). The calculation is based on the Dittus-Boelter[68] equation:

$$h_f = 0.023\,\frac{k}{D_e}\,\frac{(D_e V\rho)^{0.8}}{\mu}(Pr)^{0.4} \qquad [32]$$

where

h_f = cladding-to-coolant heat transfer coefficient

k = thermal conductivity of coolant (Btu/hr ft °F)

D_e = equivalent diameter of coolant passage (in.)
V = coolant velocity (ft/sec)
ρ = coolant density (lbs/ft^3)
μ = coolant viscosity (lb/ft-sec)
Pr = Prandtl number = $C_p \mu/k$

All coolant properties are evaluated at the mean temperature of the coolant film. The properties of water as a function of temperature are included in the subroutine. The values used are those tabulated in Krieth.[69]

Linear Interpolation - Function TERP and TEPP

TERP and TEPP are linear interpolation functions which are called frequently to interpolate the many tables of values that are used throughout the program.

TERP accesses one array which contains values for both the dependent and independent variables.

TEPP accesses two arrays, one for each of the dependent and independent variables.

APPENDIX D

INPUT VALUES TO GAPCON-THERMAL-2 USED AS PART OF THE CODE EVALUATION

Sample No. HPR-129 IFA-117 (Pin #1)

Alphabetical Listing of Input Parameters for GAPCON-THERMAL-2

ATMOS 1.0	FR35 0.06	LVOIDZ 2.5	SIGHF 25000.0
DBO -	FR40 -	MINI 0	*TIME
DCI 0.5539	FR41 -	NCLAD 0	
DCO 0.6140	HBC -	NCON 0	TINLET 464.0
DE -	HGACEL -	NFLX 9 (1)	TM 2[illegible]
DFS 0.5455	ICDF 0	NFUEL 0	TPLAS 120C°C
DSINZ -	ICREP 0	NOH 0	V -
DTEMP ~~100°F~~ 20	IDENSF 0	NPOW ~~10~~ 4	VPLENZ 0.293
DVOIDZ 0.126	IFLUX 0	NPRFIL 1	XCO -
EXTP -	IGAS 0	NTIME 14 (1)	XH -
FRACAR -	IPEAK 1	PRCDH 2.0	XN -
FRACH -	IRELOC 1	*PROFIL (1,1)	ZCLAD -
FRACHE 1.0	IRELSE 0		
FRACKR -	IRL 0	*PSEUDO	
FRACN -	ISTOR 0		
FRACXE -	IT	RADS 0.2333	
FRDEN 0.97	KB 0	ROUC 0.2E-4	
FRPUO2 -	KOOL	ROUF 0.39E-4	
FRSIN -	LFUEL 19.705	S -	

(1) See Attachment A

*PROFIL (1,1) = 0.85, 0.9, 0.99, 1.0, 0.99

*PSEUDO (1) = See Attachment A

*TIME (1) = See Attachment A

NOTE: All input variables initialized to zero except as shown above.

ATTACHMENT A (IFA-117 Pin #1)

Flux Depression Values

0.0	1.0
0.126	1.0
0.1857	1.0078
0.2457	1.0289
0.3056	1.0618
0.3655	1.1059
0.4253	1.1614
0.4852	1.2289
0.5455	1.3092

Power History Case

PSEUDO (1) = 19.9, 19.9, 20.7, 22.6, 23.6, 23.3, 21.9, 19.5,
20.2, 20.2, 20.4, 21.0, 20.9, 20.7,

TIME (1) = 0.0, 3.1, 11.3, 15.5, 24.9, 37.5, 56.7, 83.9,
98.0, 109.6, 124.3, 137.8, 147.3, 158.7

Controlled Cycle Case

NTIME = 13

PSEUDO (1) = 20.83, 20.83, 20.7, 16.58, 12.43, 8.29, 4.14, 0.0,
4.14, 8.29, 12.43, 16.58, 20.7

TIME (1) = 0.0, 140.0, 140.1, 140.2, 140.3, 140.4, 140.5,
140.6, 140.7, 140.8, 140.9, 141.0, 141.1

Sample No. HPR-129 IFA-117 (Pin #3)

Alphabetical Listing of Input Parameters for GAPCON-THERMAL-2

ATMOS	1.0	FR35	0.06	LVOIDZ	19.7	SIGHF	25000.0
DBO	-	FR40	-	MINI	-	*TIME	
DCI	0.5539	FR41	-	NCLAD	-		
DCO	0.614	HBC	-	NCON		TINLET	464.0
DE	0	HGACEL	-	NFLX	9 (1)	TM	2790°C
DFS	0.5455	ICDF	-	NFUEL	-	TPLAS	1200°C
DSINZ	-	ICREP	-	NOH	-	V	-
DTEMP	~~100°F~~ 20.0	IDENSF	-	NPOW	~~10~~ 4	VPLENZ	0.293
DVOIDZ	0.126	IFLUX	-	NPRFIL	1	XCO	-
EXTP	-	IGAS	-	NTIME	14 (1)	XH	-
FRACAR	-	IPEAK	1	PRCDH	2.0	XN	-
FRACH	-	IRELOC	1	*PROFIL	(1,1)	ZCLAD	-
FRACHE	1.0	IRELSE	-				
FRACKR	-	IRL	-	*PSEUDO			
FRACN	-	ISTOR	-				
FRACXE	-	IT		RADS	0.2333	(1) See Attachment B	
FRDEN	0.97	KB	-	ROUC	0.2E-04		
FRPUO2	-	KOOL	-	ROUF	0.39E-04		
FRSIN	-	LFUEL	19.705	S	-		

*PROFIL (1,1) = 0.85, 0.9, 0.99, 1.0, 0.99

*PSEUDO (1) = See Attachment B

*TIME (1) = See Attachment B

NOTE: All input variables initialized to zero except as shown above.

ATTACHMENT B (IFA-117 Pin #3)

Flux Depression Values

0.0	1.0
0.126	1.0
0.1857	1.0078
0.2457	1.0289
0.3056	1.0618
0.3655	1.1059
0.4253	1.1614
0.4852	1.2289
0.5455	1.3092

Power History Case

PSEUDO (1) = 17.4, 17.4, 18.1, 19.8, 20.7, 24.3, 22.8, 20.3
20.6, 21.1, 21.9, 22.0, 21.8, 21.6

TIME (1) = 0.0, 3.1, 11.3, 15.5, 24.9, 37.5, 46.7, 83.9
98.0, 109.6, 124.3, 137.8, 147.3, 158.7

Controlled Power Cycle

NTIME = 13

PSEUDO (1) = 21.08, 21.08, 21.6, 17.29, 12.97, 8.6
4.3, 0.0, 4.3, 8.6, 12.97, 17.29, 21.6

TIME (1) = 0.0, 140.0, 140.1, 140.2, 140.3, 140.4, 140.5,
140.6, 140.7, 140.8, 140.9, 141.0, 141.1

Sample No. HPR-129 IFA-117 (Pin #5)

Alphabetical Listing of Input Parameters for GAPCON-THERMAL-2

ATMOS 1.0	FR35 0.06	LVOIDZ 2.5	SIGHF 25000.0
DBO -	FR40 -	MINI -	*TIME
DCI 0.5538	FR41 -	NCLAD -	
DCO 0.614	HBC -	NCON -	TINLET 464.0
DE -	HGACEL -	NFLX 9 (1)	TM 2790°C
DFS 0.5455	ICDF -	NFUEL -	TPLAS 1200°C
DSINZ -	ICREP -	NOH -	V -
DTEMP ~~100°F~~ 20.0	IDENSF -	NPOW ~~10~~ 4	VPLENZ 0.293
DVOIDZ 0.126	IFLUX -	NPRFIL 1	XCO -
EXTP -	IGAS -	NTIME 14 (1)	XH -
FRACAR -	IPEAK 1	PRCDH 2.0	XN -
FRACH -	IRELOC 1	*PROFIL (1,1)	ZCLAD -
FRACHE 1.0	IRELSE -		
FRACKR -	IRL -	*PSEUDO	
FRACN -	ISTOR -		
FRACXE -	IT	RADS 0.2333	(1) See Attachment C
FRDEN 0.913	KB -	ROUC 0.2E-4	
FRPUO2 -	KOOL -	ROUF 0.39E-4	
FRSIN -	LFUEL 19.7	S -	

*PROFIL (1,1) = 0.85, 0.9, 0.99, 1.0, 0.99

*PSEUDO (1) = See Attachment C

*TIME (1) = See Attachment C

NOTE: All input variables initialized to zero except as shown above.

ATTACHMENT C (IFA-117 Pin #5)

Flux Depression Values

0.0	1.0
0.126	1.0
0.1857	1.0069
0.2457	1.0257
0.3056	1.0548
0.3655	1.0939
0.4253	1.1430
0.4852	1.2024
0.5455	1.2729

Power History Case

PSEUDO (1) = 17.4, 17.4, 18.1, 19.8, 20.7, 24.4, 21.2, 18.9, 19.4, 19.6, 20.2, 20.4, 20.3, 20.1

TIME (1) = 0.0, 3.1, 11.3, 15.5, 24.9, 37.5, 46.7, 83.9, 98.0, 109.6, 124.3, 137.8, 147.3, 158.7

Controlled Power Cycle

NTIME = 13

PSEUDO (1) = 20.02, 20.02, 20.1, 16.1, 12.8, 4.0, 0.0, 4.0, 8.0, 12.0, 16.1, 20.1, 21.6

TIME (1) = 0.0, 140.0, 140.1, 140.2, 140.3, 140.4, 140.5, 140.6, 140.7, 140.8, 140.9, 141.0, 141.1

Sample No. HPR-129 IFA-117 (Pin #6)

Alphabetical Listing of Input Parameters for GAPCON-THERMAL-2

ATMOS 1.0	FR35 0.06	LVOIDZ 2.5	SIGHF 25000.0
DBO -	FR40 -	MINI -	*TIME
DCI 0.5531	FR41 -	NCLAD -	
DCO 0.614	HBC -	NCON -	TINLET 464.0
DE -	HGACEL -	NFLX 9 (1)	TM 2790°C
DFS 0.5452	ICDF -	NFUEL -	TPLAS 1200°C
DSINZ -	ICREP -	NOH -	V -
DTEMP ~~100°F~~ 20.0	IDENSF -	NPOW ~~10~~ 4	VPLENZ 0.293
DVOIDZ 0.126	IFLUX -	NPRFIL 1	XCO -
EXTP 0	IGAS -	NTIME 14 (1)	XH -
FRACAR -	IPEAK 1	PRCDH 2.0	XN -
FRACH -	IRELOC 1	*PROFIL (1,1)	ZCLAD -
FRACHE 1.0	IRELSE -		
FRACKR -	IRL -	*PSEUDO	
FRACN -	ISTOR -		
FRACXE -	IT	RADS 0.2333	(1) See Attachment D
FRDEN 0.914	KB -	ROUC 0.2E-4	
FRPUO2 -	KOOL -	ROUF 0.39E-4	
FRSIN -	LFUEL 19.685	S -	

*PROFIL (1,1) = 0.9, 0.8, 0.7, 0.62, 0.54

*PSEUDO (1) = See Attachment D

*TIME (1) = See Attachment D

NOTE: All input variables initialized to zero except as shown above.

ATTACHMENT D (IFA-117 Pin #6)

Flux Depression Values

0.0	1.0
0.126	1.0
0.1857	1.0069
0.2457	1.0257
0.3056	1.0548
0.3655	1.0939
0.4253	1.1430
0.4852	1.2024
0.5452	1.2729

Power History Case

PSEUDO (1) = 15.7, 15.7, 15.0, 15.4, 16.2, 15.9, 15.5,
15.3, 15.2, 15.9, 16.3, 16.6, 16.4, 16.3

TIME (1) = 0.0, 3.1, 11.3, 15.5, 24.9, 37.5, 46.7,
83.9, 98.0, 109.6, 124.3, 137.8, 147.3, 158.7

Controlled Power Cycle

NTIME = 13

PSEUDO (1) = 15.7, 15.7, 16.3, 13.0, 9.78, 6.52, 3.26,
0.0, 3.26, 6.52, 9.78, 13.0, 16.3

TIME (1) = 0.0, 140.0, 140.1, 140.2, 140.3, 140.4, 140.5,
140.6, 140.7, 140.8, 140.9, 141.0, 141.1

Sample No. HPR-129 IFA-116 Pin #1

Alphabetical Listing of Input Parameters for GAPCON-THERMAL-2

ATMOS	1.0	FR35	0.0601	LVOIDZ	2.5	SIGHF	25000.0
DBO	-	FR40	-	MINI	-	*TIME	
DCI	0.5538	FR41	-	NCLAD	-		
DCO	0.614	HBC	-	NCON		TINLET	464
DE	-	HGACEL	-	NFLX	9 (1)	TM	2790°C
DFS	0.5455	ICDF	-	NFUEL	-	TPLAS	1200°C
DSINZ	-	ICREP	-	NOH	-	V	-
DTEMP	~~100°F~~ 20	IDENSF	-	NPOW	~~10~~ 4	VPLENZ	0.293
DVOIDZ	0.126	IFLUX	-	NPRFIL	1	XCO	-
EXTP	-	IGAS	-	NTIME	13	XH	-
FRACAR	-	IPEAK	1	PRCDH	2.0	XN	-
FRACH	-	IRELOC	1	*PROFIL	(1,1)	ZCLAD	-
FRACHE	1.0	IRELSE	-				
FRACKR	-	IRL	-	*PSEUDO			
FRACN	-	ISTOR	-				
FRACXE	-	IT		RADS	0.2333		
FRDEN	0.969	KB	-	ROUC	0.20E-4		
FRPUO2	-	KOOL	-	ROUF	0.39E-4		
FRSIN	-	LFUEL	19.685	S	-		

(1) See Attachment E

*PROFIL (1,1) = 0.85, 0.9, 0.99, 1.0, 0.99

*PSEUDO (1) = See Attachment E

*TIME (1) = See Attachment E

NOTE: All input variables initialized to zero except as shown above.

ATTACHMENT E (IFA-116 Pin #1)

Flux Depression Values	Pin #1
0.0	1.0
0.126	1.0
0.1857	1.0078
0.2457	1.0289
0.3056	1.0618
0.3655	1.1059
0.4253	1.1614
0.4852	1.2289
0.5455	1.3092

Power History Case

PSEUDO (1) = 19.13, 19.13, 18.68, 18.07, 20.35, 20.8, 17.65, 20.51, 19.64, 18.89, 18.20, 20.73, 19.88

TIME (1) = 0.0, 15.0, 30.0, 38.0, 43.0, 48.0, 50.0, 53.0, 68.0, 70.0, 74.0, 89.0, 92.0

Sample No. HPR-129 IFA-116 Pin #5

Alphabetical Listing of Input Parameters for GAPCON-THERMAL-2

ATMOS 1.0	FR35 0.0601	LVOIDZ 2.5	SIGHF 25000.0
DBO -	FR40 -	MINI -	*TIME
DCI 0.5538	FR41 -	NCLAD -	
DCO 0.614	HBC -	NCON	TINLET 464
DE -	HGACEL -	NFLX 9 (1)	TM 2790°C
DFS 0.5455	ICDF -	NFUEL -	TPLAS 1200°C
DSINZ -	ICREP -	NOH -	V -
DTEMP ~~100°F~~ 20	IDENSF -	NPOW ~~10~~ 4	VPLENZ 0.293
DVOIDZ 0.126	IFLUX -	NPRFIL 1	XCO -
EXTP -	IGAS -	NTIME 13	XH -
FRACAR -	IPEAK 1	PRCDH 2.0	XN -
FRACH -	IRELOC 1	*PROFIL (1,1)	ZCLAD -
FRACHE 1.0	IRELSE -		
FRACKR -	IRL -	*PSEUDO	
FRACN -	ISTOR -		
FRACXE -	IT	RADS 0.2333	(1) See Attachment F
FRDEN 0.913	KB -	ROUC 0.20E-4	
FRPUO2 -	KOOL -	ROUF 0.39E-4	
FRSIN -	LFUEL 19.685	S -	

*PROFIL (1,1) = 0.85, 0.9, 0.99, 1.0, 0.99

*PSEUDO (1) = See Attachment F

*TIME (1) = See Attachment F

NOTE: All input variables initialized to zero except as shown above.

ATTACHMENT F (IFA-116 Pin #5)

Flux Depression Values		Pin #1
0.0	1.0	1.0
0.126	1.0	1.0
0.1857	1.0069	1.0078
0.2457	1.0257	1.0289
0.3056	1.0548	1.0618
0.3655	1.0939	1.1059
0.4253	1.1430	1.1614
0.4852	1.2024	1.2289
0.5455	1.2729	1.3092

Power History Case

PSEUDO (1) = 19.13, 19.13, 18.68, 18.07, 20.35, 20.8 17.65, 20.51, 19.64, 18.89, 18.20, 20.73, 19.88

TIME (1) = 0.0, 15.0, 30.0, 38.0, 43,0, 48.0, 50.0, 53.0, 68.0, 70.0, 74.0, 89.0, 92.0

Sample No. IFA-130 (2 cases

Alphabetical Listing of Input Parameters for GAPCON-THERMAL-2

ATMOS 1.0	FR35 0.06	LVOIDZ -	SIGHF 10000.0
DBO -	FR40 -	MINI -	*TIME
DCI 0.5024	FR41 -	NCLAD -	
DCO 0.5575	HBC -	NCON -	TINLET 464.0
DE -	HGACEL -	NFLX 9 (1)	TM 2790°C
DFS 0.4902	ICDF -	NFUEL -	TPLAS 1200°C
DSINZ -	ICREP -	NOH -	V -
DTEMP ~~100°F~~ 20.0	IDENSF -	NPOW ~~10~~ 1	VPLENZ 0.2
DVOIDZ 0.069	IFLUX -	NPRFIL 1	XCO -
EXTP -	IGAS -	NTIME 5	XH -
FRACAR -	IPEAK -	PRCDH -	XN -
FRACH -	IRELOC 1	*PROFIL (1,1)	ZCLAD -
FRACHE 1.0	IRELSE -		
FRACKR -	IRL -	*PSEUDO	
FRACN -	ISTOR -		
FRACXE -	IT	RADS	(1) See Attachment G
FRDEN 0.90 & 0.94	KB -	ROUC 0.1E-3	
FRPUO2 -	KOOL -	ROUF 0.4E-3	
FRSIN -	LFUEL 18.3	S -	

*PROFIL (1,1) = 1.0, 1.0

*PSEUDO (1) = 3.048, 6.096, 9.144, 12.192, 15.24

*TIME (1) = 0.0, 0.1, 0.2, 0.3, 0.4

NOTE: All input variables initialized to zero except as shown above.

ATTACHMENT G (IFA-130 & IFA-131)

Flux Depression Values[88]

0.0	1.0
0.126	1.0
0.1857	1.0069
0.2457	1.0257
0.3056	1.0548
0.3655	1.0939
0.4253	1.1430
0.4852	1.2024
0.5451	1.2729

Sample No. IFA-131 (3 cases)

Alphabetical Listing of Input Parameters for GAPCON-THERMAL-2

ATMOS 1.0	FR35 0.06	LVOIDZ -	SIGHF 10000
DBO -	FR40 -	MINI -	*TIME
DCI 0.5024	FR41 -	NCLAD -	
DCO 0.5575	HBC -	NCON -	TINLET 464
DE -	HGACEL -	NFLX 9 (1)	TM 2790°C
DFS .4902,.4933,.4964	ICDF -	NFUEL -	TPLAS 1200°C
DSINZ -	ICREP -	NOH -	V -
DTEMP ~~100°F~~ 20	IDENSF -	NPOW ~~10~~ 1	VPLENZ 0.2
DVOIDZ 0.069	IFLUX -	NPRFIL 1	XCO -
EXTP -	IGAS -	NTIME 5	XH -
FRACAR -	IPEAK -	PRCDH -	XN -
FRACH -	IRELOC 1	*PROFIL (1,1)	ZCLAD -
FRACHE 1.0	IRELSE -		
FRACKR -	IRL -	*PSEUDO	
FRACN -	ISTOR -		
FRACXE -	IT	RADS	(1) See Attachment G
FRDEN 0.94	KB -	ROUC 0.1E-3	
FRPUO2 -	KOOL -	ROUF 0.4E-3	
FRSIN -	LFUEL 18.3	S -	

*PROFIL (1,1) = 1.0, 1.0

*PSEUDO (1) = 3.048, 6.096, 9.144, 12.192, 15.24

*TIME (1) = 0.0, 0.1, 0.2, 0.3, 0.4

NOTE: All input variables initialized to zero except as shown above.

Sample No. WCAP-2923 Capsule I Startup

Alphabetical Listing of Input Parameters for GAPCON-THERMAL-2

ATMOS 1.0	FR35 0.0064	LVOIDZ -	SIGHF -
DBO -	FR40 -	MINI -	*TIME
DCI 1.2745	FR41 -	NCLAD -1	
DCO 1.3245	HBC -	NCON -	TINLET 250
DE -	HGACEL -	NFLX -	TM 2790°C
DFS 1.25	ICDF -	NFUEL -	TPLAS 1200°C
DSINZ -	ICREP -	NOH -	V -
DTEMP 100°F	IDENSF -	NPOW 10 1	VPLENZ 1.0
DVOIDZ 0.068	IFLUX -	NPRFIL 1	XCO -
EXTP -	IGAS -	NTIME 8	XH -
FRACAR -	IPEAK -	PRCDH -	XN -
FRACH -	IRELOC	*PROFIL (1,1)	ZCLAD -
FRACHE 1.0	IRELSE -		
FRACKR -	IRL -	*PSEUDO	
FRACN -	ISTOR -		
FRACXE -	IT	RADS -	
FRDEN 0.95	KB -	ROUC 0.1E-4	
FRPUO2 -	KOOL -	ROUF 0.4E-4	
FRSIN -	LFUEL 4.5	S -	

*PROFIL (1,1) = 1.0, 1.0

*PSEUDO (1) = 6, 6, 8, 10.4, 13.6, 15.3, 20.1, 20.9

*TIME (1) =

NOTE: All input variables initialized to zero except as shown above.

Sample No. WCAP-2923 Capsule I "Steady State"

Alphabetical Listing of Input Parameters for GAPCON-THERMAL-2

ATMOS 1.0	FR35 0.0064	LVOIDZ -	SIGHF -
DBO -	FR40 -	MINI -	*TIME -
DCI 1.2745	FR41 -	NCLAD -1	
DCO 1.3245	HBC -	NCON -	TINLET 245
DE -	HGACEL -	NFLX -	TM 2790°C
DFS 1.25	ICDF -	NFUEL -	TPLAS 1200°C
DSINZ -	ICREP -	NOH -	V -
DTEMP 100°F	IDENSF -	NPOW 1	VPLENZ 0.44
DVOIDZ 0.068	IFLUX -	NPRFIL 1	XCO -
EXTP -	IGAS -	NTIME 8	XH -
FRACAR -	IPEAK -	PRCDH -	XN -
FRACH -	IRELOC 1	*PROFIL (1,1)	ZCLAD -
FRACHE 1.0	IRELSE -		
FRACKR -	IRL -	*PSEUDO	
FRACN -	ISTOR -		
FRACXE -	IT	RADS -	
FRDEN 0.95	KB -	ROUC 0.1E-4	
FRPUO2 -	KOOL -	ROUF 0.4E-4	
FRSIN -	LFUEL 4.5	S -	

*PROFIL (1,1) = 1.0, 1.0

*PSEUDO (1) = 16.21, 21.21, 20.82, 21.18, 21.73, 21.94, 22.34, 22.92

*TIME (1) = 0.0, 0.06, 0.12, 0.25, 0.42, 0.48, 0.58, 0.73

NOTE: All input variables initialized to zero except as shown above.

Sample No. WCAP-2923 Capsule II (2 cases)

Alphabetical Listing of Input Parameters for GAPCON-THERMAL-2

ATMOS 1.0	FR35 0.0082	LVOIDZ 0	SIGHF 10000
DBO -	FR40 -	MINI -	*TIME
DCI 1.2745	FR41 -	NCLAD -1	
DCO 1.3244	HBC -	NCON -	TINLET 245
DE -	HGACEL -	NFLX -	TM 2790°C
DFS 1.25	ICDF -	NFUEL -	TPLAS 1200°C
DSINZ -	ICREP -	NOH -	V -
DTEMP 100°F	IDENSF -	NPOW 1	VPLENZ 0.44
DVOIDZ 0.068	IFLUX -	NPRFIL 1	XCO -
EXTP -	IGAS -	NTIME 12	XH -
FRACAR -	IPEAK -	PRCDH -	XN -
FRACH -	IRELOC 0 & 1	*PROFIL (1,1)	ZCLAD -
FRACHE 1.0	IRELSE -		
FRACKR -	IRL -	*PSEUDO	
FRACN -	ISTOR -		
FRACXE -	IT	RADS	
FRDEN 0.95	KB -	ROUC 0.1E-4	
FRPUO2 -	KOOL -	ROUF 0.4E-4	
FRSIN -	LFUEL 4.5	S -	

*PROFIL (1,1) = 1.0, 1.0

*PSEUDO (1) = 2.16, 2.16,0.82,1.34,1.66,1.90,2.07,2.18,2.36,2.40,2.47,2.60

*TIME (1) = 0.0, 0.06,0.1,0.13,0.20,0.25,0.29,0.35,0.43,0.56,0.81,1.2

NOTE: All input variables initialized to zero except as shown above.

DISTRIBUTION

No. of Copies	
OFFSITE	
1	ERDA Chicago Patent Group 9800 Cass Avenue Argonne, Illinois 60439 A. A. Churm
245	Basic Distribution Under NRC-1
61	Supplementary NRC-3 Distribution List
25	Nuclear Regulatory Commission, Division of Technical Review, Chief, Core Performance Branch
ON-SITE	
1	ERDA, Richland Operations Office B. J. Melton
38	Battelle-Northwest W. J. Bailey C. E. Beyer J. A. Christensen M. D. Freshley S. Goldsmith C. R. Hann (20) D. D. Lanning R. R. Lewis R. K. Marshall R. P. Marshall C. L. Mohr P. J. Pankaskie F. E. Panisko L. J. Parchen R. E. Williford Technical Information Files (3) Technical Publications